Density Model for Fin Whale (*Balaenoptera physalus*) for the U.S. East Coast: Supplementary Report

Duke University Marine Geospatial Ecology Lab*

Model Version 9.4 - 2016-04-21

Citation

When referencing our methodology or results generally, please cite our open-access article:

Roberts JJ, Best BD, Mannocci L, Fujioka E, Halpin PN, Palka DL, Garrison LP, Mullin KD, Cole TVN, Khan CB, McLellan WM, Pabst DA, Lockhart GG (2016) Habitat-based cetacean density models for the U.S. Atlantic and Gulf of Mexico. Scientific Reports 6: 22615. doi: 10.1038/srep22615

To reference this specific model or Supplementary Report, please cite:

Roberts JJ, Best BD, Mannocci L, Fujioka E, Halpin PN, Palka DL, Garrison LP, Mullin KD, Cole TVN, Khan CB, McLellan WM, Pabst DA, Lockhart GG (2016) Density Model for Fin Whale (*Balaenoptera physalus*) for the U.S. East Coast Version 9.4, 2016-04-21, and Supplementary Report. Marine Geospatial Ecology Lab, Duke University, Durham, North Carolina.

Copyright and License

Revision History

Version	Date	Description of changes
1	2013-05-10	Initial version.
2	2014-03-01	Switched from four seasonal models to two. Reformulated density model using a Horvitz-Thompson estimator. Eliminated GAM for group size (consequence of above). Added group size as a candidate covariate in detection functions (benefit of above). Added survey ID as a candidate covariate in NOAA NARWSS detection functions. Took more care in selecting right-truncation distances. Fitted models with contemporaneous predictors, for comparison to climatological. Switched SST and SST fronts predictors from NOAA Pathfinder to GHRSST CMC0.2deg L4. Changed SST fronts algorithm to use Canny operator instead of Cayula-Cornillon. Switched winds predictors from SCOW to CCMP (SCOW only gives climatol. estimates.) Added DistToEddy predictors, based on Chelton et al. (2011) eddy database. Added cumulative VGPM predictors, summing productivity for 45, 90, and 180 days. Added North Atlantic Oscillation (NAO) predictor; included 3 and 6 month lags. Transformed predictors more carefully, to better minimize leverage of outliers. Implemented hybrid hierarchical-forward / exhaustive model selection procedure. Model selection procedure better avoids concurvity between predictors. Allowed GAMs to select between multiple formulations of dynamic predictors. Adjusted land mask to eliminate additional estuaries and hard-to-predict cells.
3	2014-05-20	Fixed bug in temporal variability plots. Density models unchanged.

*For questions, or to offer feedback about this model or report, please contact Jason Roberts (jason.roberts@duke.edu)

4	2013-06-02	Added Reclassification of Ambiguous Sightings section, which was accidentally omitted. Density models unchanged.
5	2014-09-02	Added surveys: NJ-DEP, Virginia Aquarium, NARWSS 2013, UNCW 2013. Extended study area up Scotian Shelf. Added SEAPODYM predictors. Switched to mgcv estimation of Tweedie p parameter (family=tw()).
6	2014-10-18	Switched to a single season model. Added Palka (2006) survey-specific g(0) estimates. Updated distance to eddy predictors using Chelton et al.'s 2014 database. Removed distance to eddy and wind speed predictors. Fixed missing pixels in several climatological predictors, which led to not all segments being utilized. Eliminated Cape Cod Bay subregion.
7	2014-11-03	Fixed error in g(0) for NEFSC Abel-J Binocular Surveys: previously used 0.87; changed to correct value, 0.32, and refitted the model. Updated documentation.
8	2014-11-10	Reconfigured detection hierarchy and adjusted NARWSS detection functions based on additional information from Tim Cole. Removed CumVGPM180 predictor. Updated documentation.
9	2014-12-03	Fixed bug that applied the wrong detection function to segments NE_narwss_1999_widgeon_hapo dataset. Refitted model. Updated documentation.
9.1	2015-02-02	Updated the documentation. No changes to the model.
9.2	2015-05-14	Updated calculation of CVs. Switched density rasters to logarithmic breaks. No changes to the model.
9.3	2015-09-26	Updated the documentation. No changes to the model.
9.4	2016-04-21	Switched calculation of monthly 5% and 95% confidence interval rasters to the method used to produce the year-round rasters. (We intended this to happen in version 9.2 but I did not implement it properly.) No changes to the other rasters or the model itself.

Survey Data

Survey	Period	Length (1000 km)	Hours	Sightings
NEFSC Aerial Surveys	1995-2008	70	412	200
NEFSC NARWSS Harbor Porpoise Survey	1999-1999	6	36	13
NEFSC North Atlantic Right Whale Sighting Survey	1999-2013	432	2330	1694
NEFSC Shipboard Surveys	1995-2004	16	1143	117
NJDEP Aerial Surveys	2008-2009	11	60	1
NJDEP Shipboard Surveys	2008-2009	14	836	26
SEFSC Atlantic Shipboard Surveys	1992-2005	28	1731	11
SEFSC Mid Atlantic Tursiops Aerial Surveys	1995-2005	35	196	6
SEFSC Southeast Cetacean Aerial Surveys	1992-1995	8	42	0
UNCW Cape Hatteras Navy Surveys	2011-2013	19	125	5
UNCW Early Marine Mammal Surveys	2002-2002	18	98	1
UNCW Jacksonville Navy Surveys	2009-2013	66	402	0
UNCW Onslow Navy Surveys	2007-2011	49	282	1
UNCW Right Whale Surveys	2005-2008	114	586	12
Virginia Aquarium Aerial Surveys	2012-2014	9	53	13
Total		895	8332	2100

Table 2: Survey effort and sightings used in this model. Effort is tallied as the cumulative length of on-effort transects and hours the survey team was on effort. Sightings are the number of on-effort encounters of the modeled species for which a perpendicular sighting distance (PSD) was available. Off effort sightings and those without PSDs were omitted from the analysis.

Season	Months	Length (1000 km)	Hours	Sightings
All_Year	All	897	8332	2100

Table 3: Survey effort and on-effort sightings having perpendicular sighting distances.

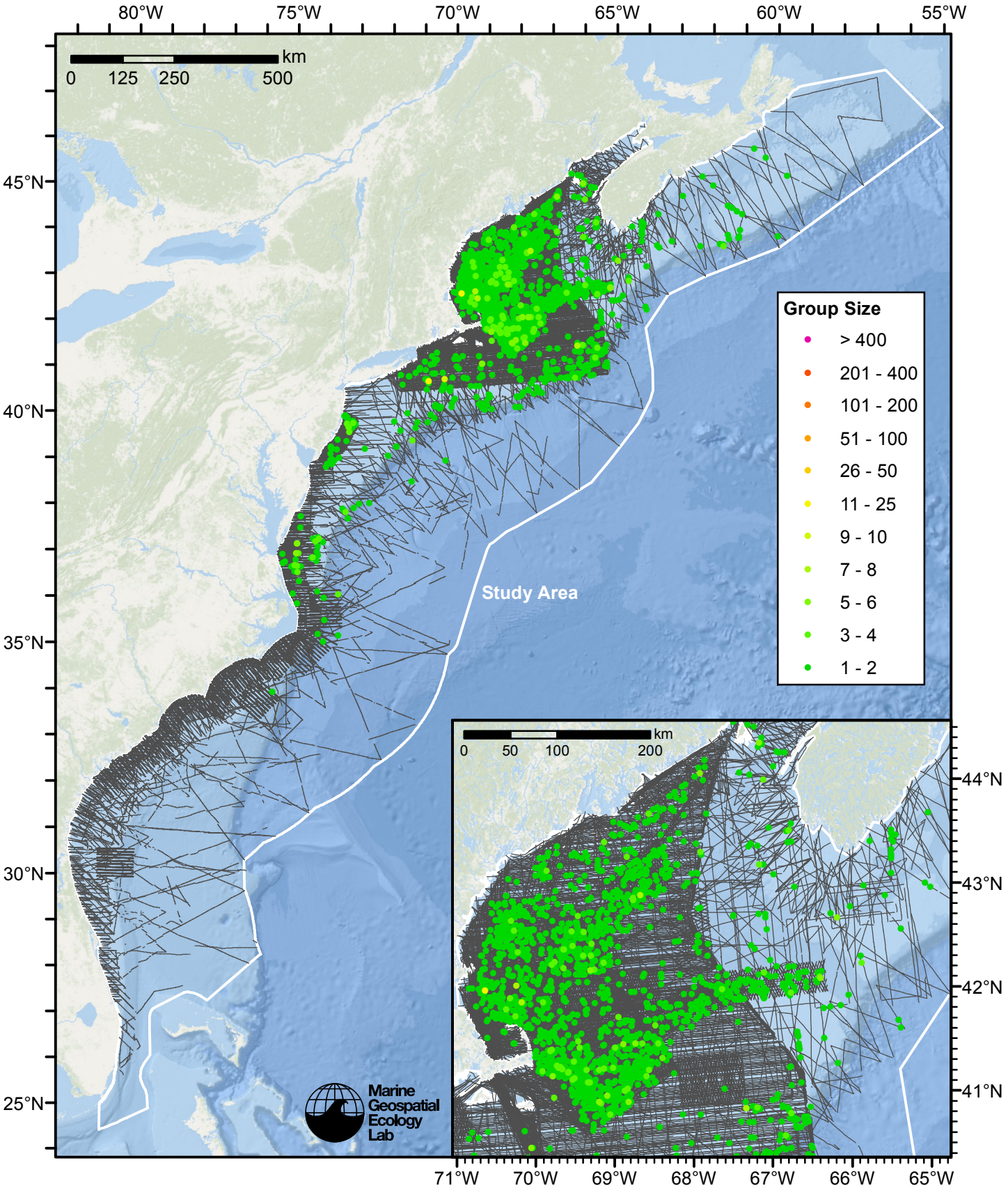

Figure 1: Fin whale sightings and survey tracklines.

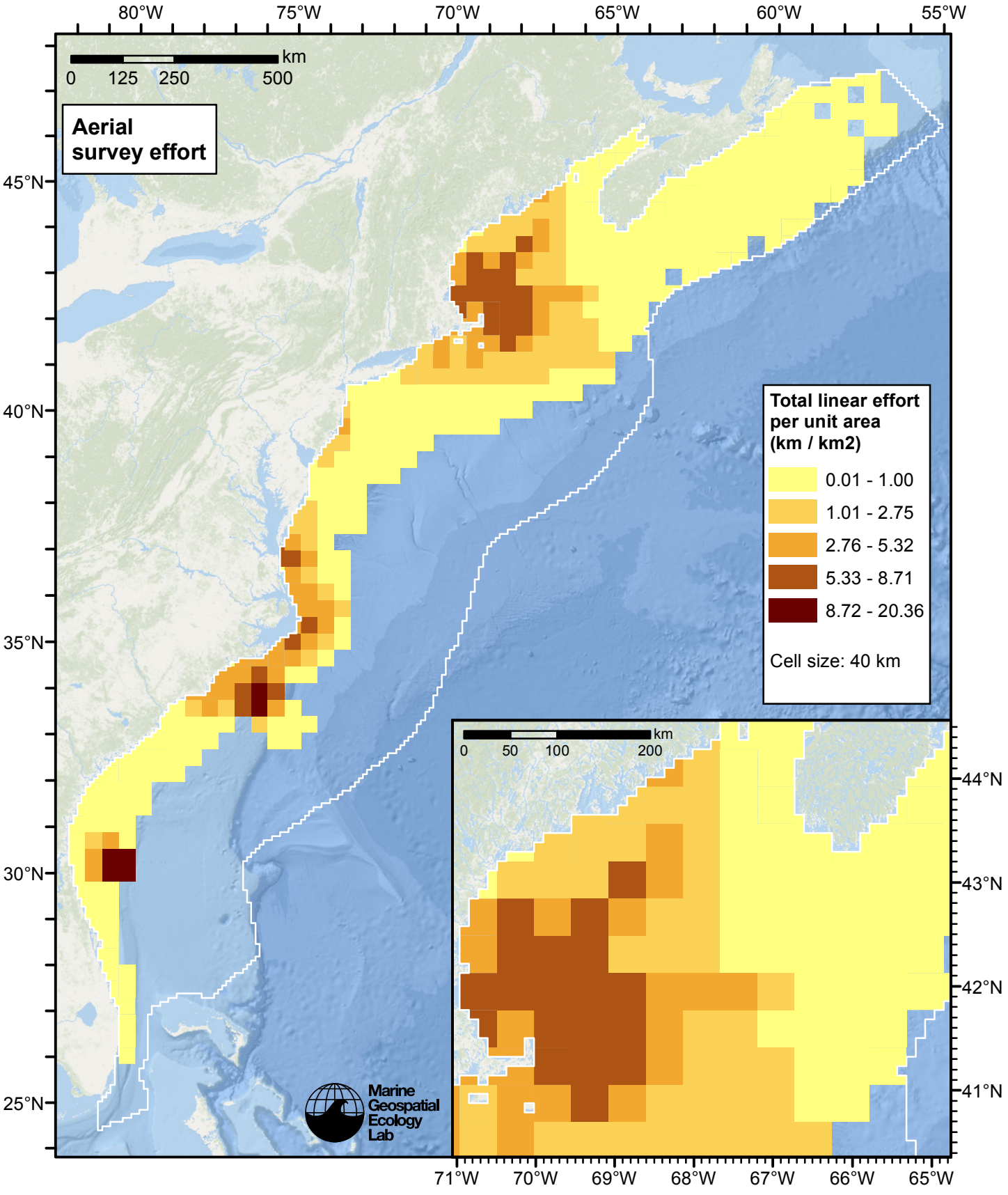

Figure 2: Aerial linear survey effort per unit area.

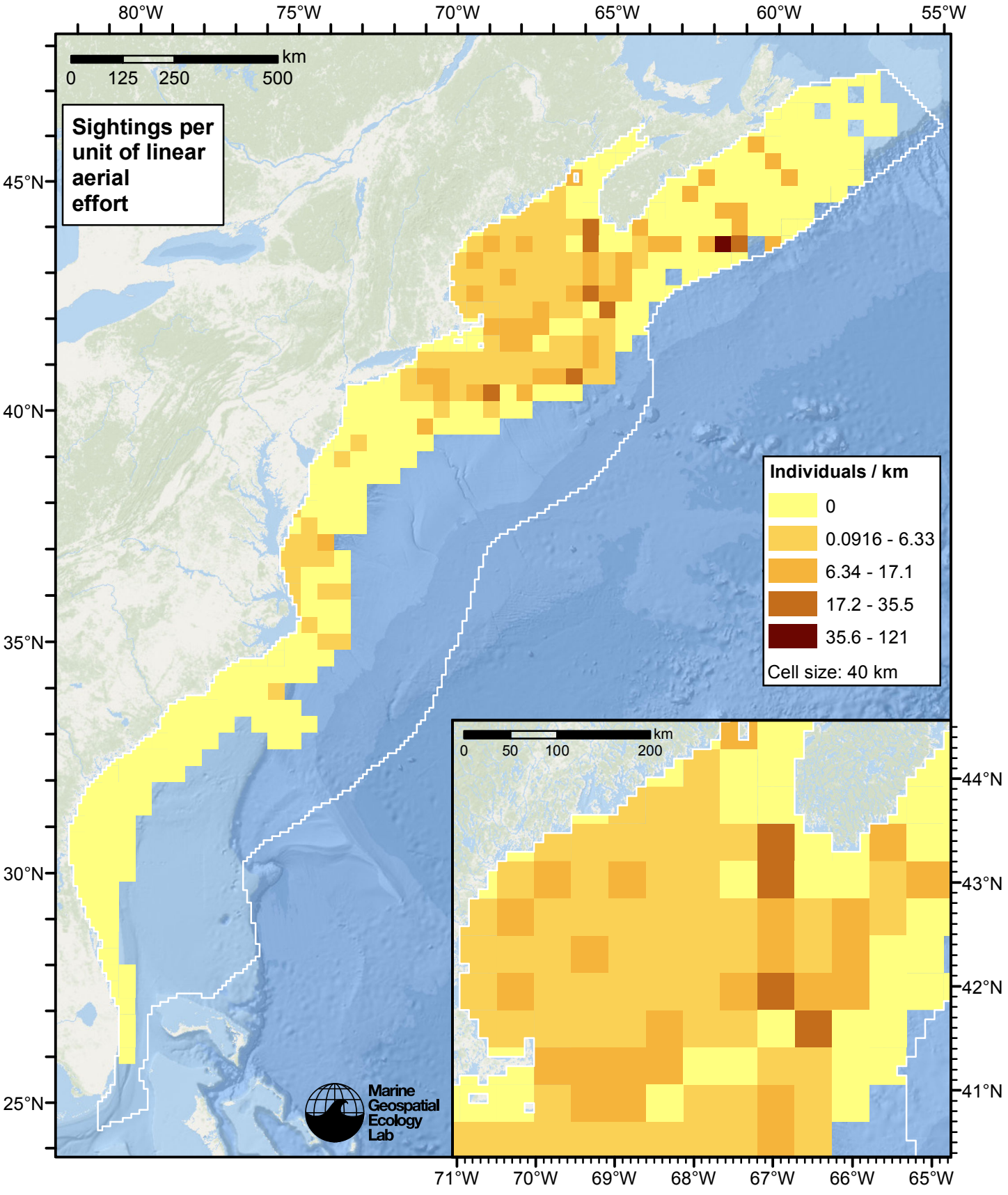

Figure 3: Fin whale sightings per unit aerial linear survey effort.

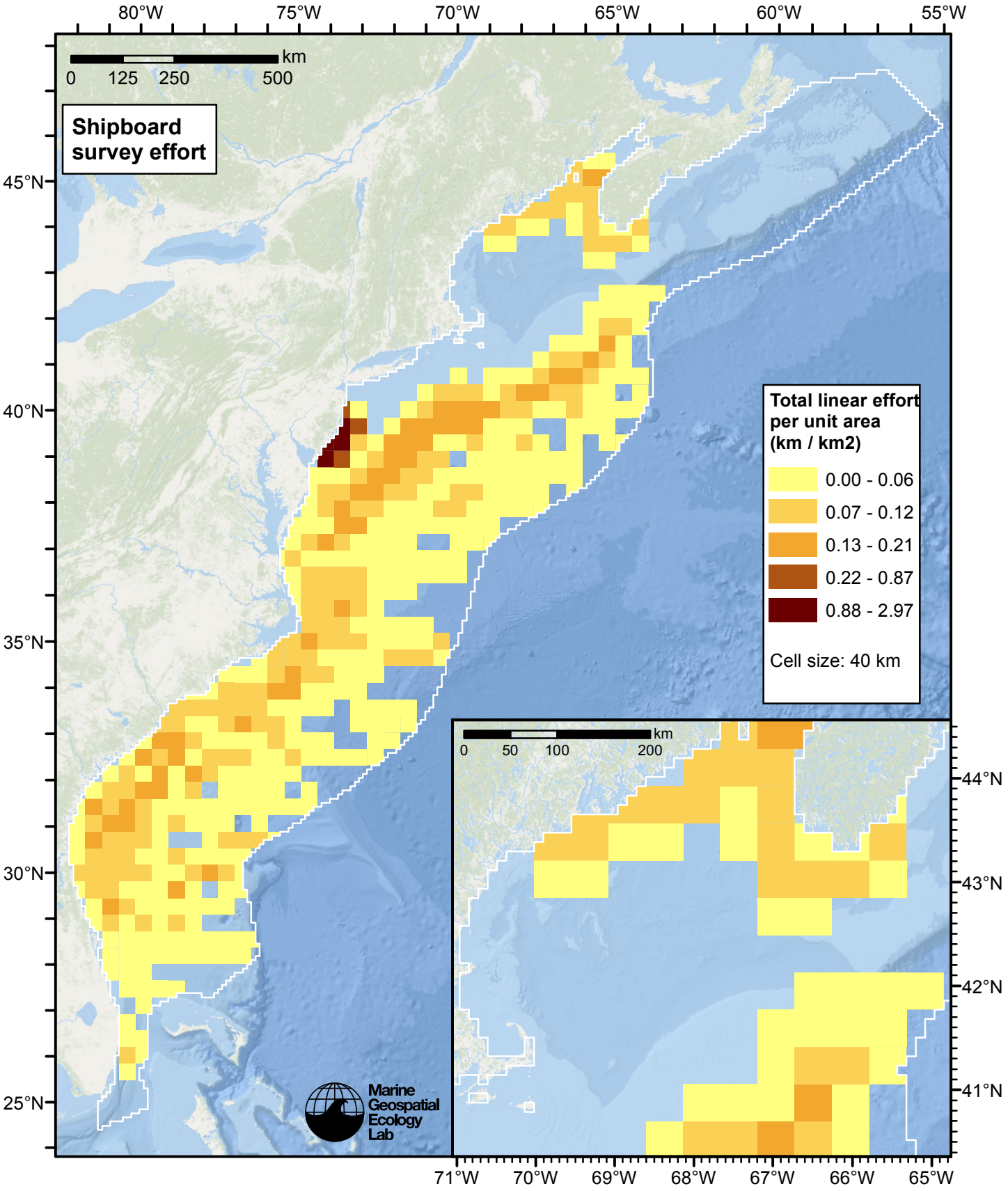

Figure 4: Shipboard linear survey effort per unit area.

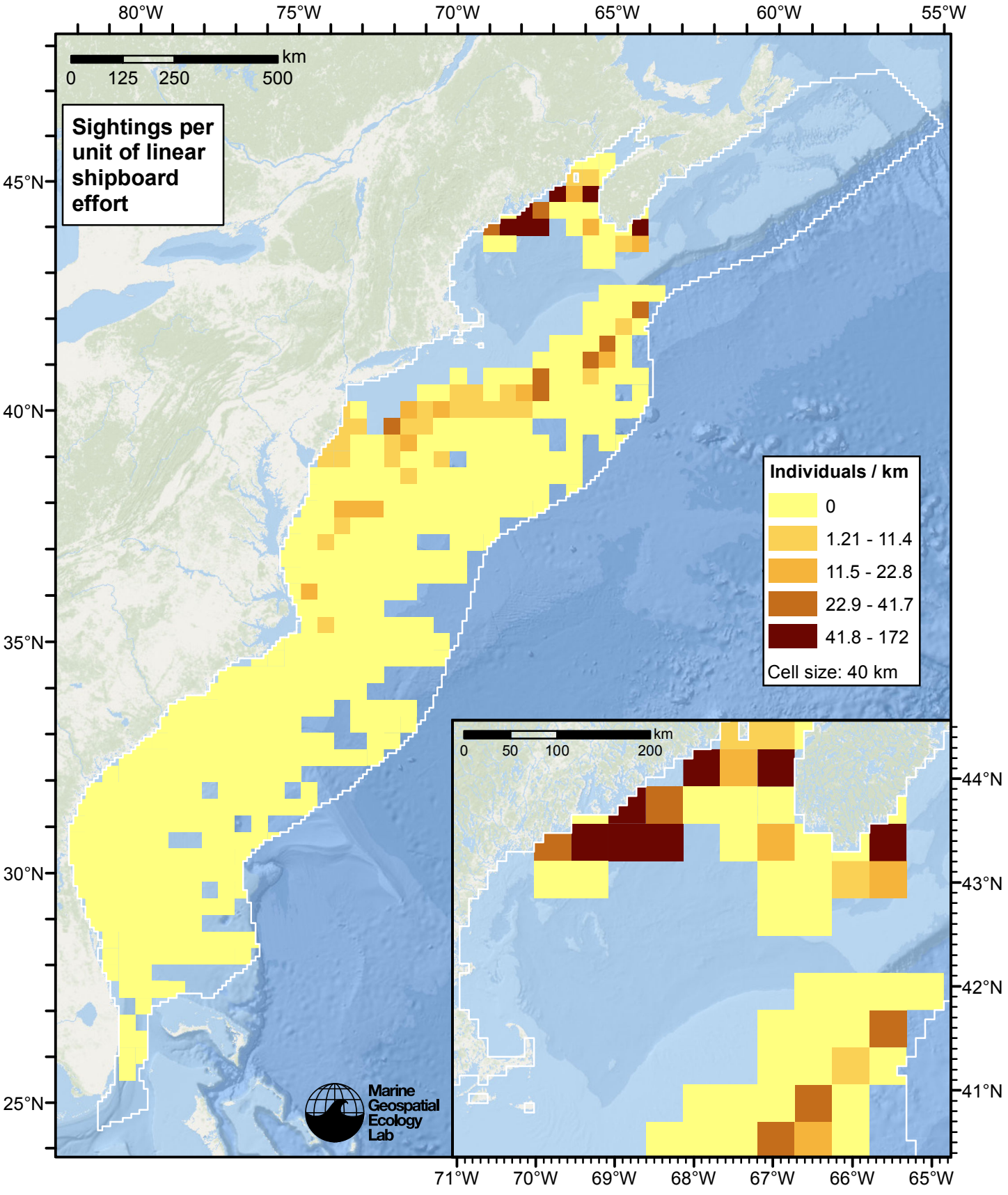

Figure 5: Fin whale sightings per unit shipboard linear survey effort.

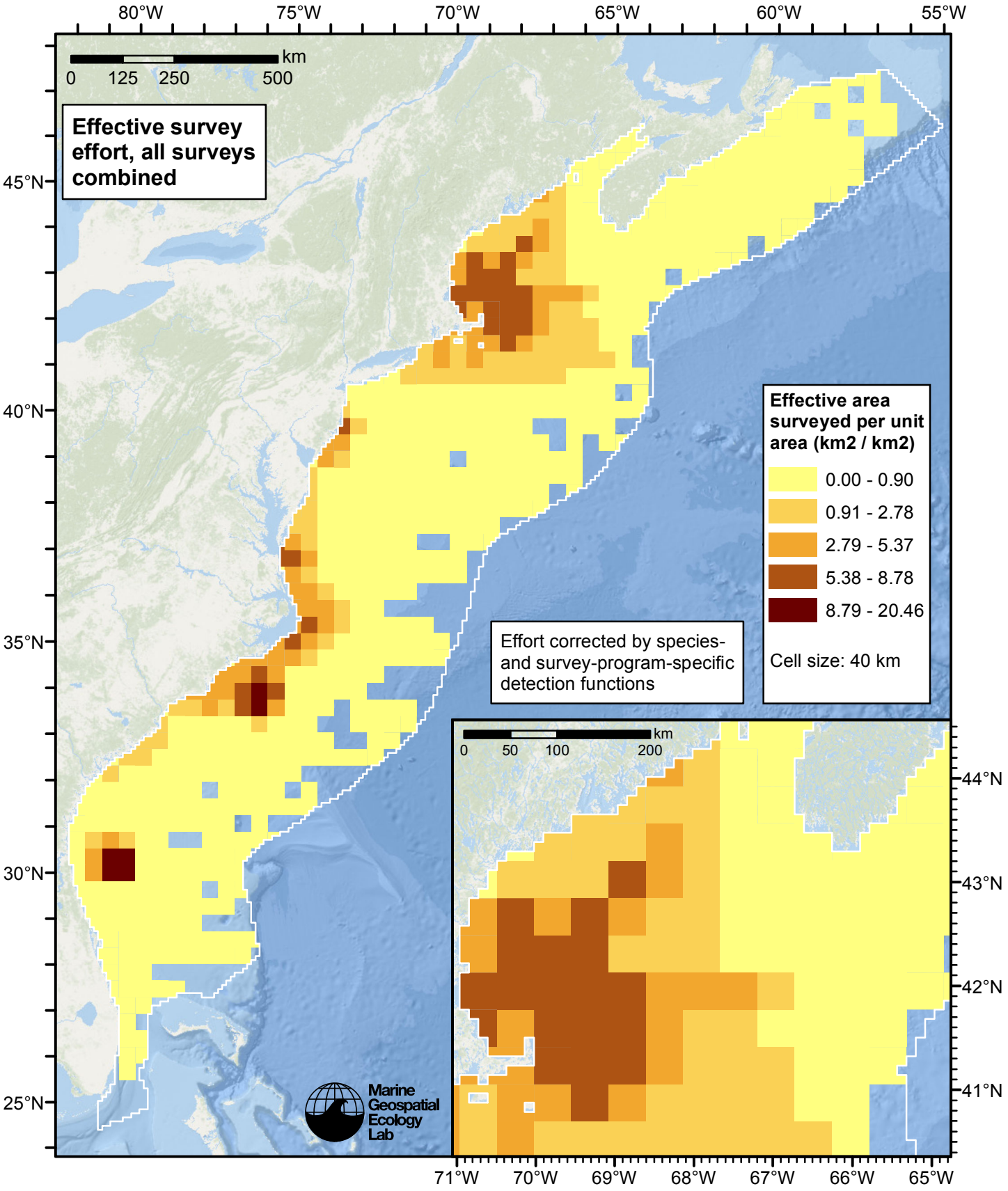

Figure 6: Effective survey effort per unit area, for all surveys combined. Here, effort is corrected by the species- and survey-program-specific detection functions used in fitting the density models.

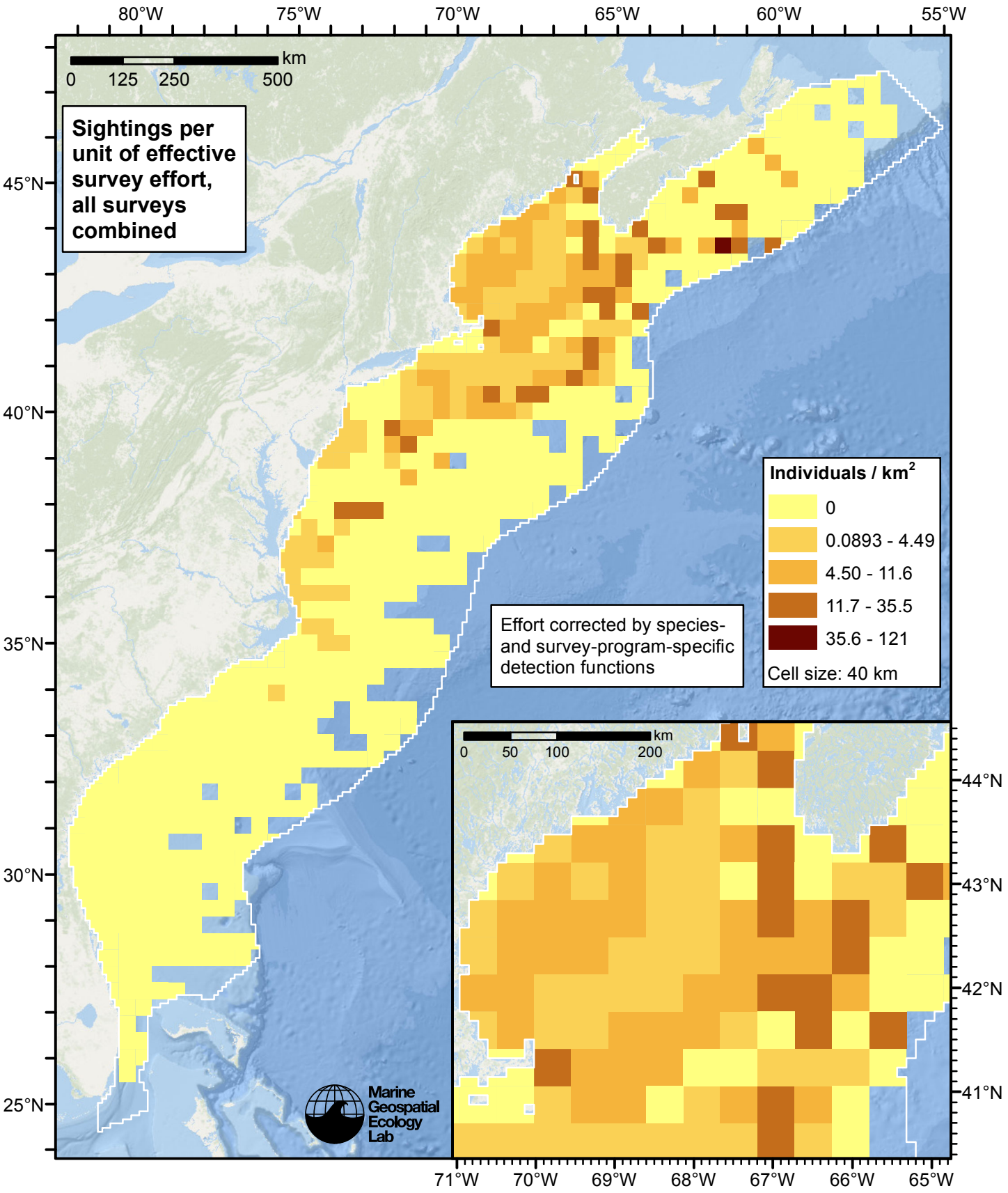

Figure 7: Fin whale sightings per unit of effective survey effort, for all surveys combined. Here, effort is corrected by the species- and survey-program-specific detection functions used in fitting the density models.

Reclassification of Ambiguous Sightings

Observers occasionally experience difficulty identifying species, due to poor sighting conditions or phenotypic similarities between the possible choices. For example, observers may not always be able to distinguish fin whales from sei whales (Tim Cole, pers. comm.). When this happens, observers will report an ambiguous identification, such as "fin or sei whale".

In our density models, we handled ambiguous identifications in three ways:

1. For sightings with very generic identifications such as "large whale", we discarded the sightings. These sightings represented a clear minority when compared to those with definitive species identifications, but they are uncounted animals and our density models may therefore underestimate density to some degree.
2. For sightings of certain taxa in which a large majority of identifications were ambiguous (e.g. "Globicephala spp.") rather than specific (e.g. "Globicephala melas" or "Globicephala macrorhynchus"), it was not tractable to model the individual species so we modeled the generic taxon instead.
3. For sightings that reported an ambiguous identification of two species (e.g. "fin or sei whale") that are known to exhibit different habitat preferences or typically occur in different group sizes, and for which we had sufficient number of definitive sightings of both species, we fitted a predictive model that classified the ambiguous sightings into one species or the other.

This section describes how we utilized the third category of ambiguous sightings in the density models presented in this report.

For the predictive model, we used the cforest classifier (Hothorn et al. 2006), an elaboration of the classic random forest classifier (Breiman, 2001). First, we trained a binary classifier using the sightings that reported definitive species identifications (e.g. "fin whale" and "sei whale"). The training data included all on-effort sightings, not just those in the focal study area. We used the species ID as the response variable and oceanographic variables or group size as predictor variables, depending on the species. We used receiver operating characteristic (ROC) curve analysis to select a threshold for classifying the probabilistic predictions of species identifications made by the model into a binary result of one species or another; for the threshold, we selected the value that maximized the Youden index (see Perkins and Schisterman, 2006).

Then, for all sightings reporting the ambiguous identification, we reclassified the sighting as either one species or the other by processing the predictor values observed for that sighting through the fitted model. We then included the reclassified sightings in the detection functions and spatial models of density. The sightings reported elsewhere in this document incorporate both the definitive sightings and the reclassified sightings.

Reclassification of "Balaenoptera borealis/physalus" in the East Coast Region

Density Histograms

These plots show the per-species distribution of each predictor variable used in the reclassification model. When a variable exhibits a substantially different distribution for each species, it is a good candidate for classifying ambiguous sightings as one species or the other.

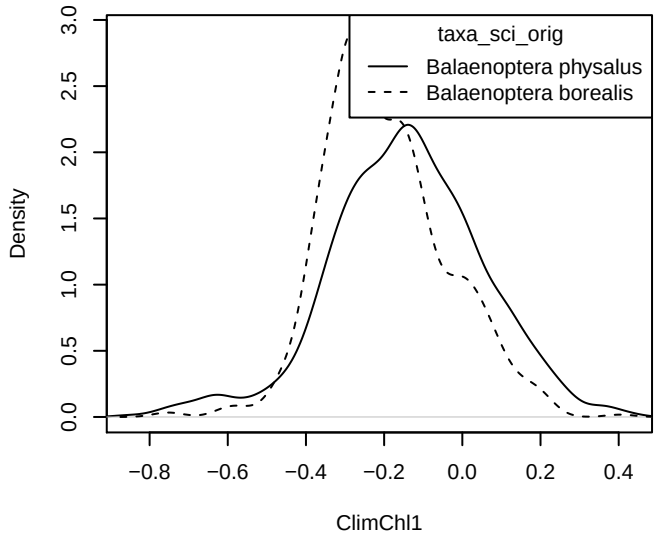
taxa_sci_orig
Balaenoptera physalus
Balaenoptera borealis
Density
ClimChl1

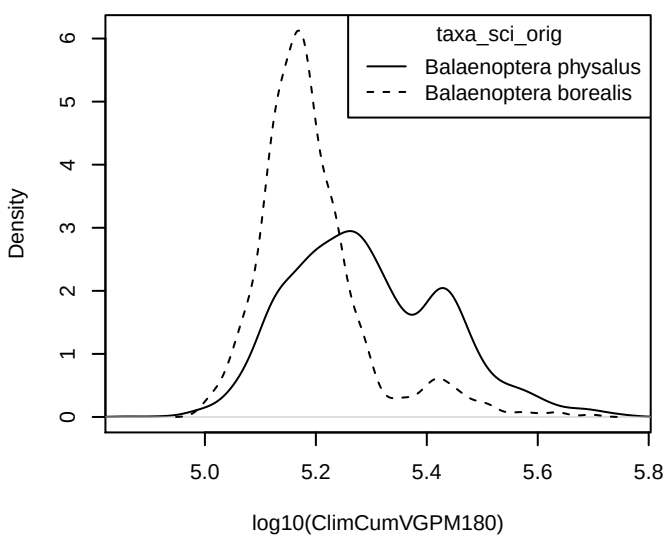
taxa_sci_orig
Balaenoptera physalus
Balaenoptera borealis
Density
log10(ClimCumVGPM180)

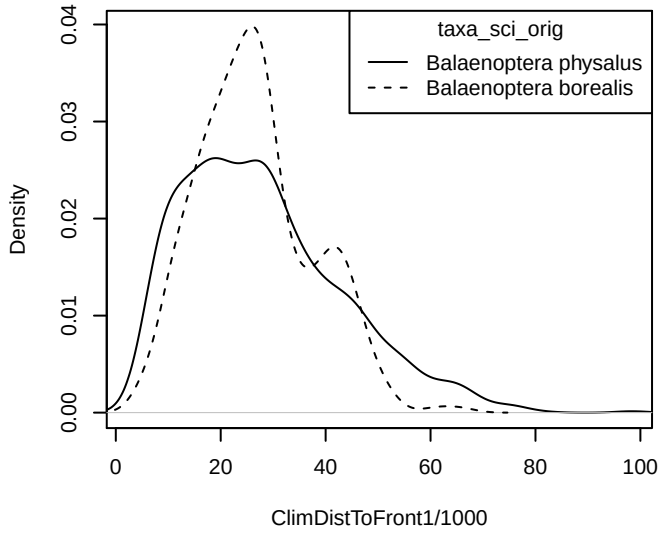
taxa_sci_orig
Balaenoptera physalus
Balaenoptera borealis
Density
ClimDistToFront1/1000

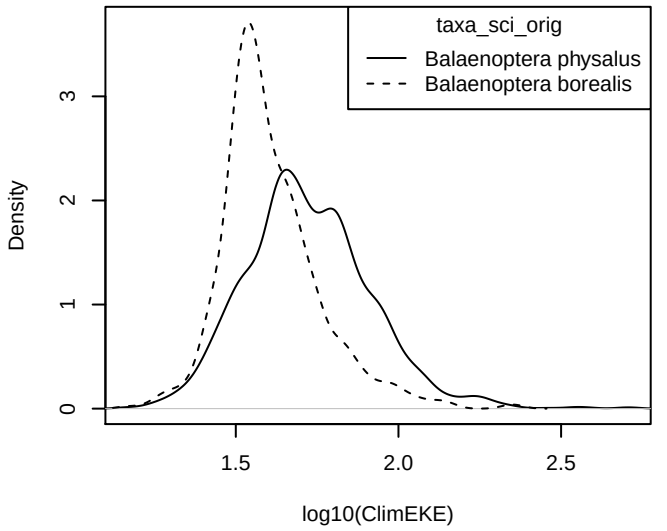
taxa_sci_orig
Balaenoptera physalus
Balaenoptera borealis
Density
log10(ClimEKE)

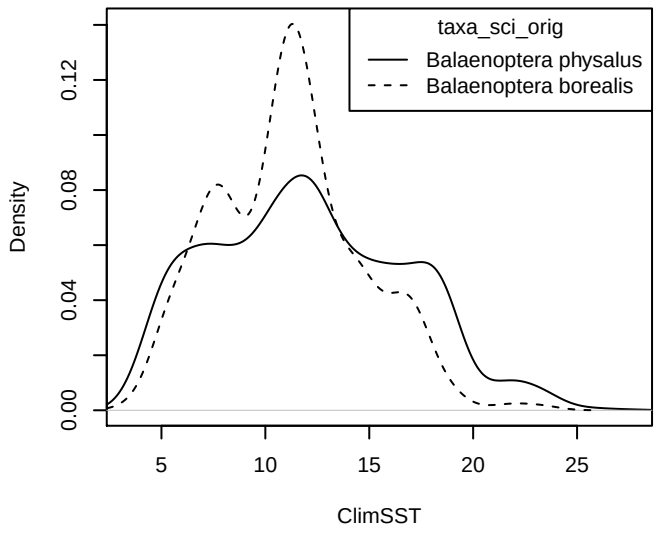
taxa_sci_orig
Balaenoptera physalus
Balaenoptera borealis
Density
ClimSST

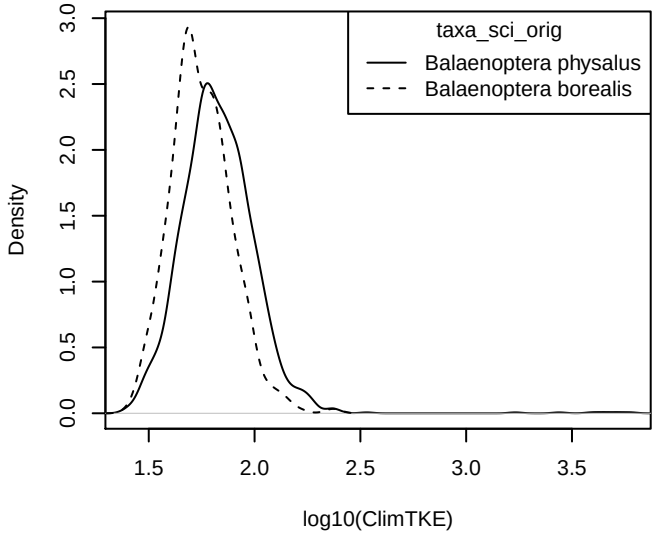
taxa_sci_orig
Balaenoptera physalus
Balaenoptera borealis
Density
log10(ClimTKE)

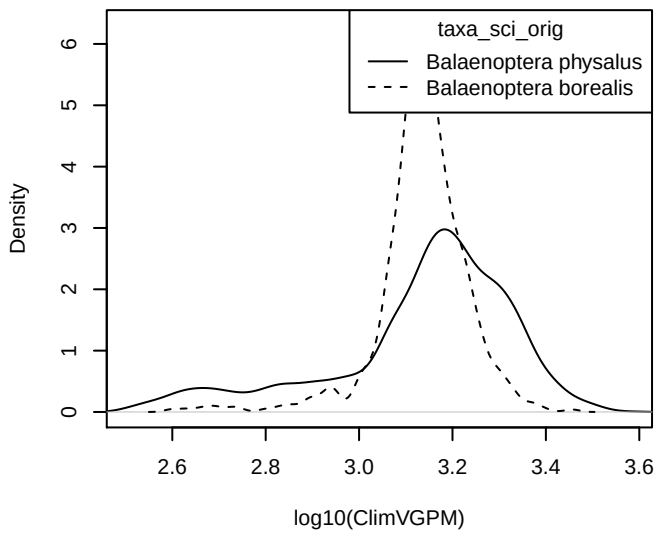
taxa_sci_orig
Balaenoptera physalus
Balaenoptera borealis
Density
log10(ClimVGPM)

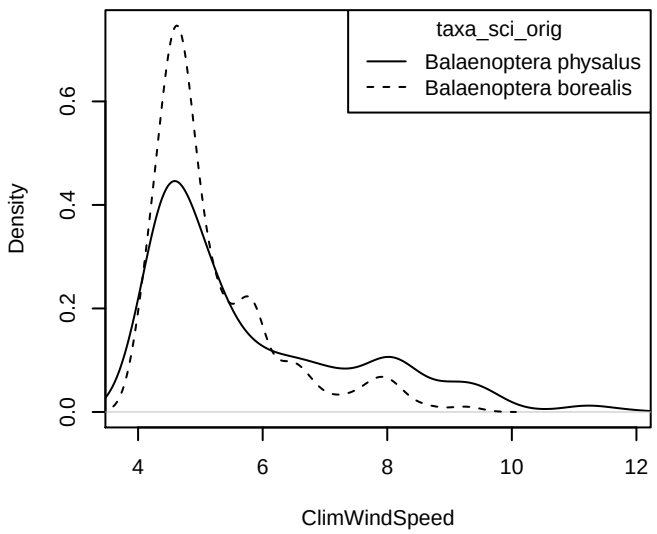
taxa_sci_orig
Balaenoptera physalus
Balaenoptera borealis
Density
ClimWindSpeed

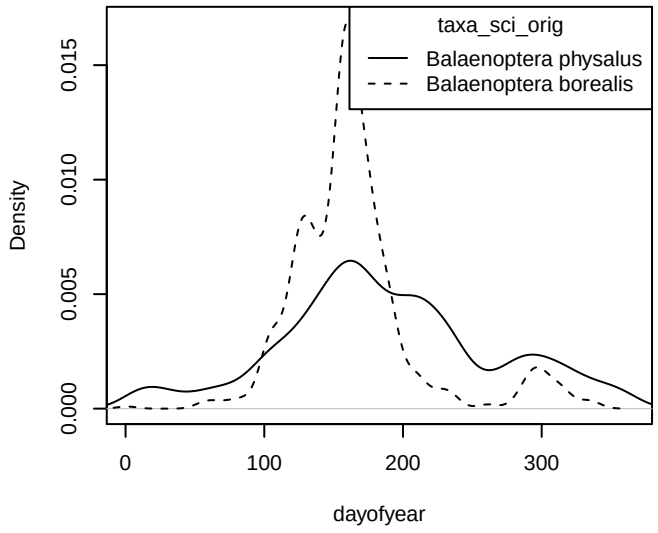
taxa_sci_orig
Balaenoptera physalus
Balaenoptera borealis
Density
dayofyear

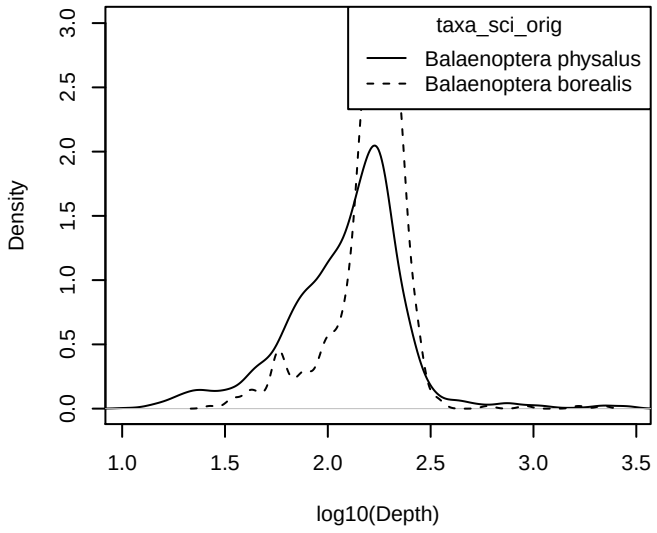
taxa_sci_orig
Balaenoptera physalus
Balaenoptera borealis
Density
log10(Depth)

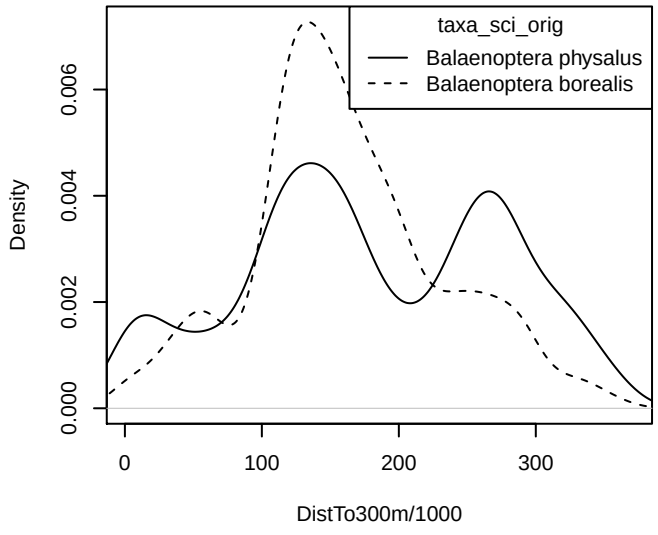
taxa_sci_orig
Balaenoptera physalus
Balaenoptera borealis
Density
DistTo300m/1000

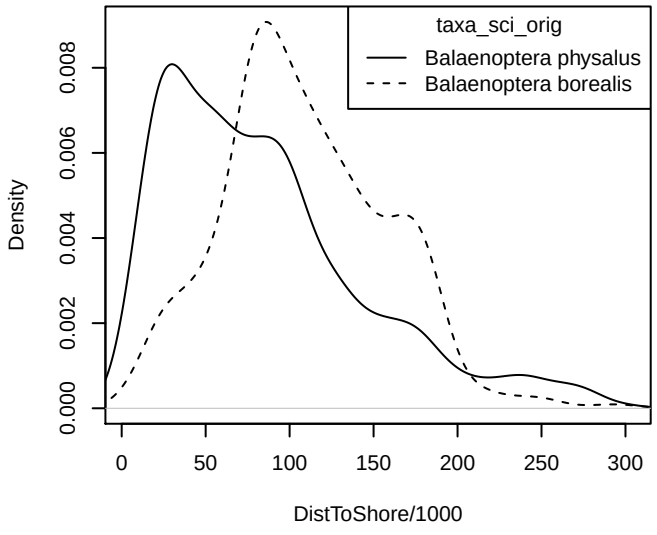
taxa_sci_orig
Balaenoptera physalus
Balaenoptera borealis
Density
DistToShore/1000

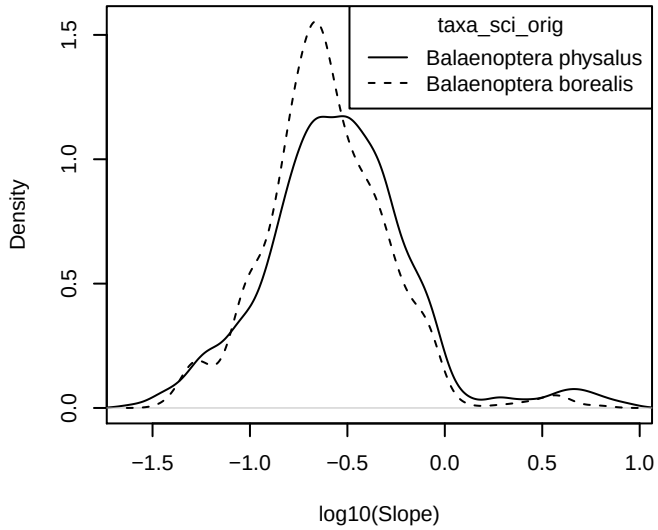

Statistical output

```
MODEL SUMMARY:
==============

     Random Forest using Conditional Inference Trees

Number of trees:  1000

Response:  factor(taxa_sci_orig)
Inputs:  dayofyear, Depth, Slope, DistToShore, DistTo300m, ClimSST, ClimDistToFront1, ClimChl1, ClimTKE, ClimE
Number of observations:  2458

Number of variables tried at each split: 5

Estimated predictor variable importance (conditional = FALSE):

                 Importance
ClimCumVGPM180      0.03383
ClimEKE             0.01948
ClimWindSpeed       0.01803
Depth               0.01777
DistToShore         0.01762
ClimVGPM            0.01171
DistTo300m          0.01154
dayofyear           0.01125
ClimChl1            0.00968
ClimSST             0.00920
Slope               0.00759
ClimTKE             0.00618
ClimDistToFront1    0.00512

MODEL PERFORMANCE SUMMARY:
==========================

Statistics calculated from the training data.

Area under the ROC curve (auc)           = 0.940
Mean cross-entropy (mxe)                 = 0.282
Precision-recall break-even point (prbe) = 0.915
```

```
Root-mean square error (rmse)            = 0.297

Cutoff selected by maximizing the Youden index = 0.721

Confusion matrix for that cutoff:

                                 Actual Balaenoptera physalus  Actual Balaenoptera borealis  Total
Predicted Balaenoptera physalus                          1587                            92   1679
Predicted Balaenoptera borealis                           255                           524    779
Total                                                    1842                           616   2458

Model performance statistics for that cutoff:

Accuracy (acc)                              = 0.859
Error rate (err)                            = 0.141
Rate of positive predictions (rpp)          = 0.683
Rate of negative predictions (rnp)          = 0.317

True positive rate (tpr, or sensitivity)    = 0.862
False positive rate (fpr, or fallout)       = 0.149
True negative rate (tnr, or specificity)    = 0.851
False negative rate (fnr, or miss)          = 0.138

Positive prediction value (ppv, or precision) = 0.945
Negative prediction value (npv)             = 0.673
Prediction-conditioned fallout (pcfall)     = 0.055
Prediction-conditioned miss (pcmiss)        = 0.327

Matthews correlation coefficient (mcc)      = 0.663
Odds ratio (odds)                           = 35.447
SAR                                         = 0.698

Cohen's kappa (K)                           = 0.655
```

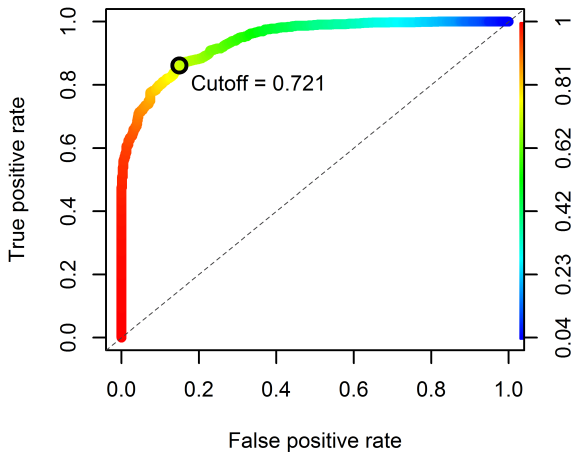

Figure 8: Receiver operating characteristic (ROC) curve illustrating the predictive performance of the model used to reclassify "Balaenoptera borealis/physalus" sightings into one species or the other.

Reclassifications Performed

Survey	Definitive B. physalus Sightings	Definitive B. borealis Sightings	Ambiguous Sightings	Reclassed to B. physalus	Reclassed to B. borealis
NEFSC Aerial Surveys	210	8	27	21	6
NEFSC NARWSS Harbor Porpoise Survey	16	0	0	0	0
NEFSC North Atlantic Right Whale Sighting Survey	1455	603	546	315	231
NEFSC Shipboard Surveys	138	6	100	100	0
NJDEP Aerial Surveys	1	0	0	0	0
NJDEP Shipboard Surveys	27	0	0	0	0
SEFSC Atlantic Shipboard Surveys	11	0	0	0	0
SEFSC Mid Atlantic Tursiops Aerial Surveys	6	0	0	0	0
UNCW Cape Hatteras Navy Surveys	5	0	0	0	0
UNCW Early Marine Mammal Surveys	2	0	0	0	0
UNCW Onslow Navy Surveys	1	0	0	0	0
UNCW Right Whale Surveys	12	0	0	0	0
Virginia Aquarium Aerial Surveys	14	0	0	0	0
Total	1898	617	673	436	237

Table 4: Counts of definitive sightings, ambiguous sightings, and what the ambiguous sightings were reclassified to. Note that this analysis was performed on all on-effort sightings, not just those in the focal study area. These counts may therefore be larger than those presented in the Survey Data section of this report, which are restricted to the focal study area.

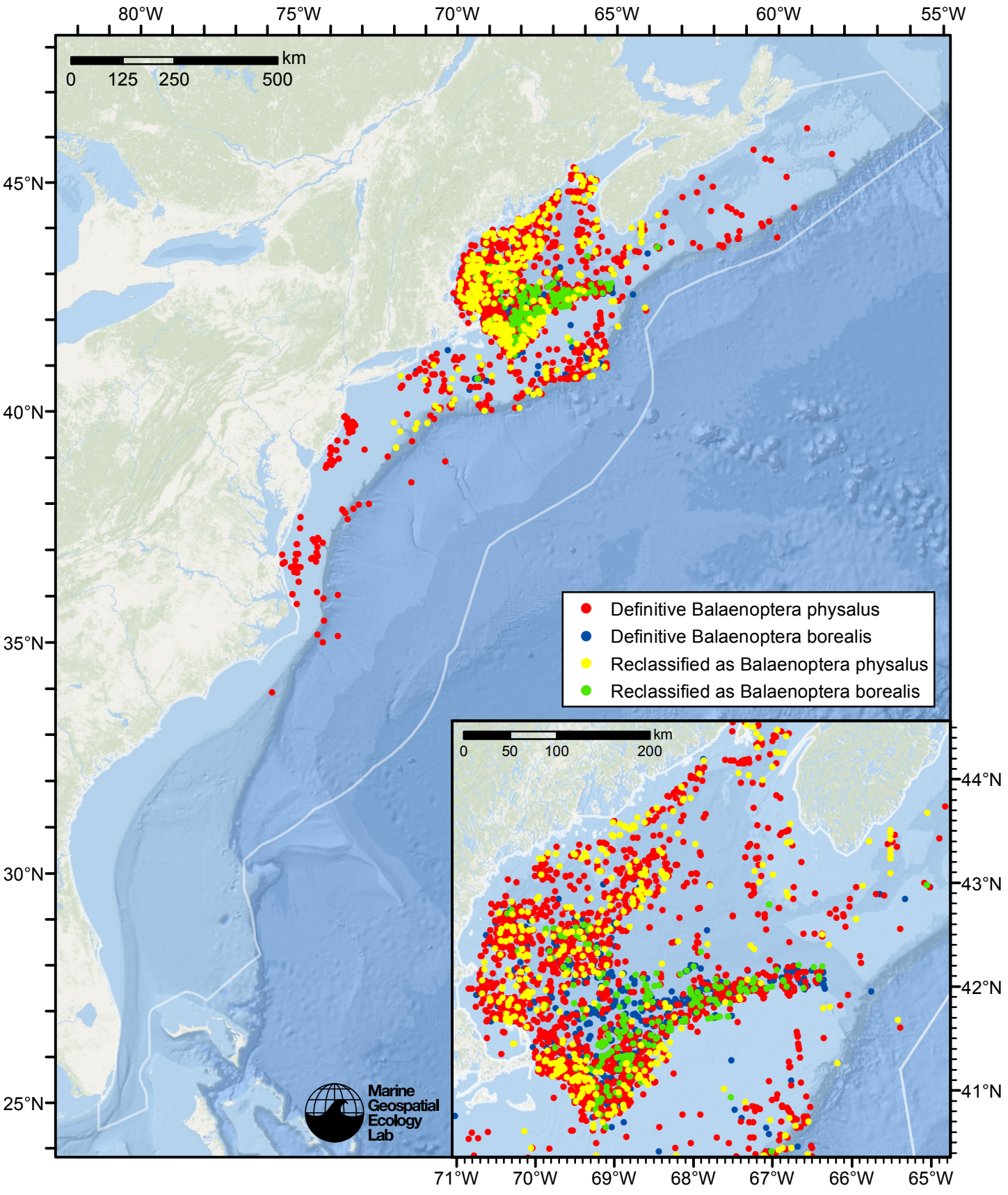

Figure 9: Definitive sightings used to train the model and ambiguous sightings reclassified by the model, by season.

Detection Functions

The detection hierarchy figures below show how sightings from multiple surveys were pooled to try to achieve Buckland et. al's (2001) recommendation that at least 60-80 sightings be used to fit a detection function. Leaf nodes, on the right, usually represent individual surveys, while the hierarchy to the left shows how they have been grouped according to how similar we believed the surveys were to each other in their detection performance.

At each node, the red or green number indicates the total number of sightings below that node in the hierarchy, and is colored green if 70 or more sightings were available, and red otherwise. If a grouping node has zero sightings–i.e. all of the surveys within it had zero sightings–it may be collapsed and shown as a leaf to save space.

Each histogram in the figure indicates a node where a detection function was fitted. The actual detection functions do not appear in this figure; they are presented in subsequent sections. The histogram shows the frequency of sightings by perpendicular sighting distance for all surveys contained by that node. Each survey (leaf node) recieves the detection function that is closest to it up the hierarchy. Thus, for common species, sufficient sightings may be available to fit detection functions deep in the hierarchy, with each function applying to only a few surveys, thereby allowing variability in detection performance between surveys to be addressed relatively finely. For rare species, so few sightings may be available that we have to pool many surveys together to try to meet Buckland's recommendation, and fit only a few coarse detection functions high in the hierarchy.

A blue Proxy Species tag indicates that so few sightings were available that, rather than ascend higher in the hierarchy to a point that we would pool grossly-incompatible surveys together, (e.g. shipboard surveys that used big-eye binoculars with those that used only naked eyes) we pooled sightings of similar species together instead. The list of species pooled is given in following sections.

Shipboard Surveys

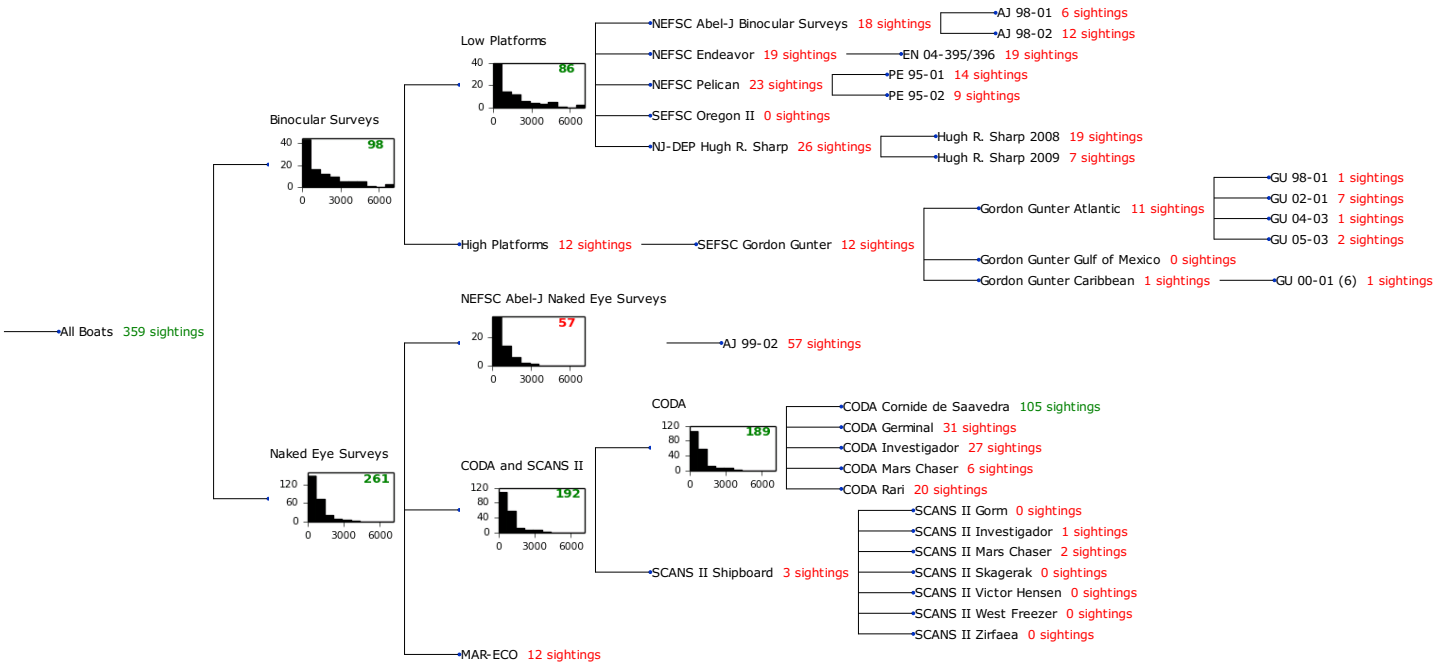

Figure 10: Detection hierarchy for shipboard surveys

Binocular Surveys

The sightings were right truncated at 5000m.

Covariate	Description

beaufort	Beaufort sea state.

Table 5: Covariates tested in candidate "multi-covariate distance sampling" (MCDS) detection functions.

Key	Adjustment	Order	Covariates	Succeeded	Δ AIC	Mean ESHW (m)
hr				Yes	0.00	1414
hr			beaufort	Yes	0.92	1505
hr	poly	4		Yes	1.85	1418
hr	poly	2		Yes	2.00	1414
hn	cos	2		Yes	2.48	1809
hn			beaufort	Yes	11.78	2540
hn	cos	3		Yes	13.12	2027
hn				Yes	14.20	2524
hn	herm	4		Yes	15.86	2515
hn	cos	1		No		

Table 6: Candidate detection functions for Binocular Surveys. The first one listed was selected for the density model.

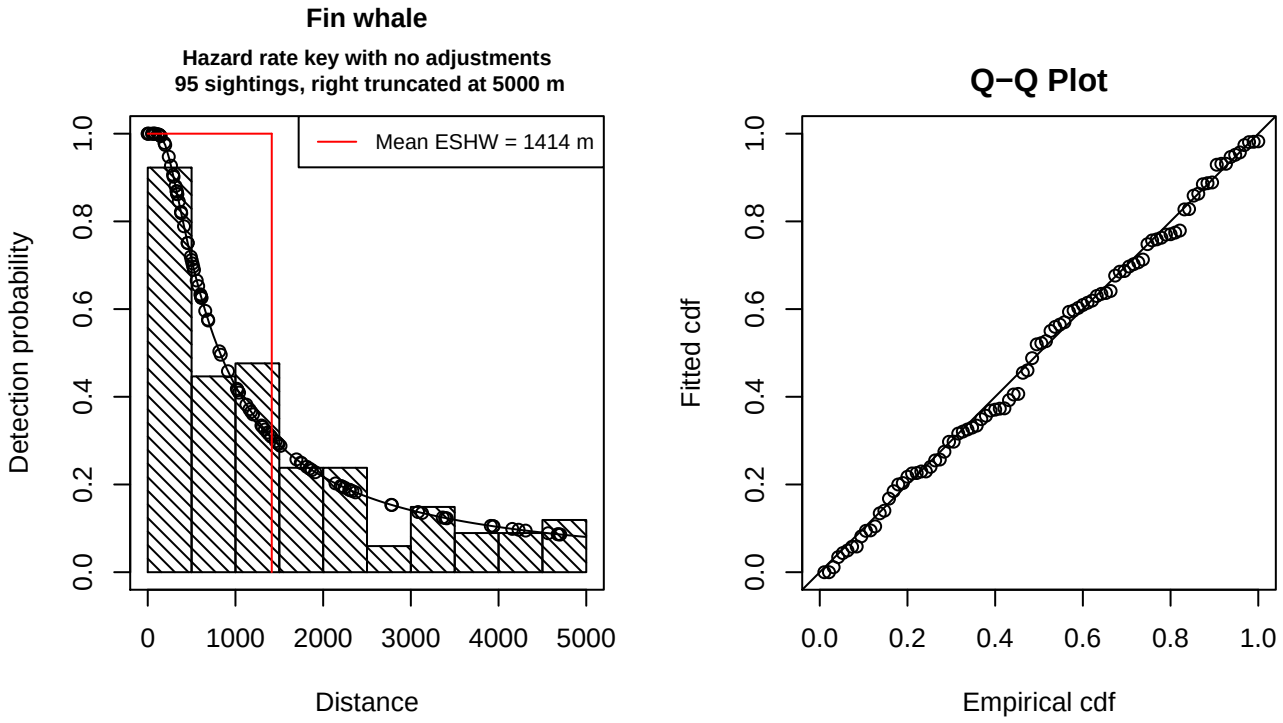

Figure 11: Detection function for Binocular Surveys that was selected for the density model

Statistical output for this detection function:

```
Summary for ds object
Number of observations :  95
Distance range         :  0  -  5000
AIC                    :  1561.759

Detection function:
 Hazard-rate key function

Detection function parameters
Scale Coefficients:
            estimate        se
(Intercept) 6.401429 0.4538613

Shape parameters:
             estimate        se
(Intercept) 0.1588674 0.2113658

                        Estimate          SE        CV
Average p              0.2827566  0.06458143 0.2283994
N in covered region 335.9780163 82.10261441 0.2443690
```

Additional diagnostic plots:

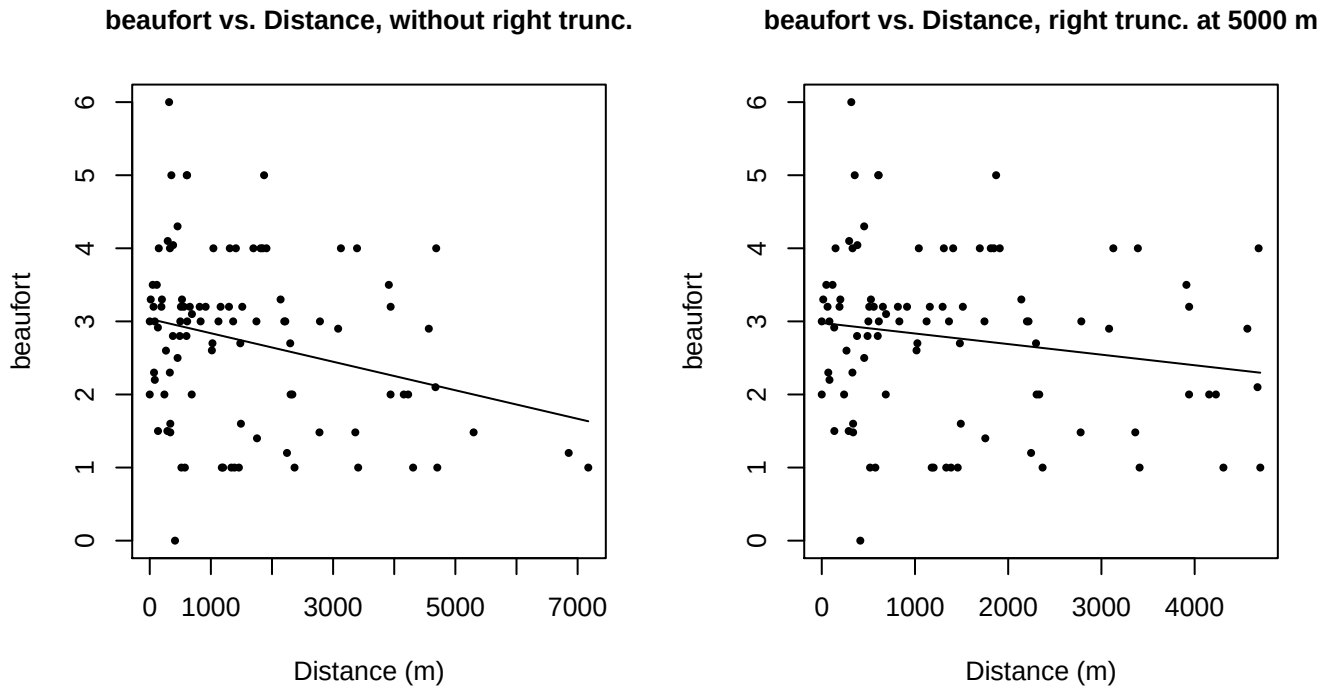

Figure 12: Scatterplots showing the relationship between Beaufort sea state and perpendicular sighting distance, for all sightings (left) and only those not right truncated (right). The line is a simple linear regression.

Low Platforms

The sightings were right truncated at 5000m.

Covariate	Description

beaufort	Beaufort sea state.

Table 7: Covariates tested in candidate "multi-covariate distance sampling" (MCDS) detection functions.

Key	Adjustment	Order	Covariates	Succeeded	Δ AIC	Mean ESHW (m)
hr				Yes	0.00	1427
hn	cos	2		Yes	1.61	1717
hr			beaufort	Yes	1.63	1463
hr	poly	4		Yes	2.00	1427
hr	poly	2		Yes	2.00	1427
hn			beaufort	Yes	12.34	2424
hn				Yes	13.27	2420
hn	cos	3		Yes	13.49	2026
hn	herm	4		Yes	14.92	2413
hn	cos	1		No		

Table 8: Candidate detection functions for Low Platforms. The first one listed was selected for the density model.

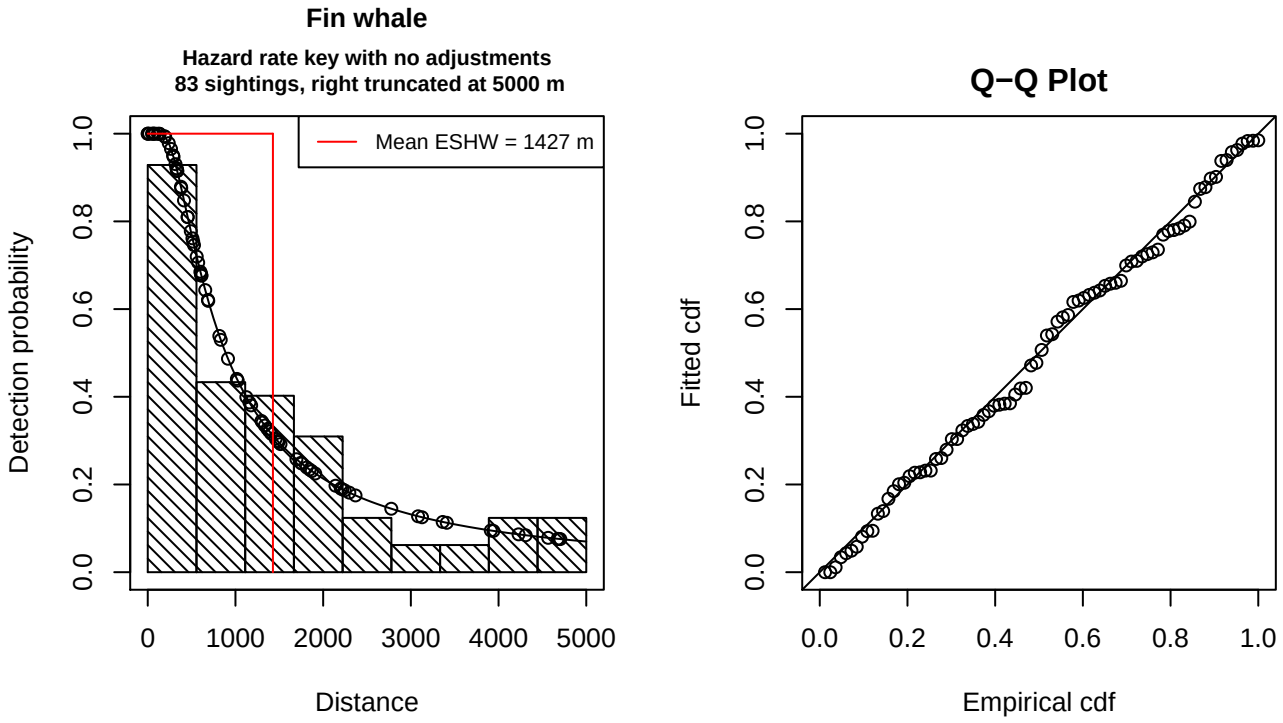

Figure 13: Detection function for Low Platforms that was selected for the density model

Statistical output for this detection function:

```
Summary for ds object
Number of observations :  83
Distance range         :  0  -  5000
AIC                    :  1358.713

Detection function:
 Hazard-rate key function

Detection function parameters
Scale Coefficients:
            estimate        se
(Intercept) 6.508864 0.4148118

Shape parameters:
             estimate        se
(Intercept) 0.2672509 0.2180009

                         Estimate          SE        CV
Average p                0.2854652  0.06275673 0.2198402
N in covered region 290.7534550 69.37901822 0.2386180
```

Additional diagnostic plots:

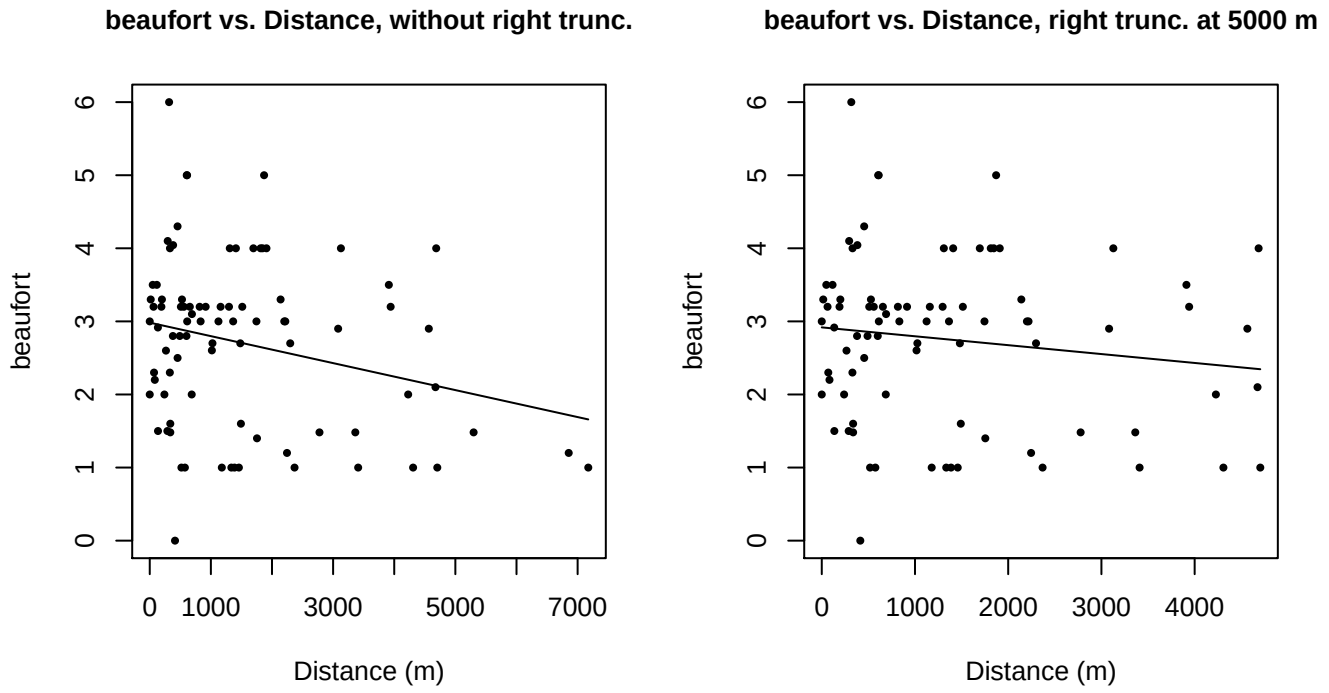

Figure 14: Scatterplots showing the relationship between Beaufort sea state and perpendicular sighting distance, for all sightings (left) and only those not right truncated (right). The line is a simple linear regression.

Naked Eye Surveys

The sightings were right truncated at 2500m.

Covariate	Description

beaufort	Beaufort sea state.
size	Estimated size (number of individuals) of the sighted group.

Table 9: Covariates tested in candidate "multi-covariate distance sampling" (MCDS) detection functions.

Key	Adjustment	Order	Covariates	Succeeded	Δ AIC	Mean ESHW (m)
hr				Yes	0.00	1164
hn			beaufort	Yes	0.62	1111
hn				Yes	0.91	1111
hr			beaufort	Yes	1.52	1182
hr	poly	4		Yes	1.59	1146
hr	poly	2		Yes	2.00	1164
hn			beaufort, size	Yes	2.01	1111
hn	cos	3		Yes	2.20	1205
hn	cos	2		Yes	2.32	1052
hn			size	Yes	2.49	1111
hn	herm	4		Yes	2.77	1108
hn	cos	1		No		
hr			size	No		
hr			beaufort, size	No		

Table 10: Candidate detection functions for Naked Eye Surveys. The first one listed was selected for the density model.

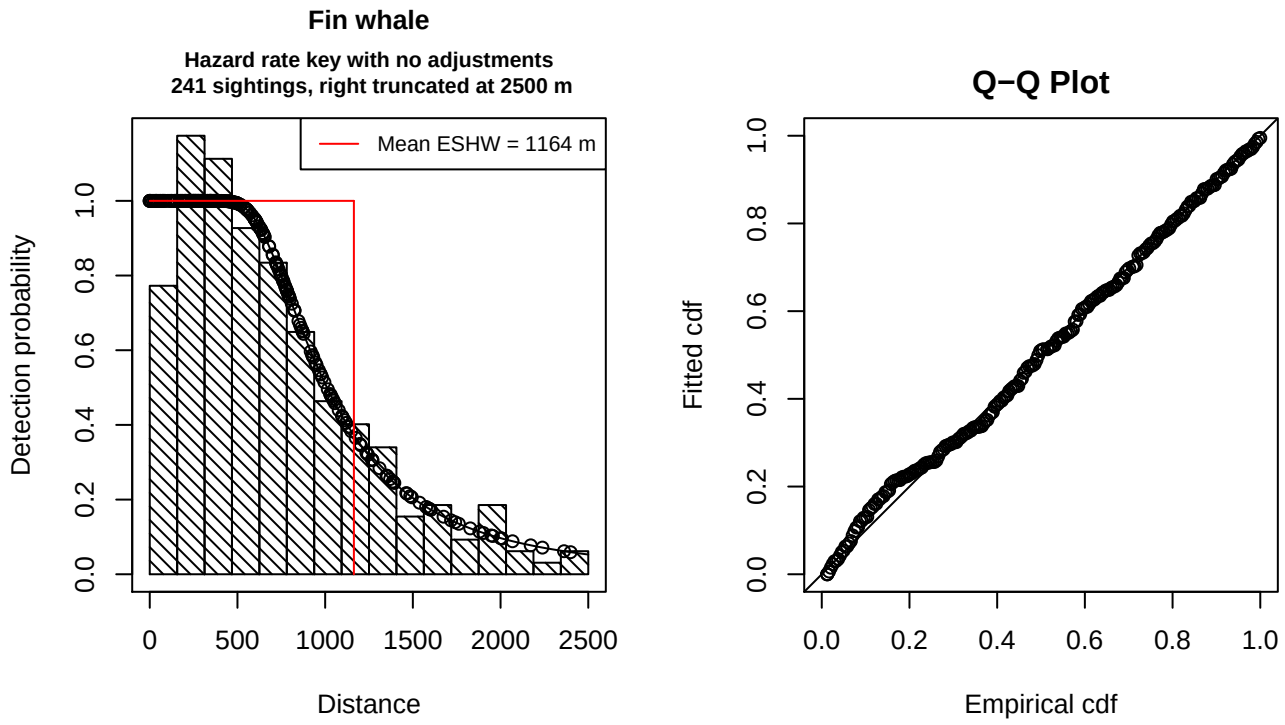

Figure 15: Detection function for Naked Eye Surveys that was selected for the density model

Statistical output for this detection function:

```
Summary for ds object
Number of observations :  241
Distance range         :  0  -  2500
AIC                    :  3611.718

Detection function:
 Hazard-rate key function

Detection function parameters
Scale Coefficients:
            estimate         se
(Intercept) 6.787624 0.09771699

Shape parameters:
            estimate        se
(Intercept) 1.033049 0.1546577

                       Estimate          SE         CV
Average p              0.4655164  0.02961268 0.06361254
N in covered region 517.7045964 40.97503174 0.07914751
```

Additional diagnostic plots:

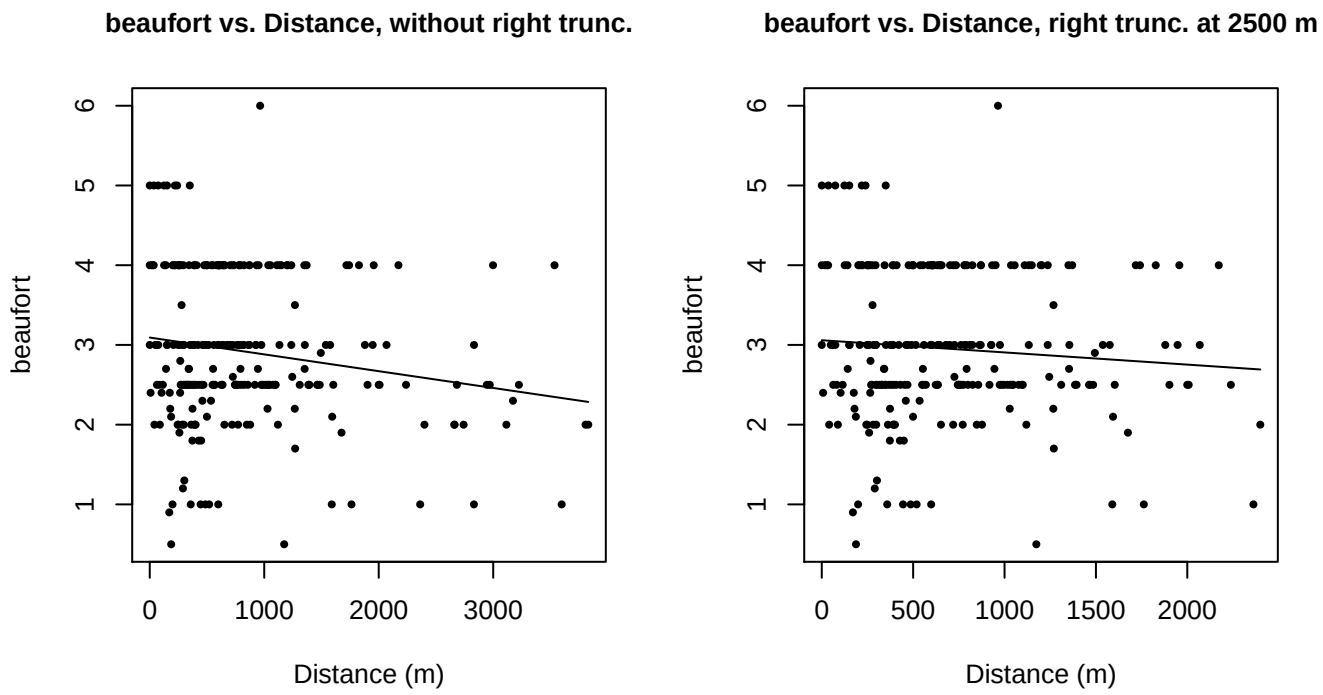

Figure 16: Scatterplots showing the relationship between Beaufort sea state and perpendicular sighting distance, for all sightings (left) and only those not right truncated (right). The line is a simple linear regression.

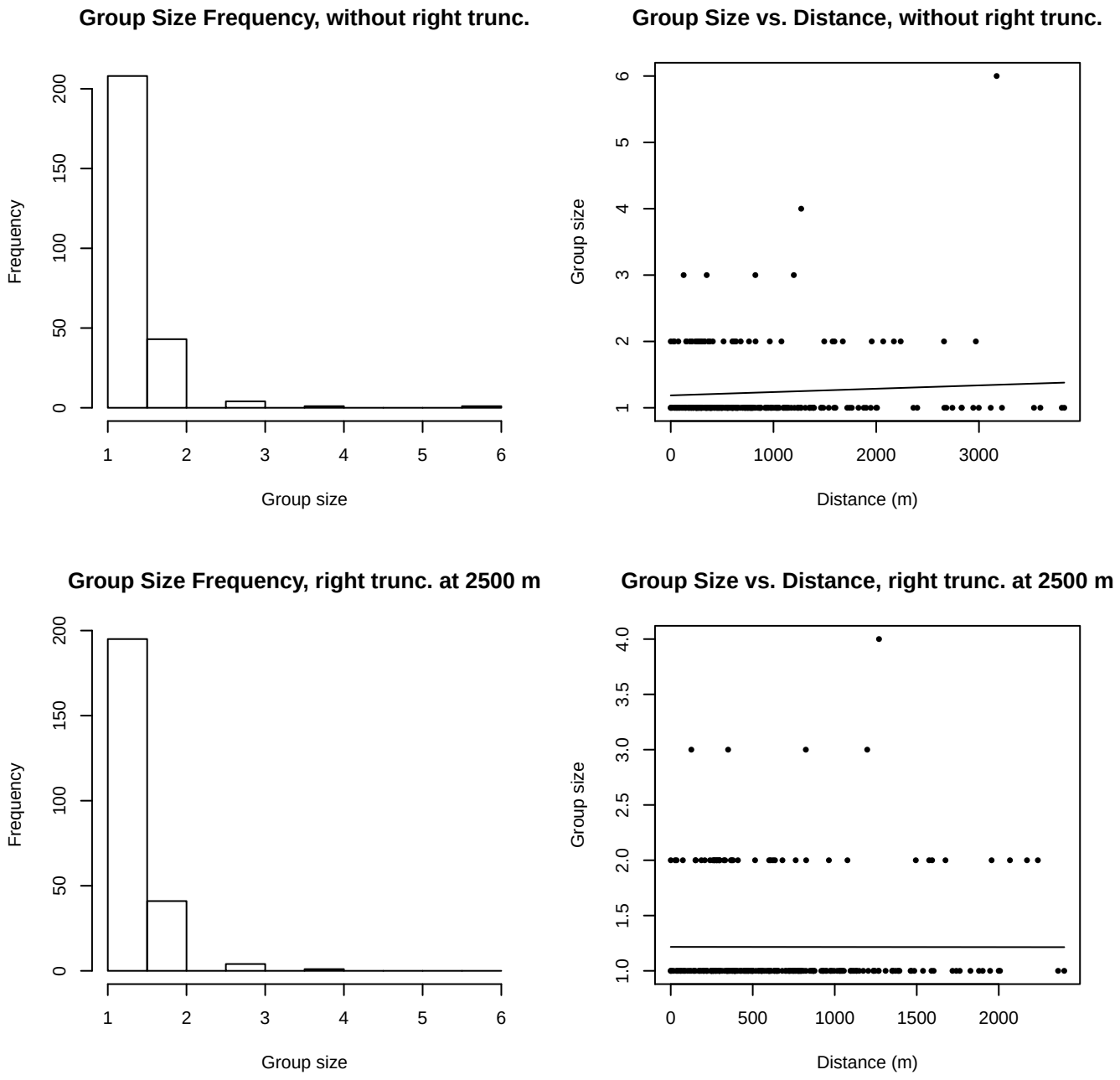

Figure 17: Histograms showing group size frequency and scatterplots showing the relationship between group size and perpendicular sighting distance, for all sightings (top row) and only those not right truncated (bottom row). In the scatterplot, the line is a simple linear regression.

NEFSC Abel-J Naked Eye Surveys

The sightings were right truncated at 3000m.

Covariate	Description
beaufort	Beaufort sea state.
quality	Survey-specific index of the quality of observation conditions, utilizing relevant factors other than Beaufort sea state (see methods).

Table 11: Covariates tested in candidate "multi-covariate distance sampling" (MCDS) detection functions.

Key	Adjustment	Order	Covariates	Succeeded	Δ AIC	Mean ESHW (m)
hn	cos	3		Yes	0.00	875
hr				Yes	0.52	957
hr	poly	4		Yes	1.64	970
hn	cos	2		Yes	2.15	1041
hn				Yes	2.41	1225
hr	poly	2		Yes	2.52	957
hn	herm	4		Yes	4.36	1222
hn			quality	Yes	4.40	1225
hn	cos	1		No		
hr			beaufort	No		
hn			beaufort	No		
hr			quality	No		
hr			beaufort, quality	No		
hn			beaufort, quality	No		

Table 12: Candidate detection functions for NEFSC Abel-J Naked Eye Surveys. The first one listed was selected for the density model.

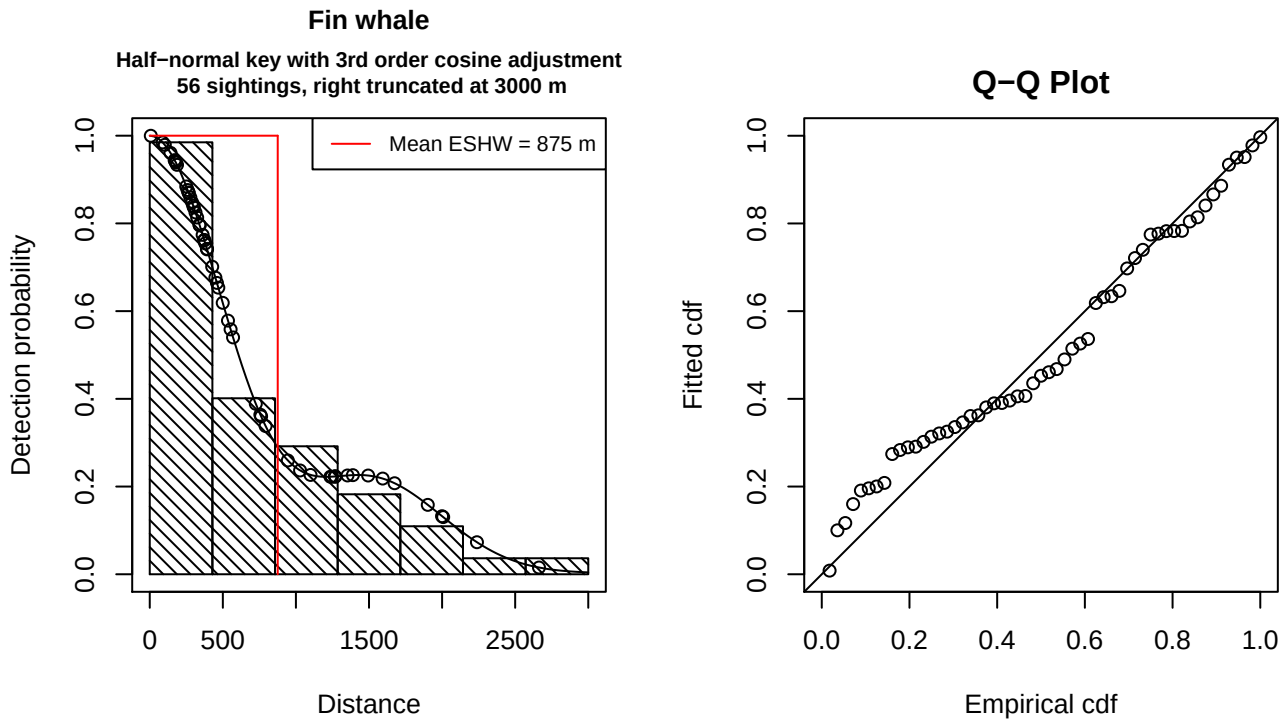

Figure 18: Detection function for NEFSC Abel-J Naked Eye Surveys that was selected for the density model

Statistical output for this detection function:

```
Summary for ds object
Number of observations :  56
Distance range         :  0  -  3000
AIC                    :  850.7126

Detection function:
 Half-normal key function with cosine adjustment term of order 3

Detection function parameters
Scale Coefficients:
            estimate         se
(Intercept)  6.90227 0.09299626

Adjustment term parameter(s):
              estimate        se
cos, order 3 0.4255273 0.1928938


Monotonicity constraints were enforced.
                       Estimate          SE        CV
Average p             0.2918325  0.04332918 0.1484728
N in covered region 191.8908987 35.74016771 0.1862525

Monotonicity constraints were enforced.
```

Additional diagnostic plots:

Figure 19: Scatterplots showing the relationship between Beaufort sea state and perpendicular sighting distance, for all sightings (left) and only those not right truncated (right). The line is a simple linear regression.

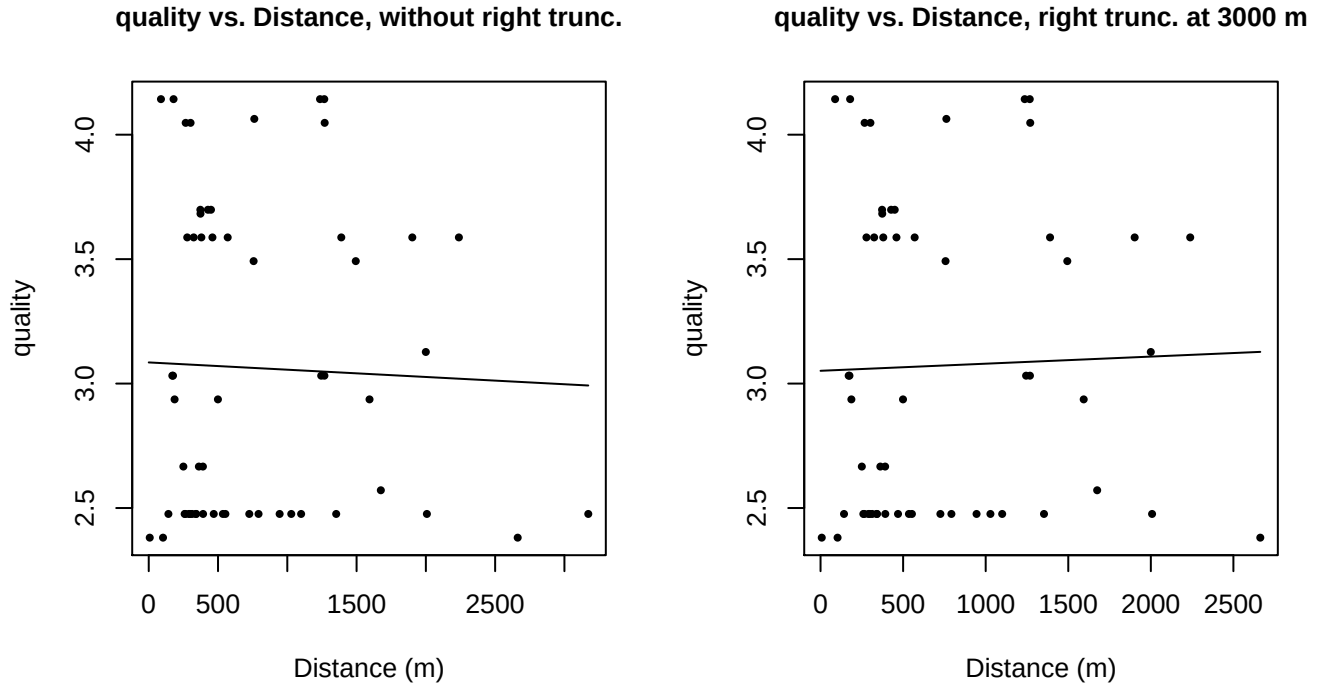

Figure 20: Scatterplots showing the relationship between the survey-specific index of the quality of observation conditions and perpendicular sighting distance, for all sightings (left) and only those not right truncated (right). Low values of the quality index correspond to better observation conditions. The line is a simple linear regression.

CODA and SCANS II

The sightings were right truncated at 2500m.

Covariate	Description
beaufort	Beaufort sea state.
quality	Survey-specific index of the quality of observation conditions, utilizing relevant factors other than Beaufort sea state (see methods).

Table 13: Covariates tested in candidate "multi-covariate distance sampling" (MCDS) detection functions.

Key	Adjustment	Order	Covariates	Succeeded	Δ AIC	Mean ESHW (m)
hr				Yes	0.00	1199
hr			beaufort	Yes	1.82	1197
hn	cos	3		Yes	1.96	1163
hr	poly	2		Yes	2.00	1199
hn				Yes	2.78	1070
hn	cos	2		Yes	4.27	1143
hn	herm	4		Yes	4.75	1070
hn			beaufort	Yes	4.76	1070
hn	cos	1		No		
hr	poly	4		No		
hr			quality	No		
hn			quality	No		
hr			beaufort, quality	No		
hn			beaufort, quality	No		

Table 14: Candidate detection functions for CODA and SCANS II. The first one listed was selected for the density model.

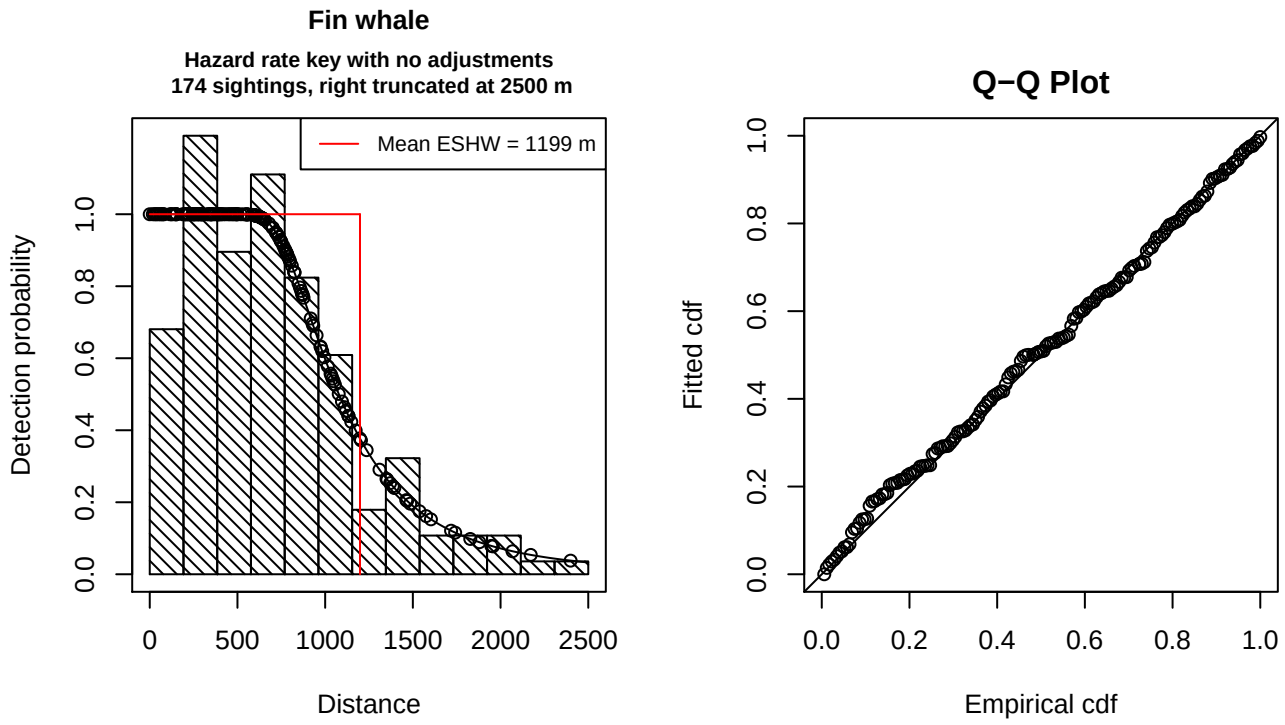

Figure 21: Detection function for CODA and SCANS II that was selected for the density model

Statistical output for this detection function:

```
Summary for ds object
Number of observations :  174
Distance range         :  0  -  2500
AIC                    :  2594.897

Detection function:
 Hazard-rate key function

Detection function parameters
Scale Coefficients:
            estimate         se
(Intercept) 6.881442 0.09192199

Shape parameters:
            estimate        se
(Intercept) 1.283454 0.1771652

                       Estimate          SE         CV
Average p              0.4794734  0.03064825 0.06392065
N in covered region 362.8981110 30.52959253 0.08412717
```

Additional diagnostic plots:

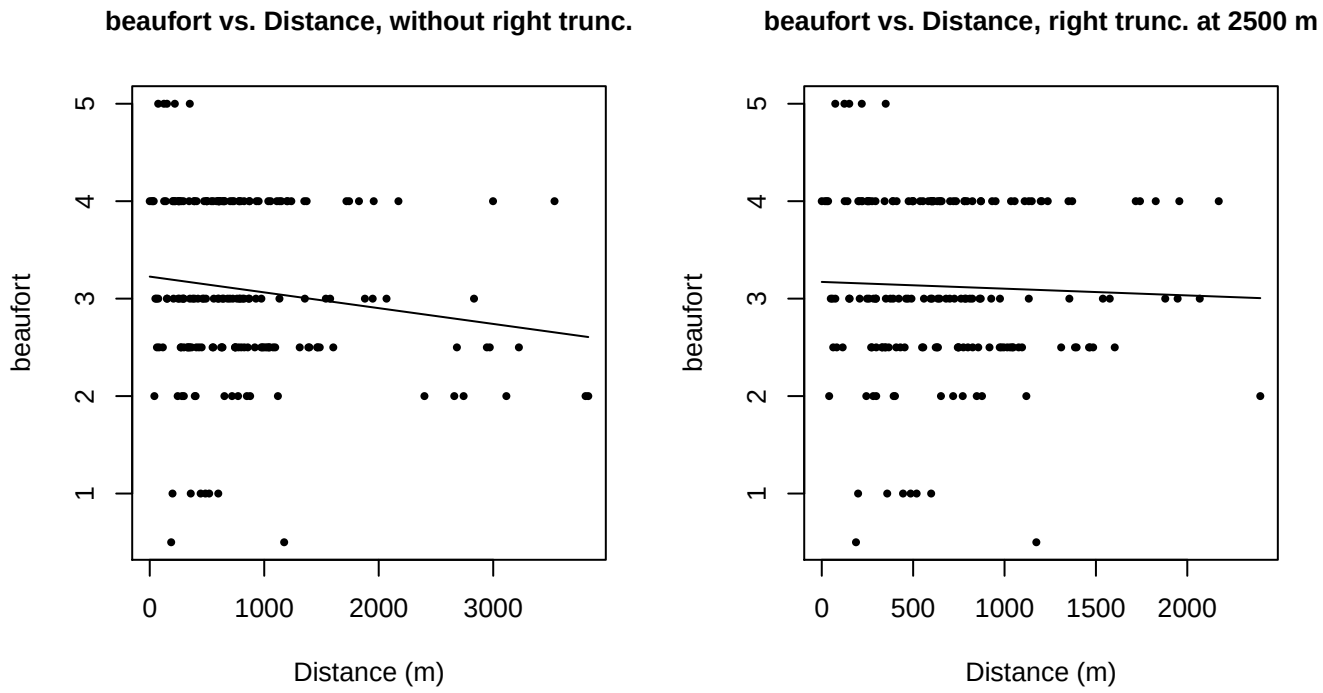

Figure 22: Scatterplots showing the relationship between Beaufort sea state and perpendicular sighting distance, for all sightings (left) and only those not right truncated (right). The line is a simple linear regression.

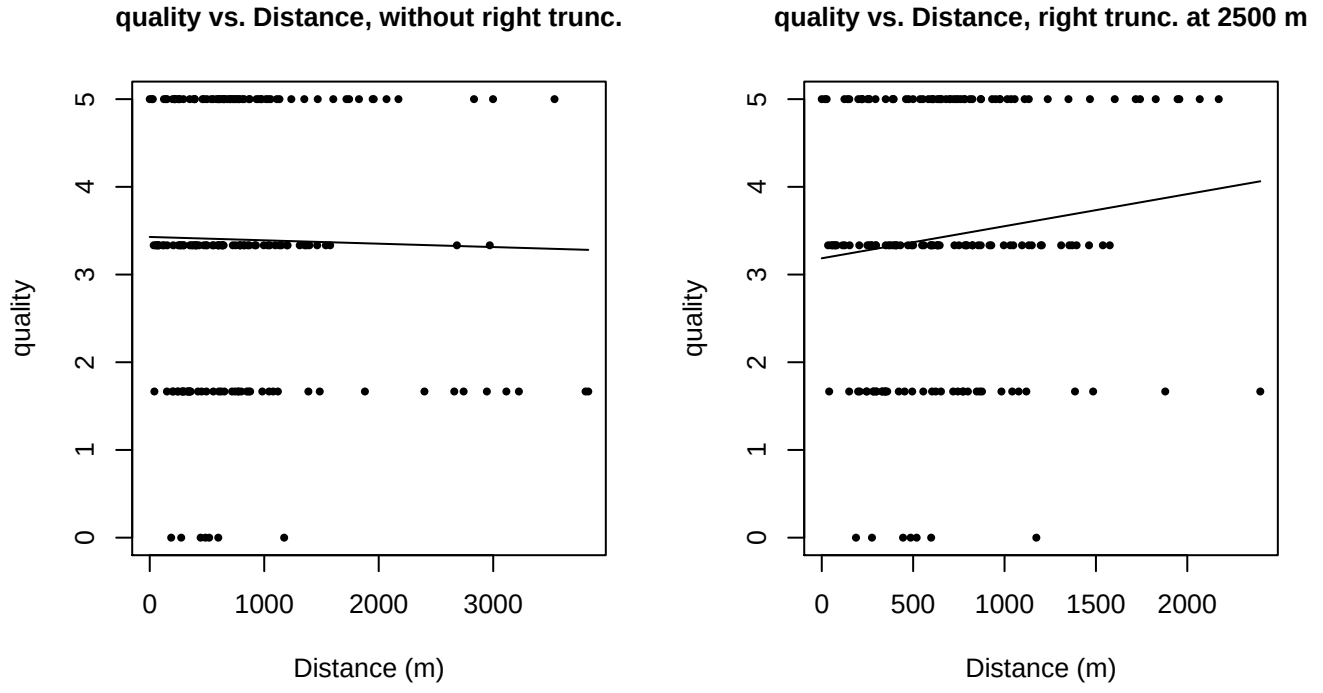

Figure 23: Scatterplots showing the relationship between the survey-specific index of the quality of observation conditions and perpendicular sighting distance, for all sightings (left) and only those not right truncated (right). Low values of the quality index correspond to better observation conditions. The line is a simple linear regression.

CODA

The sightings were right truncated at 2500m.

Covariate	Description
beaufort	Beaufort sea state.
quality	Survey-specific index of the quality of observation conditions, utilizing relevant factors other than Beaufort sea state (see methods).
vessel	Vessel from which the observation was made. This covariate allows the detection function to account for vessel-specific biases, such as the height of the survey platform.

Table 15: Covariates tested in candidate "multi-covariate distance sampling" (MCDS) detection functions.

Key	Adjustment	Order	Covariates	Succeeded	Δ AIC	Mean ESHW (m)
hr			vessel	Yes	0.00	1224
hn			vessel	Yes	0.93	1063
hn			beaufort, vessel	Yes	2.92	1064
hr				Yes	13.13	1212
hr			beaufort	Yes	15.05	1211
hr	poly	4		Yes	15.13	1212
hr	poly	2		Yes	15.13	1212
hn	cos	3		Yes	15.17	1171
hn				Yes	16.02	1078
hn	cos	2		Yes	17.34	1166
hn	herm	4		Yes	17.91	1129
hn			beaufort	Yes	18.02	1078
hn	cos	1		No		
hr			quality	No		
hn			quality	No		
hr			beaufort, quality	No		
hn			beaufort, quality	No		
hr			beaufort, vessel	No		
hr			quality, vessel	No		
hn			quality, vessel	No		
hr			beaufort, quality, vessel	No		
hn			beaufort, quality, vessel	No		

Table 16: Candidate detection functions for CODA. The first one listed was selected for the density model.

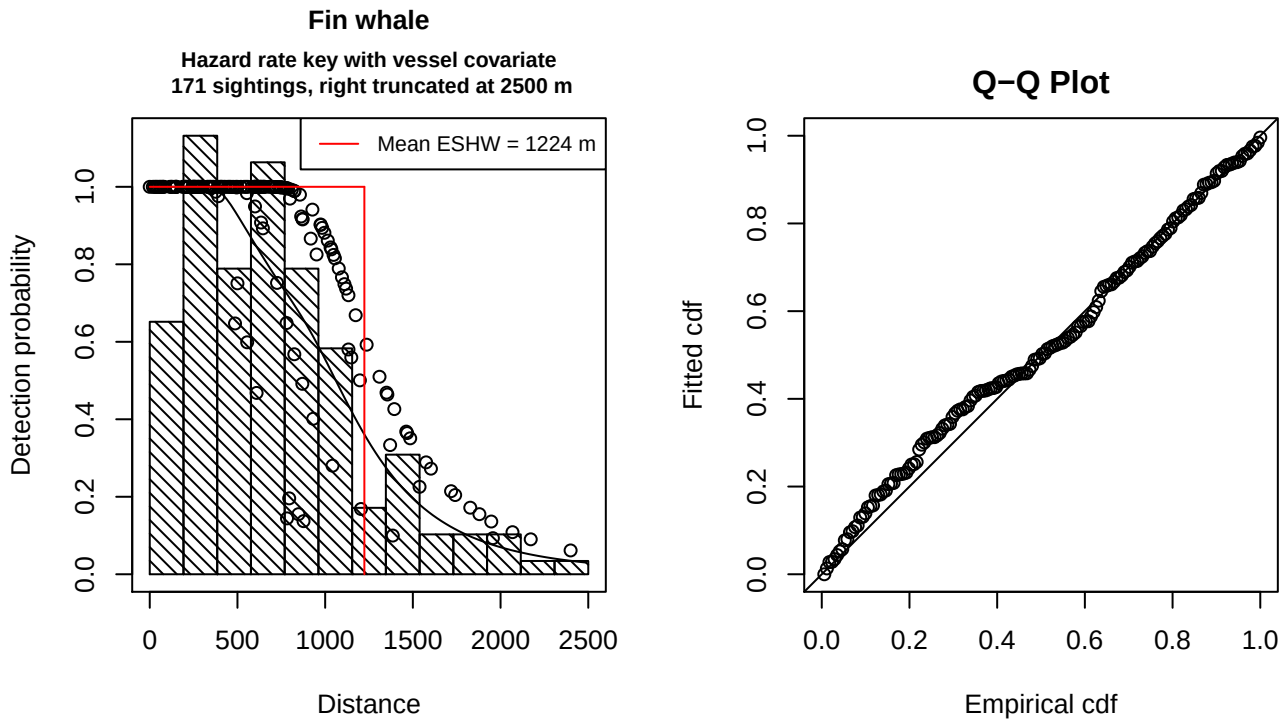

Figure 24: Detection function for CODA that was selected for the density model

Statistical output for this detection function:

```
Summary for ds object
Number of observations :  171
Distance range         :  0  -  2500
AIC                    :  2539.201

Detection function:
 Hazard-rate key function

Detection function parameters
Scale Coefficients:
                     estimate        se
(Intercept)         7.09305901 0.1036583
vesselGerminal     -0.09607018 0.1742353
vesselInvestigador -0.42257998 0.1645327
vesselMars Chaser  -0.89591669 0.2901733
vesselRari         -0.79600484 0.1784771

Shape parameters:
            estimate        se
(Intercept) 1.384925 0.2114039

                       Estimate          SE         CV
Average p             0.4511392  0.02913001 0.06456988
N in covered region 379.0404360 33.05029595 0.08719464
```

Additional diagnostic plots:

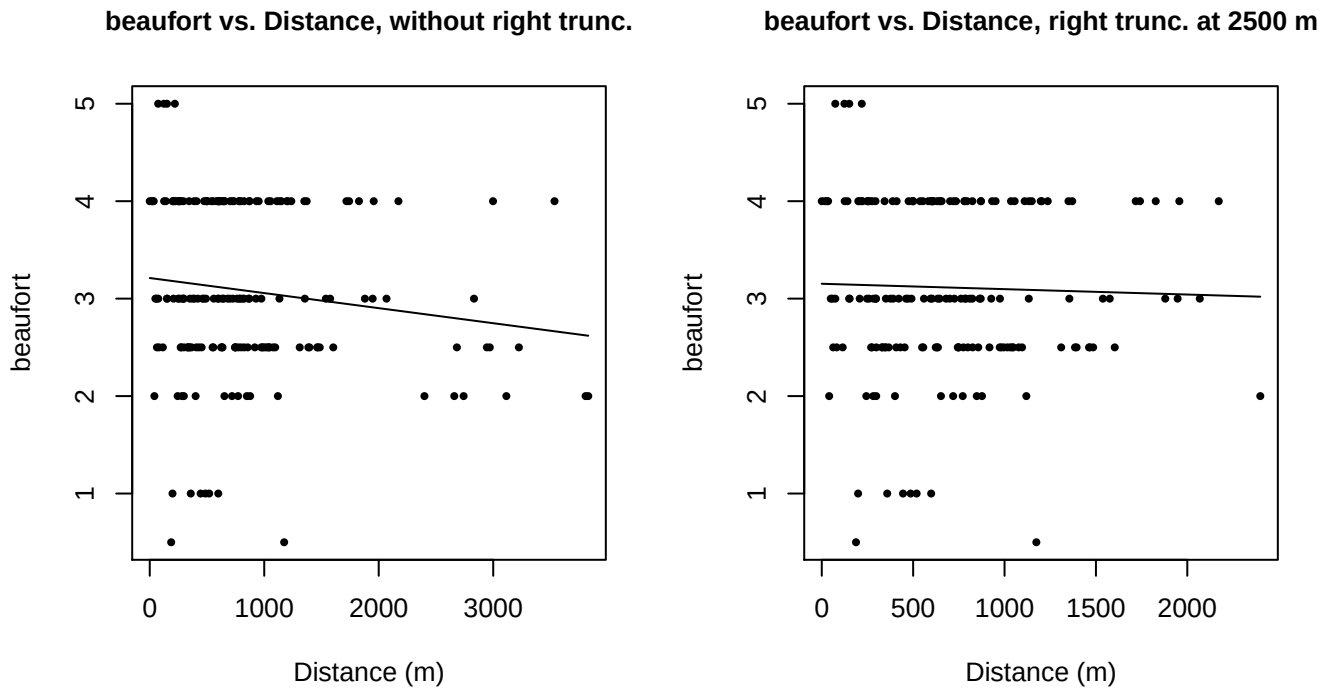

Figure 25: Scatterplots showing the relationship between Beaufort sea state and perpendicular sighting distance, for all sightings (left) and only those not right truncated (right). The line is a simple linear regression.

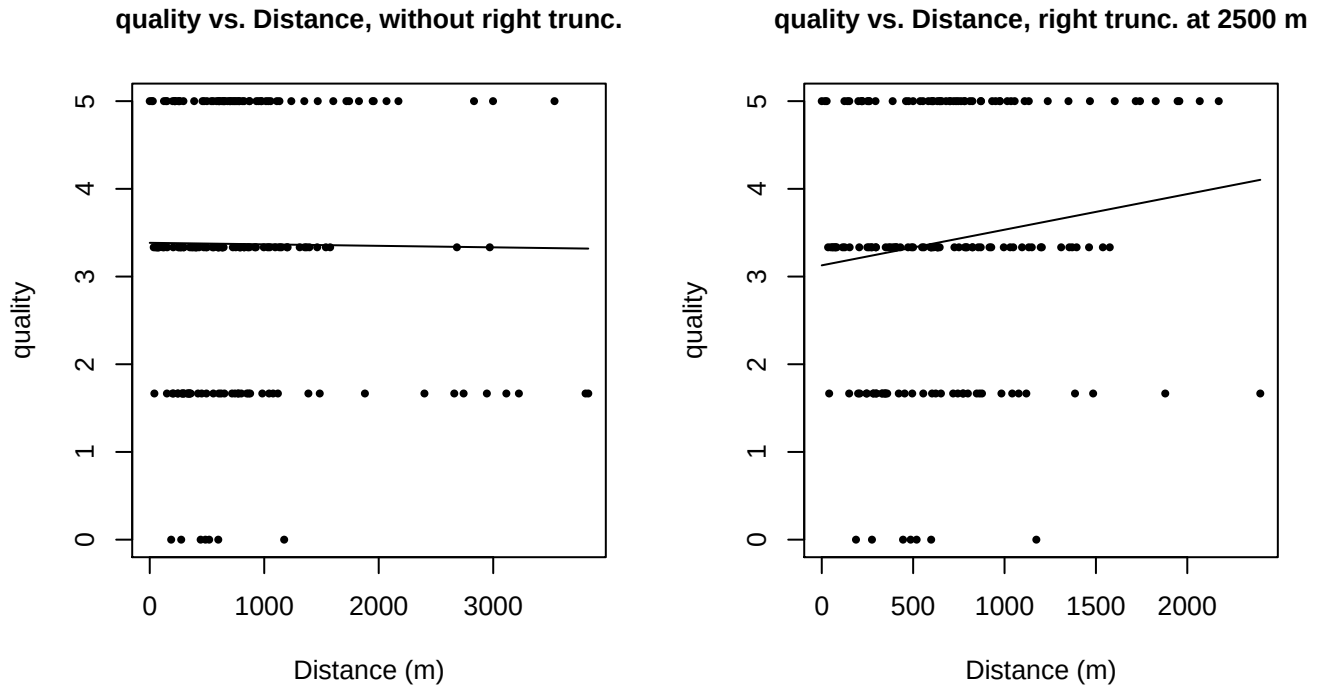

Figure 26: Scatterplots showing the relationship between the survey-specific index of the quality of observation conditions and perpendicular sighting distance, for all sightings (left) and only those not right truncated (right). Low values of the quality index correspond to better observation conditions. The line is a simple linear regression.

Aerial Surveys

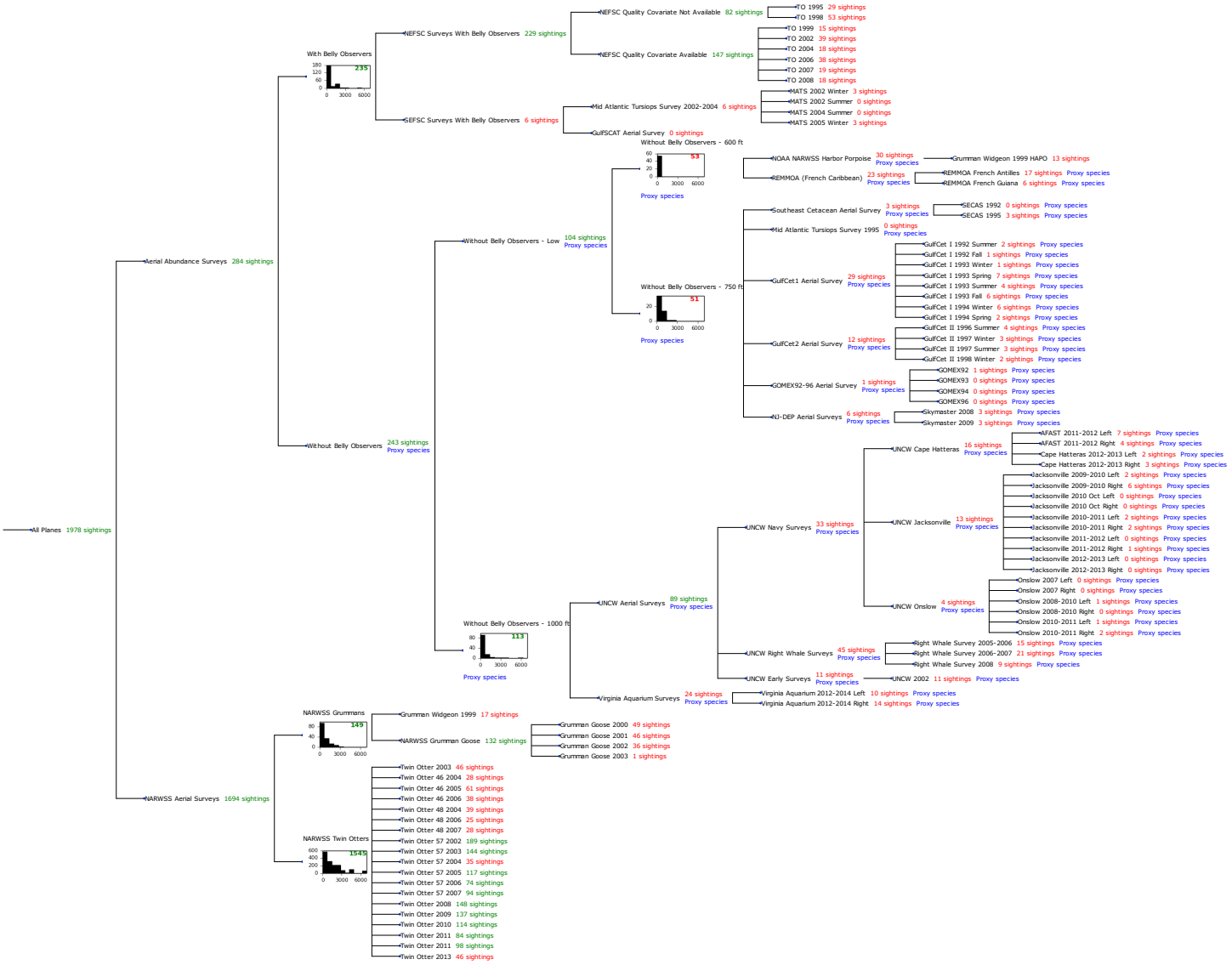

Figure 27: Detection hierarchy for aerial surveys

With Belly Observers

The sightings were right truncated at 1000m.

Covariate	Description
beaufort	Beaufort sea state.
size	Estimated size (number of individuals) of the sighted group.

Table 17: Covariates tested in candidate “multi-covariate distance sampling” (MCDS) detection functions.

Key	Adjustment	Order	Covariates	Succeeded	Δ AIC	Mean ESHW (m)
hn				Yes	0.00	474

hn	cos	3		Yes	1.22	436
hn	herm	4		Yes	1.79	485
hn			size	Yes	1.94	474
hn	cos	2		Yes	1.99	470
hr	poly	2		Yes	2.06	453
hr	poly	4		Yes	4.09	422
hr				Yes	6.16	525
hr			size	Yes	8.15	525
hn			beaufort	No		
hr			beaufort	No		
hn			beaufort, size	No		
hr			beaufort, size	No		

Table 18: Candidate detection functions for With Belly Observers. The first one listed was selected for the density model.

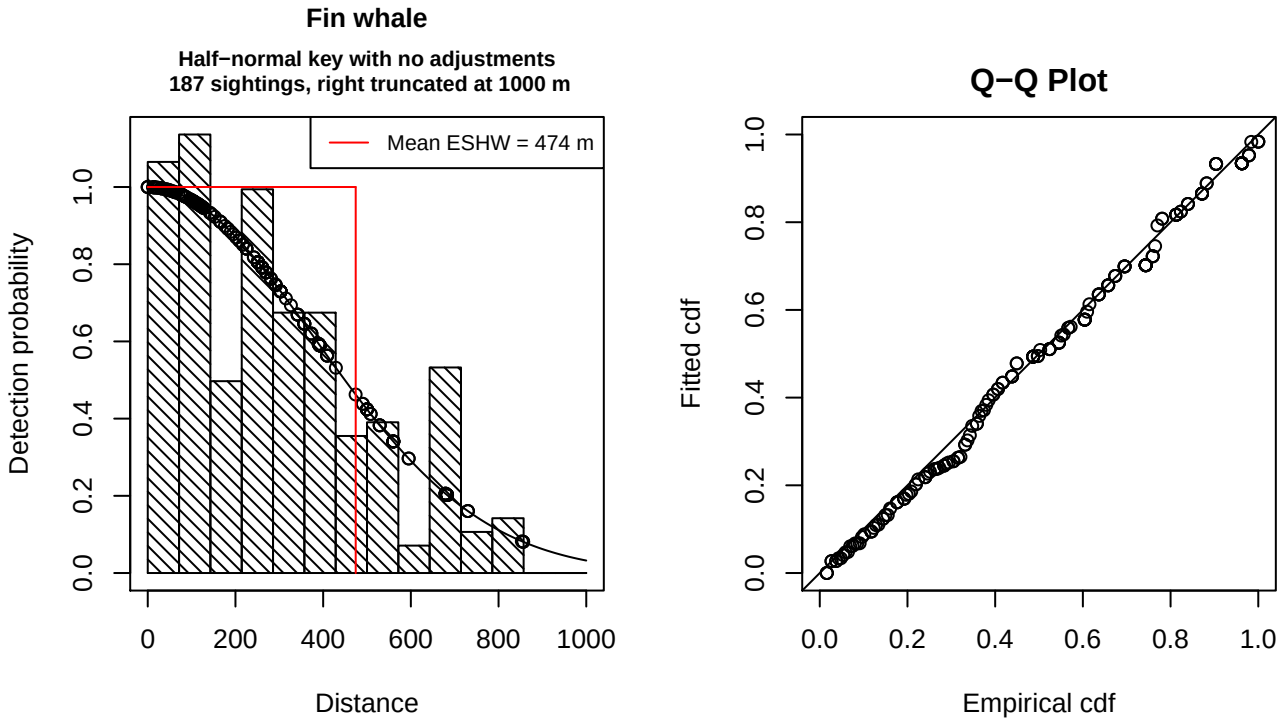

Figure 28: Detection function for With Belly Observers that was selected for the density model

Statistical output for this detection function:

```
Summary for ds object
Number of observations :  187
Distance range         :  0  -  1000
AIC                    :  2480.693
```

```
Detection function:
 Half-normal key function

Detection function parameters
Scale Coefficients:
            estimate         se
(Intercept) 5.944659 0.06291675

                        Estimate          SE         CV
Average p               0.4741924  0.02780043 0.05862690
N in covered region 394.3547098 31.17378165 0.07905011
```

Additional diagnostic plots:

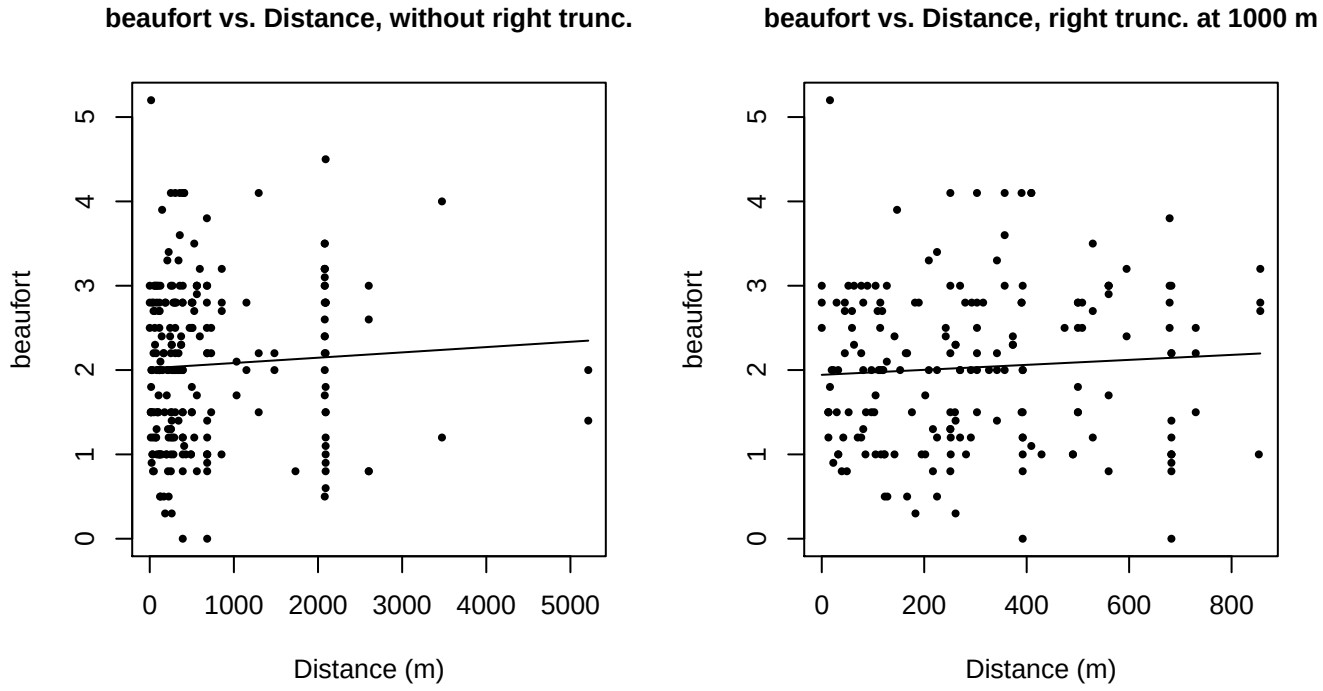

Figure 29: Scatterplots showing the relationship between Beaufort sea state and perpendicular sighting distance, for all sightings (left) and only those not right truncated (right). The line is a simple linear regression.

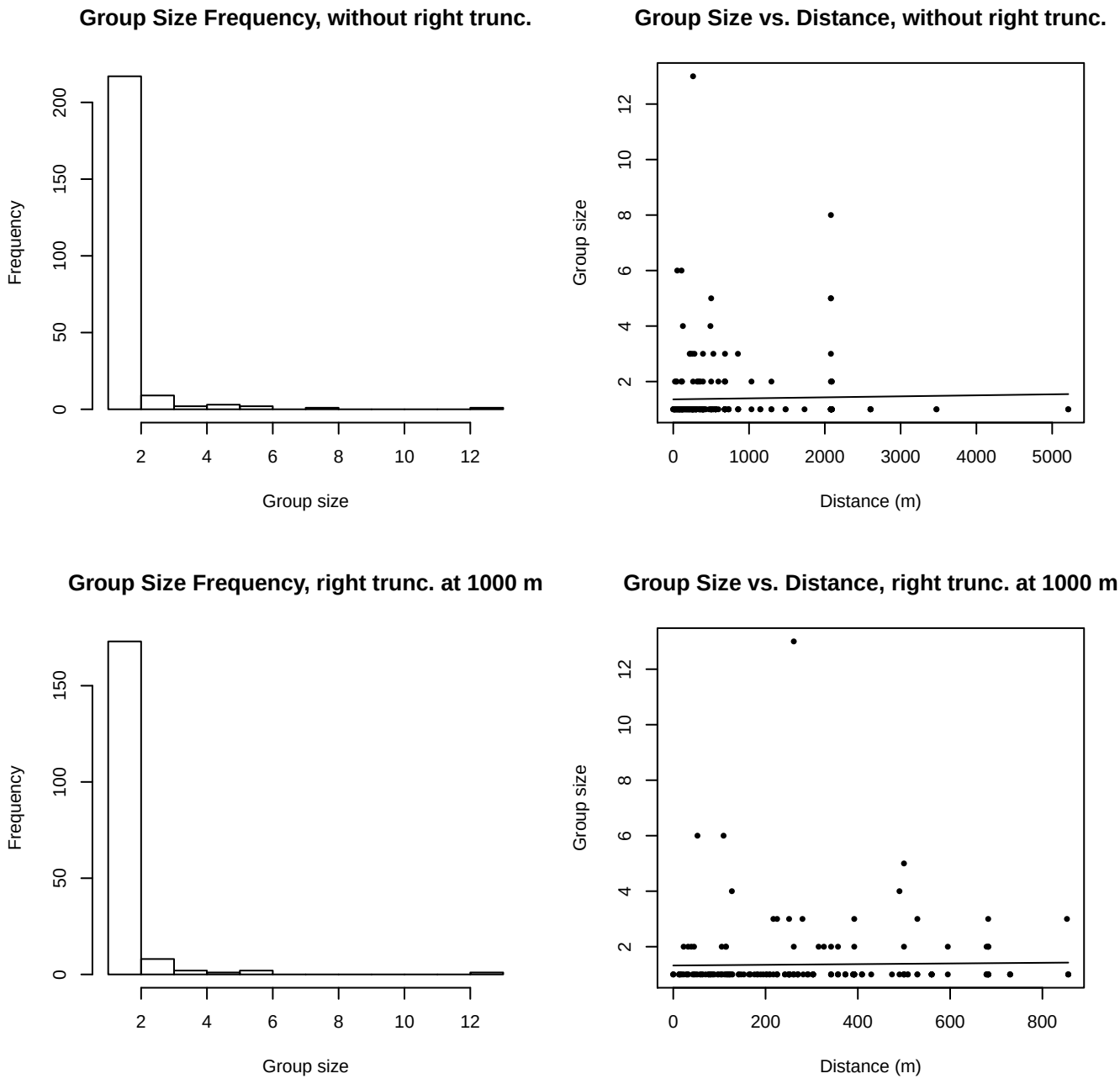

Figure 30: Histograms showing group size frequency and scatterplots showing the relationship between group size and perpendicular sighting distance, for all sightings (top row) and only those not right truncated (bottom row). In the scatterplot, the line is a simple linear regression.

Without Belly Observers - 600 ft

Because this taxon was sighted too infrequently to fit a detection function to its sightings alone, we fit a detection function to the pooled sightings of several other species that we believed would exhibit similar detectability. These "proxy species" are listed below.

Reported By Observer	Common Name	n
Balaenoptera	Balaenopterid sp.	2
Balaenoptera acutorostrata	Minke whale	8

Balaenoptera borealis	Sei whale	0
Balaenoptera borealis/edeni	Sei or Bryde's whale	0
Balaenoptera borealis/physalus	Fin or Sei whale	0
Balaenoptera edeni	Bryde's whale	0
Balaenoptera musculus	Blue whale	0
Balaenoptera physalus	Fin whale	15
Eubalaena glacialis	North Atlantic right whale	2
Eubalaena glacialis/Megaptera novaeangliae	Right or humpback whale	0
Megaptera novaeangliae	Humpback whale	16
Physeter macrocephalus	Sperm whale	10
Total		53

Table 19: Proxy species used to fit detection functions for Without Belly Observers - 600 ft. The number of sightings, n, is before truncation.

The sightings were right truncated at 600m. Due to a reduced frequency of sightings close to the trackline that plausibly resulted from the behavior of the observers and/or the configuration of the survey platform, the sightings were left truncted as well. Sightings closer than 32 m to the trackline were omitted from the analysis, and it was assumed that the the area closer to the trackline than this was not surveyed. This distance was estimated by inspecting histograms of perpendicular sighting distances.

Covariate	Description
beaufort	Beaufort sea state.
size	Estimated size (number of individuals) of the sighted group.

Table 20: Covariates tested in candidate "multi-covariate distance sampling" (MCDS) detection functions.

Key	Adjustment	Order	Covariates	Succeeded	Δ AIC	Mean ESHW (m)
hn				Yes	0.00	293
hr				Yes	1.14	318
hn			beaufort	Yes	1.57	293
hn	cos	3		Yes	1.65	311
hn	herm	4		Yes	1.93	291
hr			beaufort	Yes	1.97	326
hn	cos	2		Yes	1.97	283
hr	poly	2		Yes	3.14	318
hr	poly	4		Yes	3.14	318
hn			size	No		
hr			size	No		
hn			beaufort, size	No		
hr			beaufort, size	No		

Table 21: Candidate detection functions for Without Belly Observers - 600 ft. The first one listed was selected for the density model.

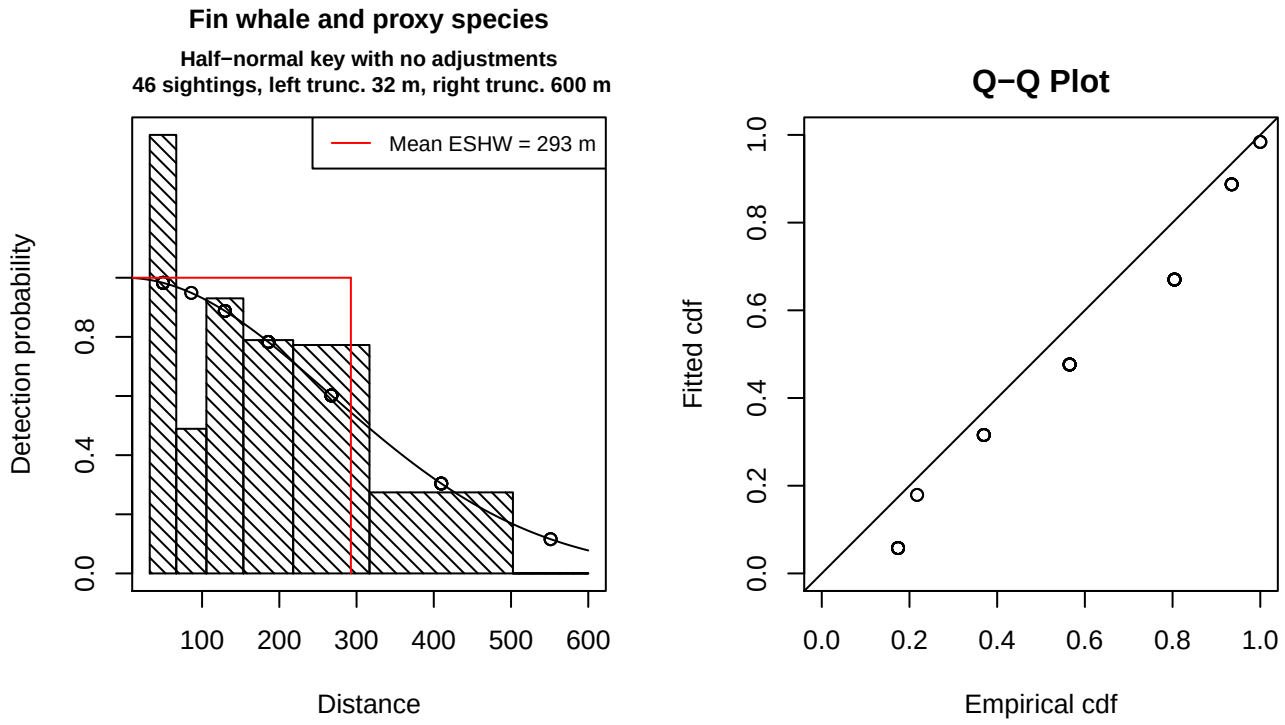

Figure 31: Detection function for Without Belly Observers - 600 ft that was selected for the density model

Statistical output for this detection function:

```
Summary for ds object
Number of observations :  46
Distance range         :  32.24668  -  600
AIC                    :  177.4011

Detection function:
 Half-normal key function

Detection function parameters
Scale Coefficients:
            estimate        se
(Intercept) 5.581559 0.1339955

                     Estimate          SE        CV
Average p            0.487738  0.06208134 0.1272842
N in covered region 94.312922 15.59372100 0.1653402
```

Additional diagnostic plots:

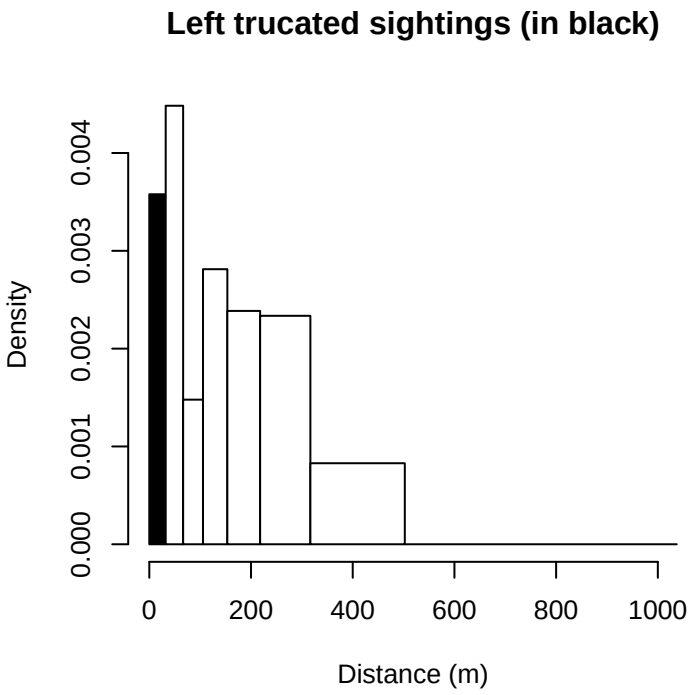

Figure 32: Density of sightings by perpendicular distance for Without Belly Observers - 600 ft. Black bars on the left show sightings that were left truncated.

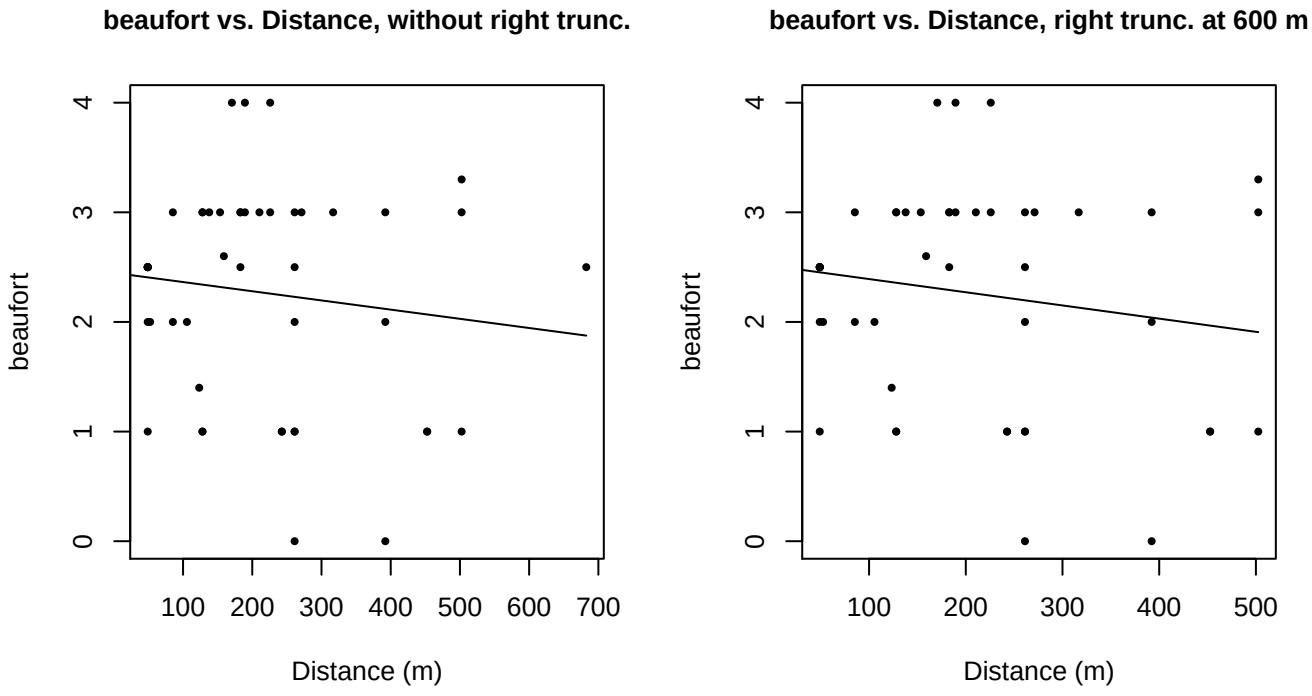

Figure 33: Scatterplots showing the relationship between Beaufort sea state and perpendicular sighting distance, for all sightings (left) and only those not right truncated (right). The line is a simple linear regression.

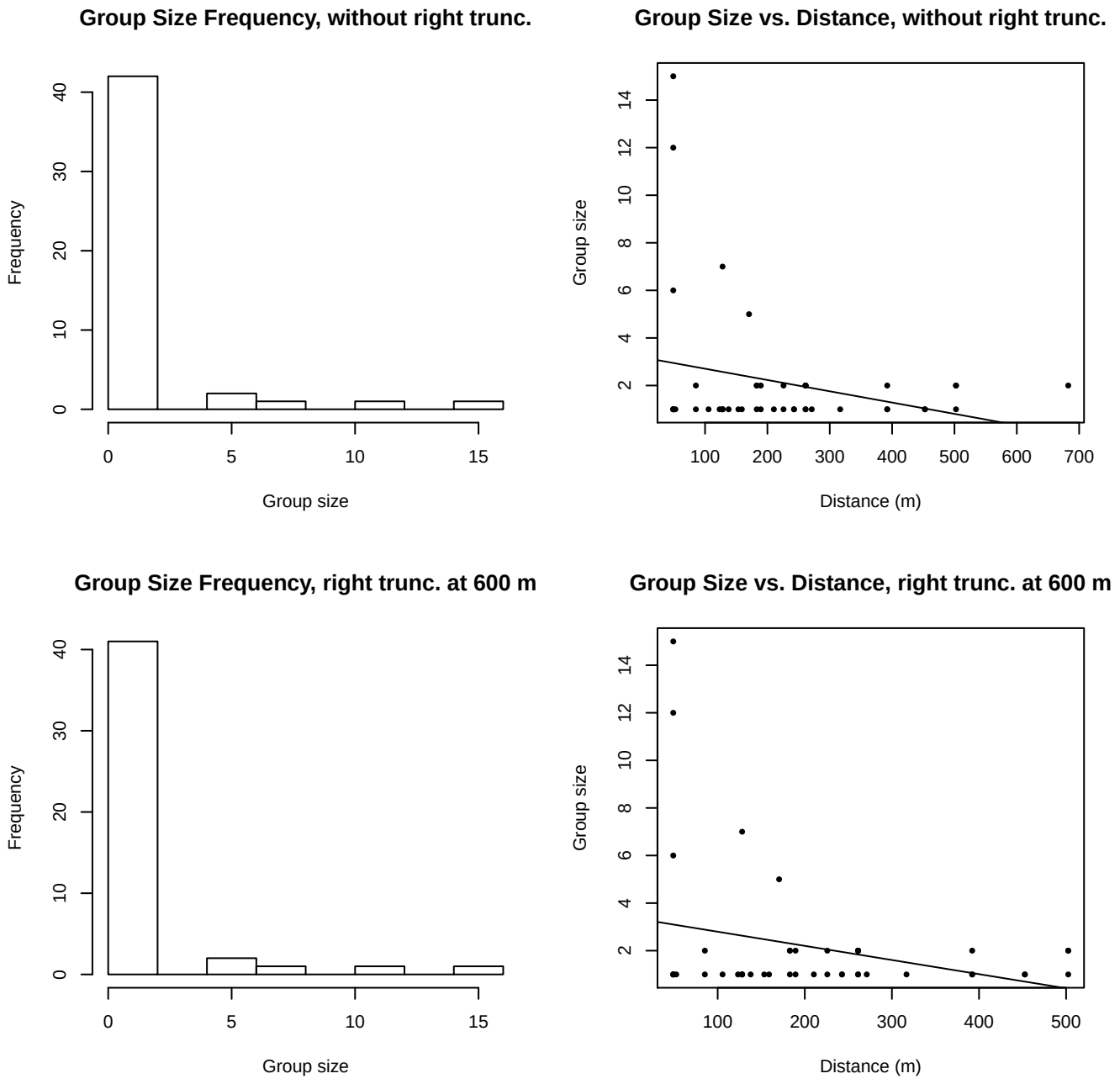

Figure 34: Histograms showing group size frequency and scatterplots showing the relationship between group size and perpendicular sighting distance, for all sightings (top row) and only those not right truncated (bottom row). In the scatterplot, the line is a simple linear regression.

Without Belly Observers - 750 ft

Because this taxon was sighted too infrequently to fit a detection function to its sightings alone, we fit a detection function to the pooled sightings of several other species that we believed would exhibit similar detectability. These "proxy species" are listed below.

Reported By Observer	Common Name	n
Balaenoptera	Balaenopterid sp.	1
Balaenoptera acutorostrata	Minke whale	0

Balaenoptera borealis	Sei whale	0
Balaenoptera borealis/edeni	Sei or Bryde's whale	2
Balaenoptera borealis/physalus	Fin or Sei whale	0
Balaenoptera edeni	Bryde's whale	3
Balaenoptera musculus	Blue whale	0
Balaenoptera physalus	Fin whale	2
Eubalaena glacialis	North Atlantic right whale	0
Eubalaena glacialis/Megaptera novaeangliae	Right or humpback whale	0
Megaptera novaeangliae	Humpback whale	6
Physeter macrocephalus	Sperm whale	37
Total		51

Table 22: Proxy species used to fit detection functions for Without Belly Observers - 750 ft. The number of sightings, n, is before truncation.

The sightings were right truncated at 600m. Due to a reduced frequency of sightings close to the trackline that plausibly resulted from the behavior of the observers and/or the configuration of the survey platform, the sightings were left truncted as well. Sightings closer than 40 m to the trackline were omitted from the analysis, and it was assumed that the the area closer to the trackline than this was not surveyed. This distance was estimated by inspecting histograms of perpendicular sighting distances. The vertical sighting angles were heaped at 10 degree increments, so the candidate detection functions were fitted using linear bins scaled accordingly.

Key	Adjustment	Order	Covariates	Succeeded	Δ AIC	Mean ESHW (m)
hn	cos	2		Yes	0.00	216
hr				Yes	0.59	251
hn	cos	3		Yes	2.31	255
hn	herm	4		Yes	2.46	316
hr	poly	2		Yes	2.59	251
hr	poly	4		Yes	2.60	257
hn				No		

Table 23: Candidate detection functions for Without Belly Observers - 750 ft. The first one listed was selected for the density model.

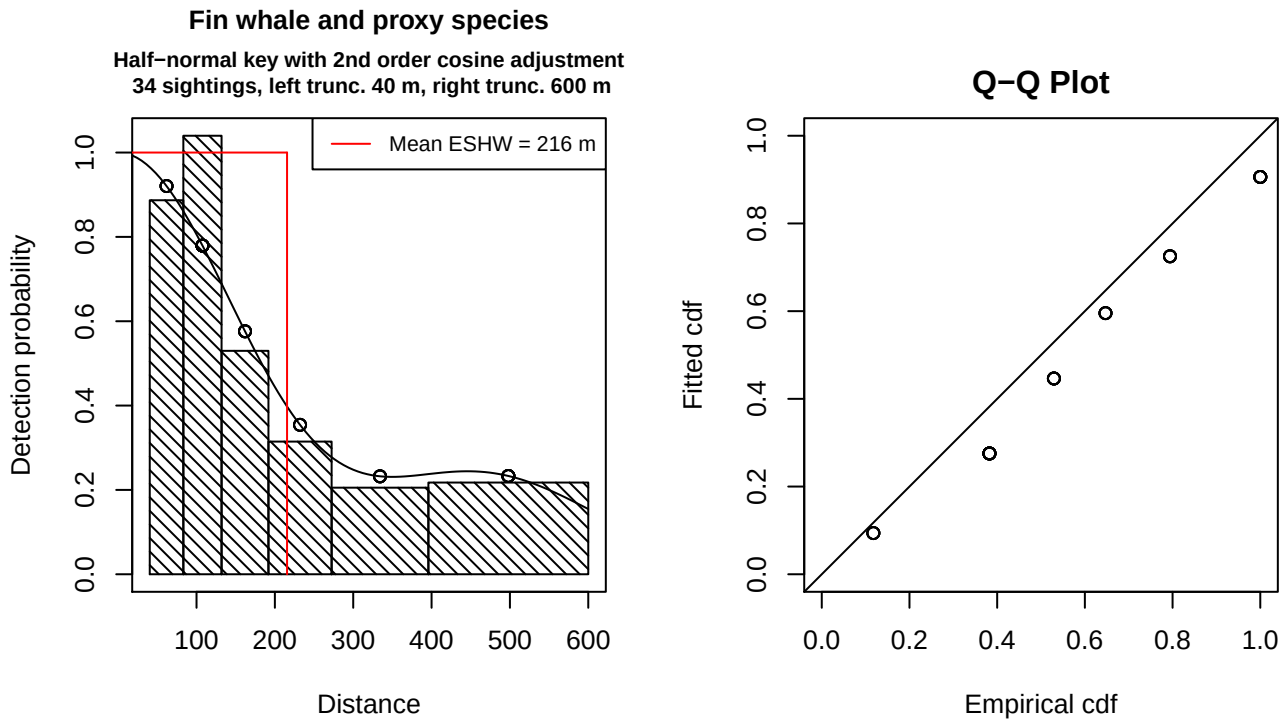

Figure 35: Detection function for Without Belly Observers - 750 ft that was selected for the density model

Statistical output for this detection function:

```
Summary for ds object
Number of observations :  34
Distance range         :  40.30835  -  600
AIC                    :  124.984

Detection function:
 Half-normal key function with cosine adjustment term of order 2

Detection function parameters
Scale Coefficients:
            estimate       se
(Intercept) 5.738324 0.1838281

Adjustment term parameter(s):
              estimate       se
cos, order 2 0.4333816 0.242253


Monotonicity constraints were enforced.
                     Estimate         SE        CV
Average p            0.3592781  0.0870934 0.2424122
N in covered region 94.6341993 26.3634683 0.2785829

Monotonicity constraints were enforced.
```

Additional diagnostic plots:

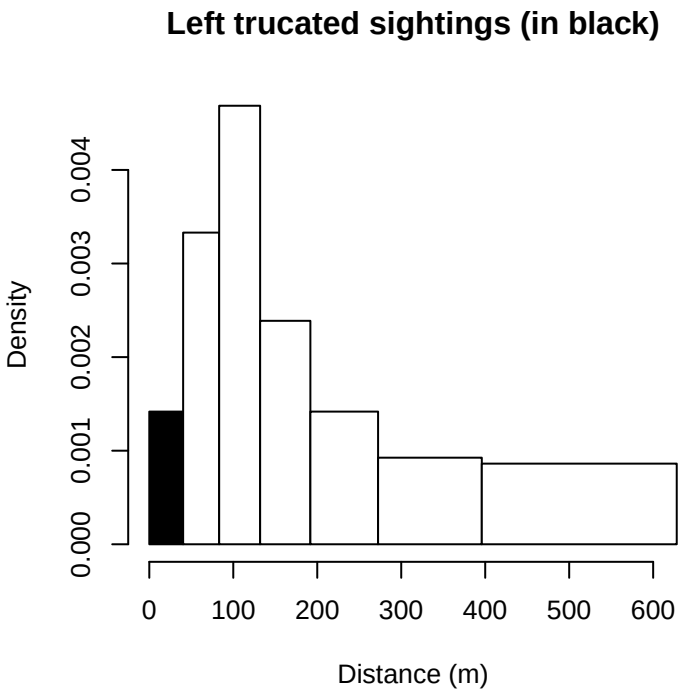

Figure 36: Density of sightings by perpendicular distance for Without Belly Observers - 750 ft. Black bars on the left show sightings that were left truncated.

Without Belly Observers - 1000 ft

Because this taxon was sighted too infrequently to fit a detection function to its sightings alone, we fit a detection function to the pooled sightings of several other species that we believed would exhibit similar detectability. These "proxy species" are listed below.

Reported By Observer	Common Name	n
Balaenoptera	Balaenopterid sp.	1
Balaenoptera acutorostrata	Minke whale	16
Balaenoptera borealis	Sei whale	0
Balaenoptera borealis/edeni	Sei or Bryde's whale	0
Balaenoptera borealis/physalus	Fin or Sei whale	0
Balaenoptera edeni	Bryde's whale	0
Balaenoptera musculus	Blue whale	0
Balaenoptera physalus	Fin whale	32
Eubalaena glacialis	North Atlantic right whale	34
Eubalaena glacialis/Megaptera novaeangliae	Right or humpback whale	0
Megaptera novaeangliae	Humpback whale	30
Total		113

Table 24: Proxy species used to fit detection functions for Without Belly Observers - 1000 ft. The number of sightings, n, is before truncation.

The sightings were right truncated at 1500m.

Covariate	Description
beaufort	Beaufort sea state.
quality	Survey-specific index of the quality of observation conditions, utilizing relevant factors other than Beaufort sea state (see methods).
size	Estimated size (number of individuals) of the sighted group.

Table 25: Covariates tested in candidate "multi-covariate distance sampling" (MCDS) detection functions.

Key	Adjustment	Order	Covariates	Succeeded	Δ AIC	Mean ESHW (m)
hr				Yes	0.00	434
hr	poly	4		Yes	1.58	424
hn	cos	2		Yes	1.71	462
hr	poly	2		Yes	1.92	427
hr			quality	Yes	1.96	433
hn	cos	3		Yes	3.64	418
hn				Yes	11.03	585
hn	herm	4		No		
hn			beaufort	No		
hr			beaufort	No		
hn			quality	No		
hn			size	No		
hr			size	No		
hn			beaufort, quality	No		
hr			beaufort, quality	No		
hn			beaufort, size	No		
hr			beaufort, size	No		
hn			quality, size	No		
hr			quality, size	No		
hn			beaufort, quality, size	No		
hr			beaufort, quality, size	No		

Table 26: Candidate detection functions for Without Belly Observers - 1000 ft. The first one listed was selected for the density model.

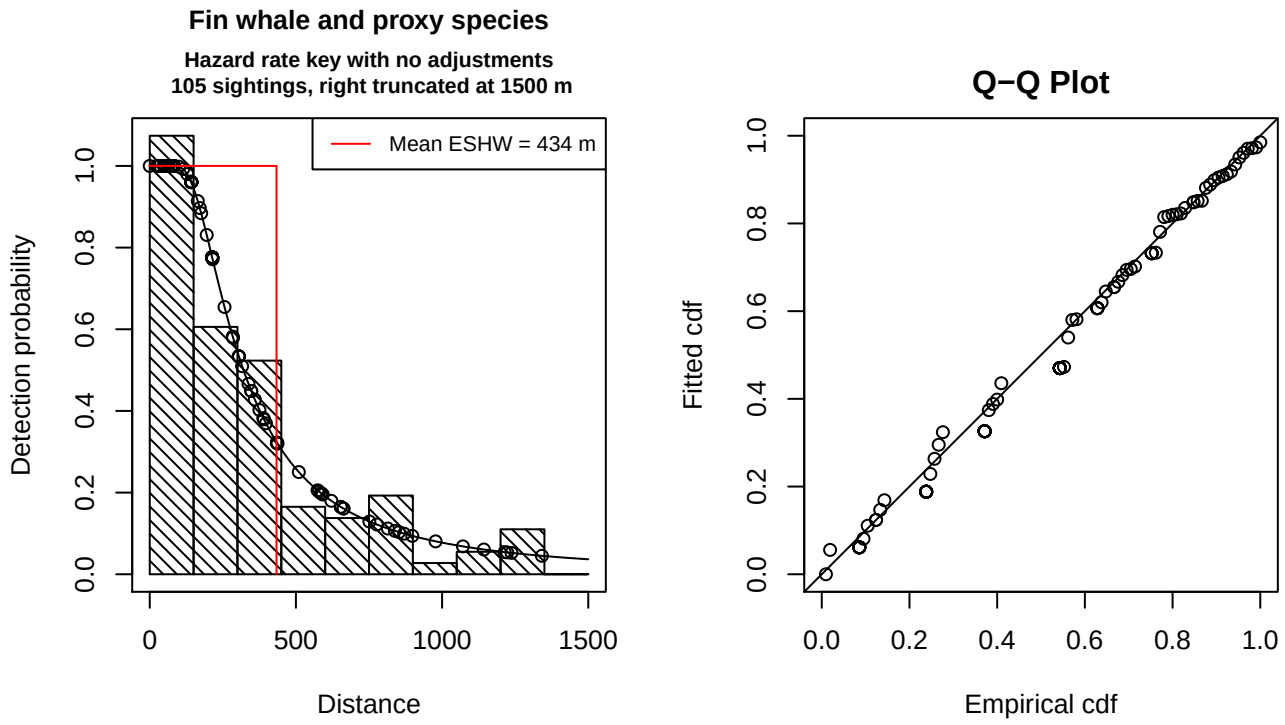

Figure 37: Detection function for Without Belly Observers - 1000 ft that was selected for the density model

Statistical output for this detection function:

```
Summary for ds object
Number of observations :  105
Distance range         :  0  -  1500
AIC                    :  1432.491

Detection function:
 Hazard-rate key function

Detection function parameters
Scale Coefficients:
            estimate        se
(Intercept) 5.576432 0.2232183

Shape parameters:
             estimate        se
(Intercept) 0.6374087 0.1752092

                       Estimate          SE        CV
Average p              0.2891295  0.03984493 0.1378100
N in covered region 363.1591175 58.28878285 0.1605048
```

Additional diagnostic plots:

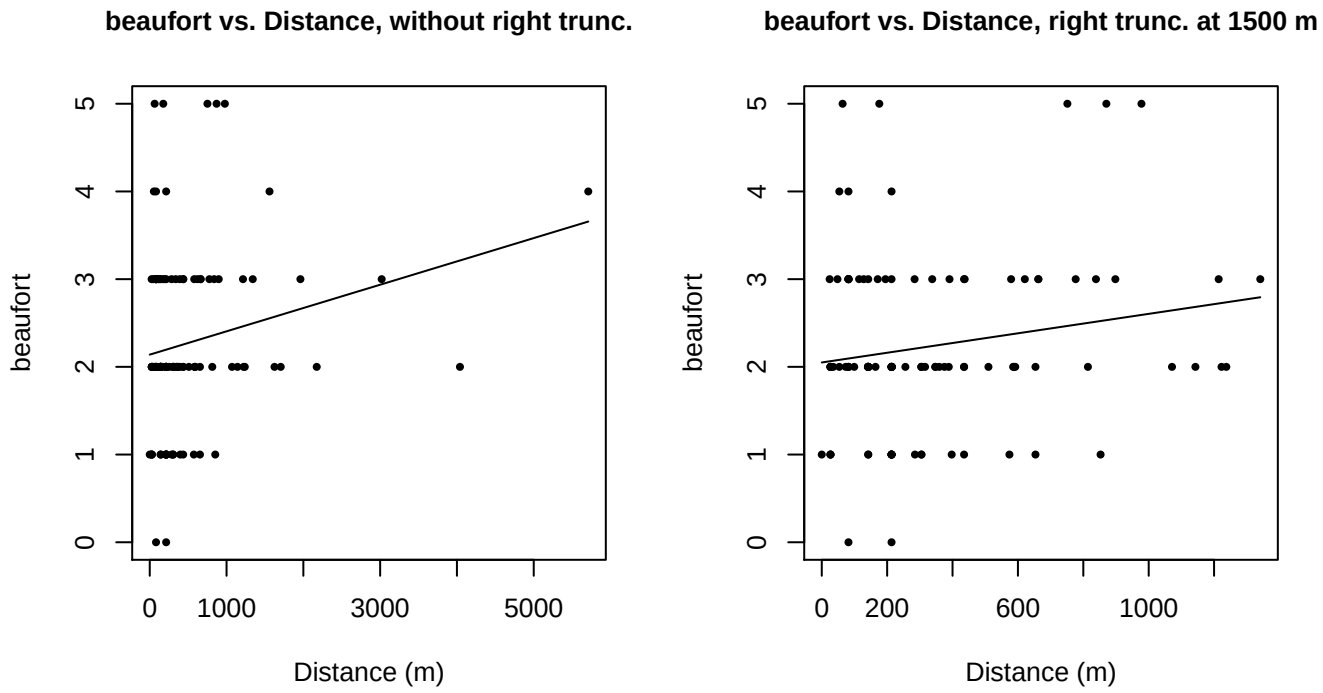

Figure 38: Scatterplots showing the relationship between Beaufort sea state and perpendicular sighting distance, for all sightings (left) and only those not right truncated (right). The line is a simple linear regression.

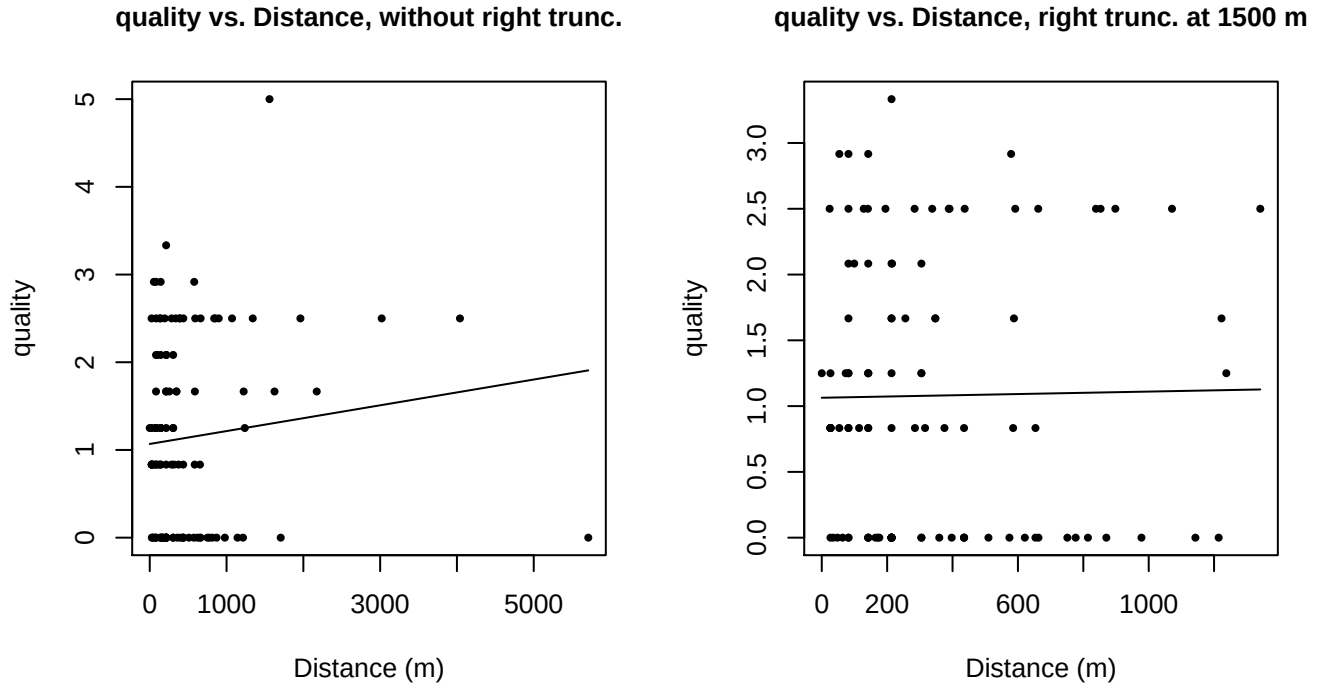

Figure 39: Scatterplots showing the relationship between the survey-specific index of the quality of observation conditions and perpendicular sighting distance, for all sightings (left) and only those not right truncated (right). Low values of the quality index correspond to better observation conditions. The line is a simple linear regression.

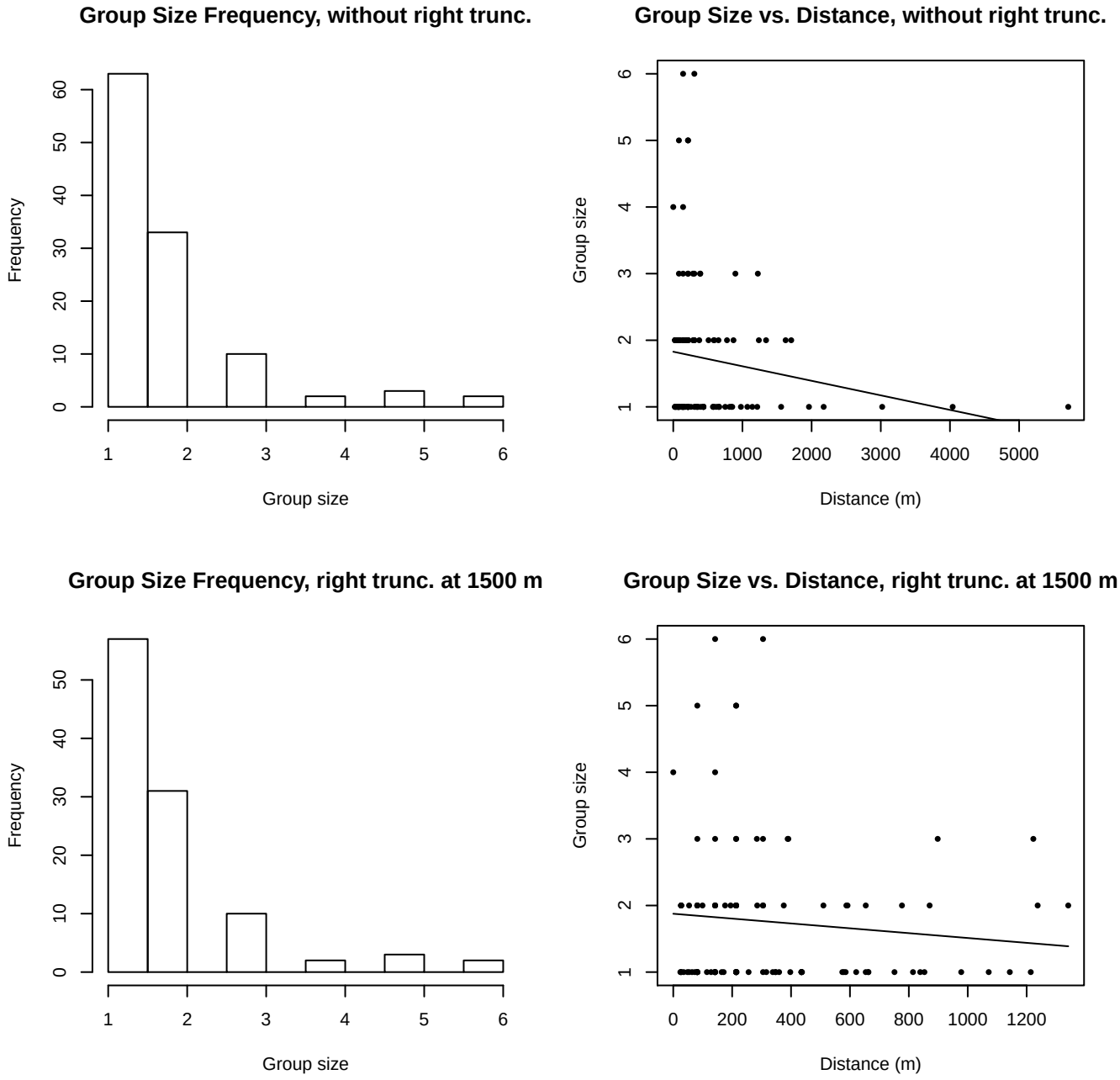

Figure 40: Histograms showing group size frequency and scatterplots showing the relationship between group size and perpendicular sighting distance, for all sightings (top row) and only those not right truncated (bottom row). In the scatterplot, the line is a simple linear regression.

NARWSS Grummans

The sightings were right truncated at 2500m. Due to a reduced frequency of sightings close to the trackline that plausibly resulted from the behavior of the observers and/or the configuration of the survey platform, the sightings were left truncted as well. Sightings closer than 107 m to the trackline were omitted from the analysis, and it was assumed that the the area closer to the trackline than this was not surveyed. This distance was estimated by inspecting histograms of perpendicular sighting distances.

Covariate	Description

beaufort	Beaufort sea state.
quality	Survey-specific index of the quality of observation conditions, utilizing relevant factors other than Beaufort sea state (see methods).
size	Estimated size (number of individuals) of the sighted group.

Table 27: Covariates tested in candidate "multi-covariate distance sampling" (MCDS) detection functions.

Key	Adjustment	Order	Covariates	Succeeded	Δ AIC	Mean ESHW (m)
hn	cos	3		Yes	0.00	600
hn	cos	2		Yes	4.14	714
hn			size	Yes	9.70	891
hn				Yes	9.95	889
hn			quality, size	Yes	11.67	891
hn			quality	Yes	11.94	889
hn	herm	4		No		
hn			beaufort	No		
hn			beaufort, quality	No		
hn			beaufort, size	No		
hn			beaufort, quality, size	No		

Table 28: Candidate detection functions for NARWSS Grummans. The first one listed was selected for the density model.

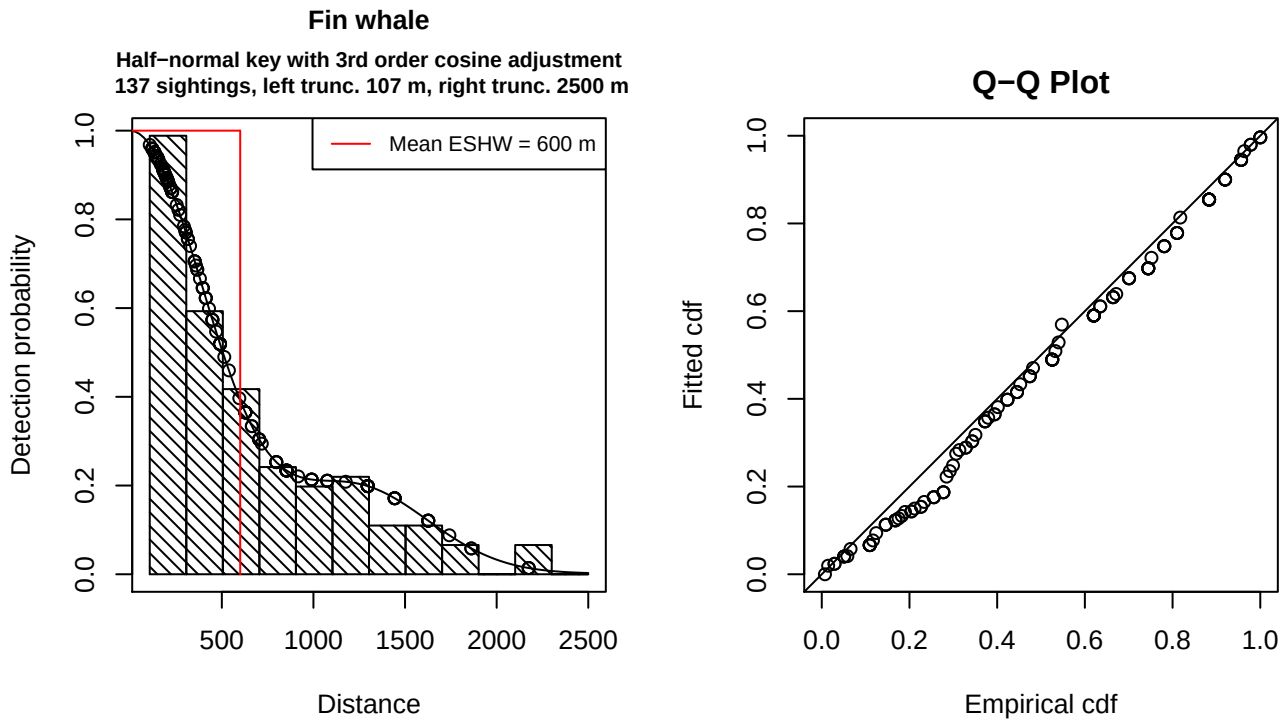

Figure 41: Detection function for NARWSS Grummans that was selected for the density model

Statistical output for this detection function:

```
Summary for ds object
Number of observations :  137
Distance range         :  106.5979  -  2500
AIC                    :  2003.07

Detection function:
 Half-normal key function with cosine adjustment term of order 3

Detection function parameters
Scale Coefficients:
            estimate         se
(Intercept)  6.67438 0.05352877

Adjustment term parameter(s):
              estimate        se
cos, order 3 0.4113226 0.1092172


Monotonicity constraints were enforced.
                       Estimate          SE        CV
Average p             0.2401048  0.02540906 0.1058248
N in covered region 570.5840865 73.83626663 0.1294047

Monotonicity constraints were enforced.
```

Additional diagnostic plots:

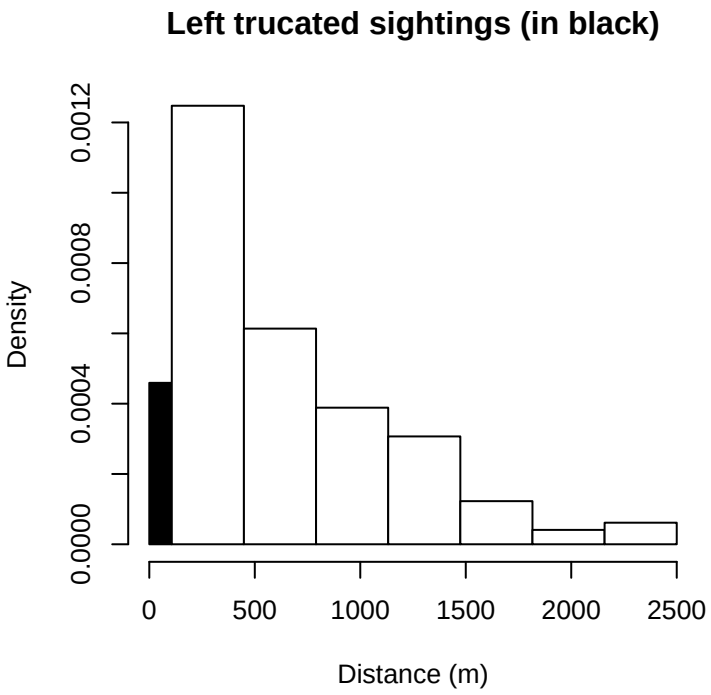

Figure 42: Density of sightings by perpendicular distance for NARWSS Grummans. Black bars on the left show sightings that were left truncated.

Figure 43: Scatterplots showing the relationship between Beaufort sea state and perpendicular sighting distance, for all sightings (left) and only those not right truncated (right). The line is a simple linear regression.

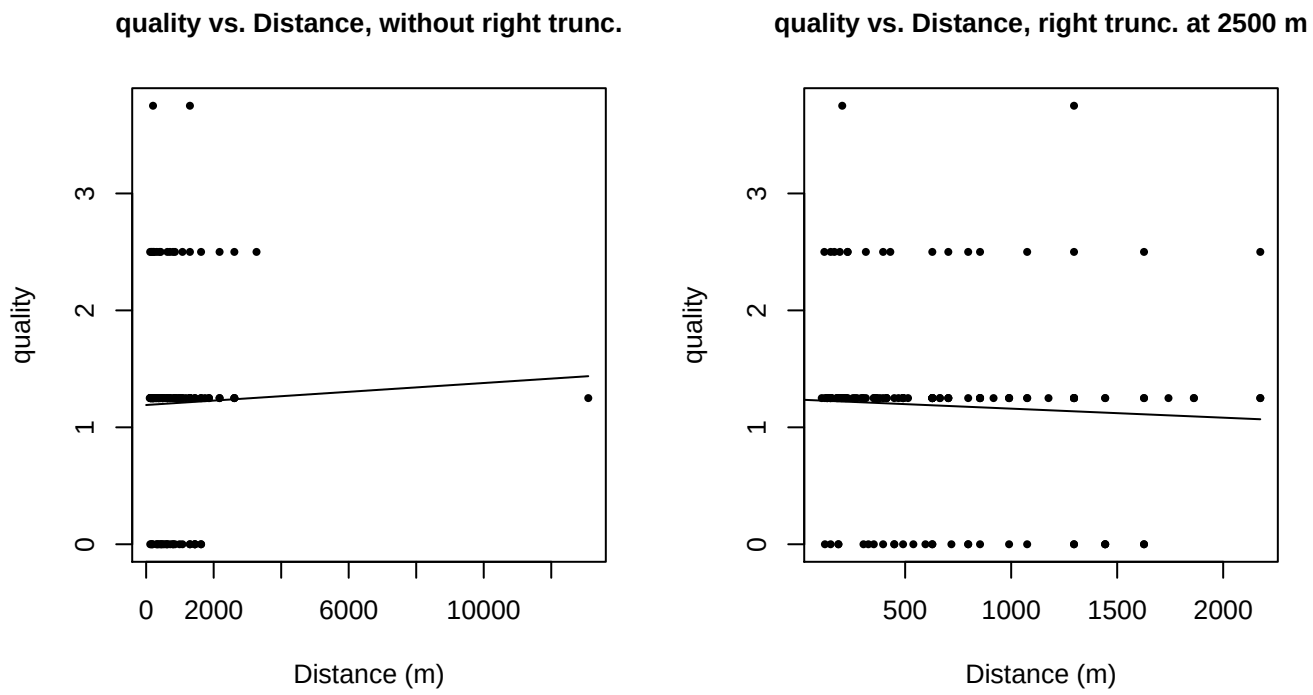

Figure 44: Scatterplots showing the relationship between the survey-specific index of the quality of observation conditions and perpendicular sighting distance, for all sightings (left) and only those not right truncated (right). Low values of the quality index correspond to better observation conditions. The line is a simple linear regression.

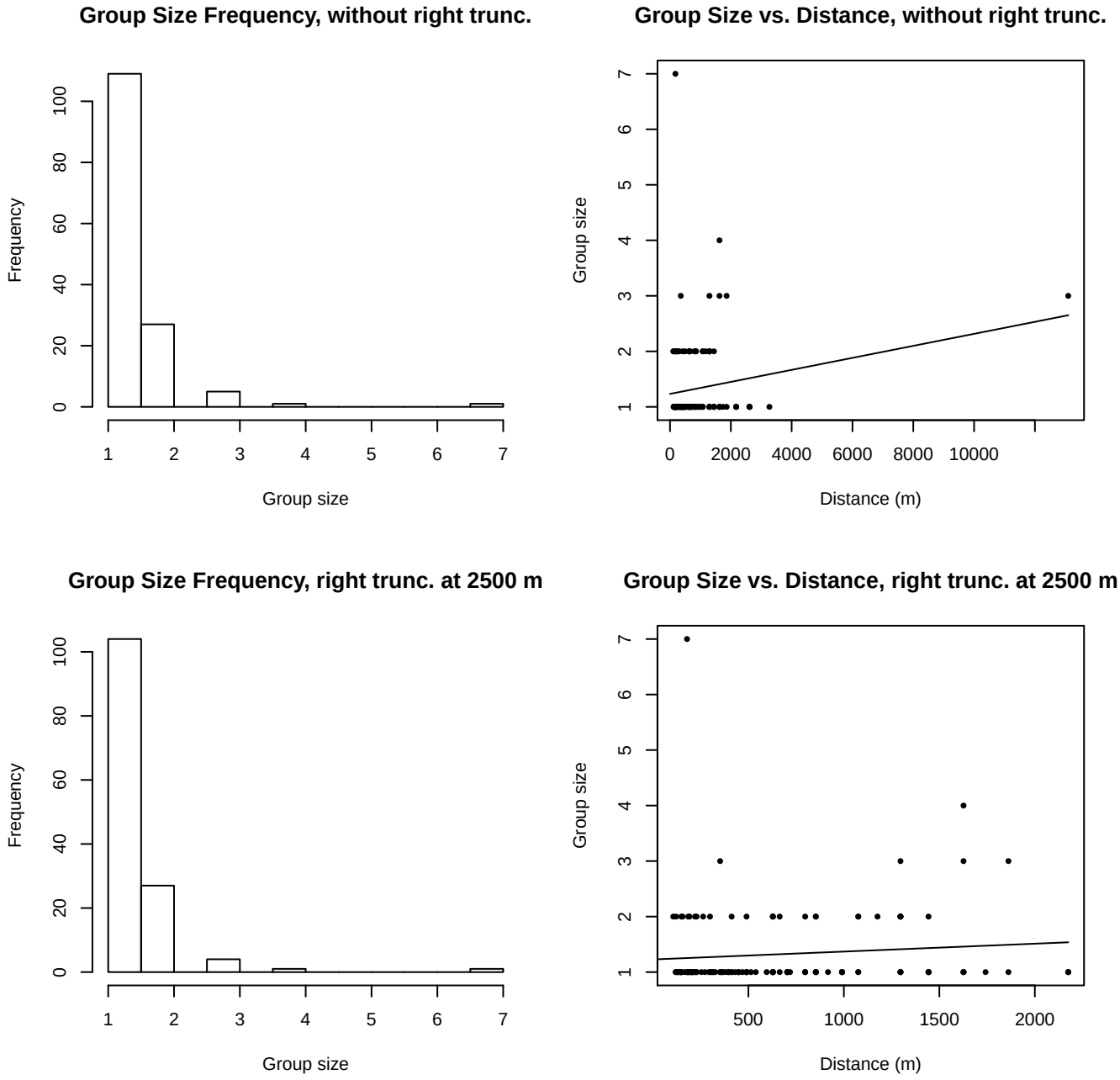

Figure 45: Histograms showing group size frequency and scatterplots showing the relationship between group size and perpendicular sighting distance, for all sightings (top row) and only those not right truncated (bottom row). In the scatterplot, the line is a simple linear regression.

NARWSS Twin Otters

The sightings were right truncated at 4000m. Due to a reduced frequency of sightings close to the trackline that plausibly resulted from the behavior of the observers and/or the configuration of the survey platform, the sightings were left truncted as well. Sightings closer than 160 m to the trackline were omitted from the analysis, and it was assumed that the the area closer to the trackline than this was not surveyed. This distance was estimated by inspecting histograms of perpendicular sighting distances. The vertical sighting angles were heaped at 10 degree increments up to 80 degrees and 1 degree increments thereafter, so the candidate detection functions were fitted using linear bins scaled accordingly.

Covariate	Description

beaufort	Beaufort sea state.
quality	Survey-specific index of the quality of observation conditions, utilizing relevant factors other than Beaufort sea state (see methods).
size	Estimated size (number of individuals) of the sighted group.

Table 29: Covariates tested in candidate "multi-covariate distance sampling" (MCDS) detection functions.

Key	Adjustment	Order	Covariates	Succeeded	Δ AIC	Mean ESHW (m)
hn	cos	3		Yes	0.00	1275
hn	cos	2		Yes	44.91	1560
hn				Yes	57.40	1778
hn	herm	4		Yes	59.39	1775
hn			beaufort	No		
hn			quality	No		
hn			size	No		
hn			beaufort, quality	No		
hn			beaufort, size	No		
hn			quality, size	No		
hn			beaufort, quality, size	No		

Table 30: Candidate detection functions for NARWSS Twin Otters. The first one listed was selected for the density model.

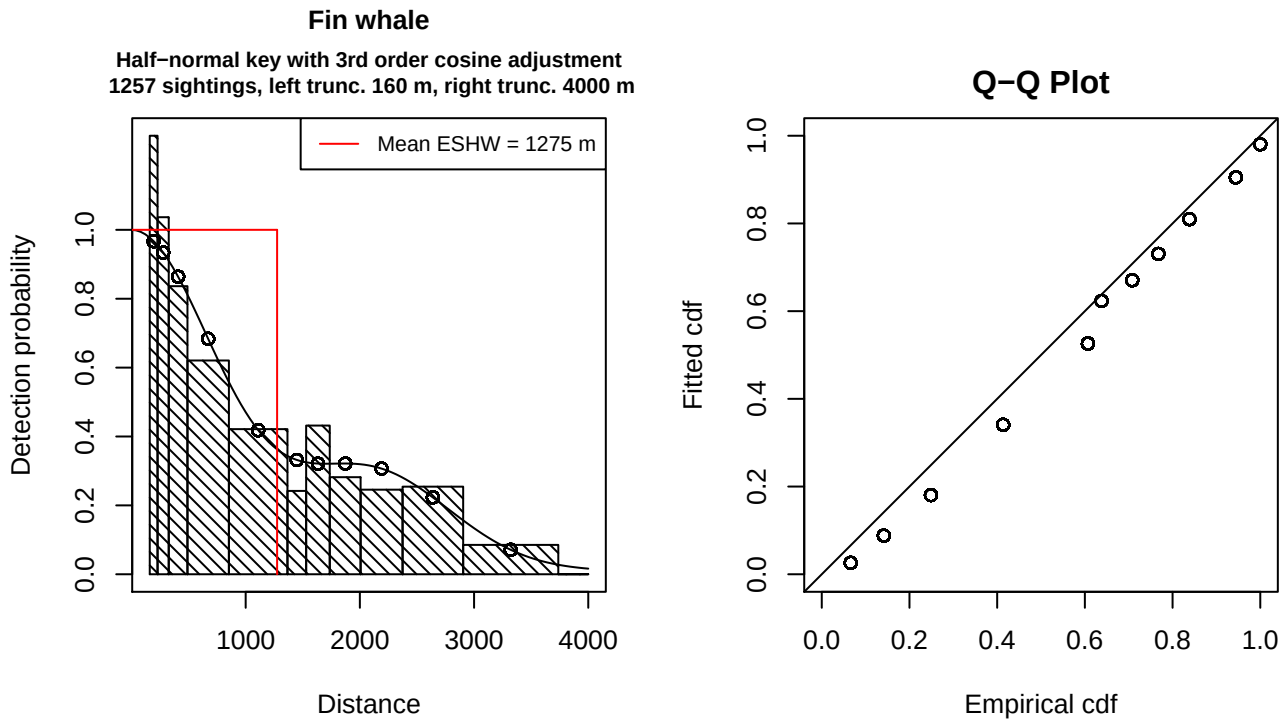

Figure 46: Detection function for NARWSS Twin Otters that was selected for the density model

Statistical output for this detection function:

```
Summary for ds object
Number of observations :  1257
Distance range         :  160.0674  -  4000
AIC                    :  5773.451

Detection function:
 Half-normal key function with cosine adjustment term of order 3

Detection function parameters
Scale Coefficients:
            estimate         se
(Intercept) 7.329061 0.02310891

Adjustment term parameter(s):
              estimate         se
cos, order 3 0.3224317 0.04029934


Monotonicity constraints were enforced.
                        Estimate          SE         CV
Average p              0.3188383   0.01438781 0.04512572
N in covered region 3942.4374543 200.18212149 0.05077623

Monotonicity constraints were enforced.
```

Additional diagnostic plots:

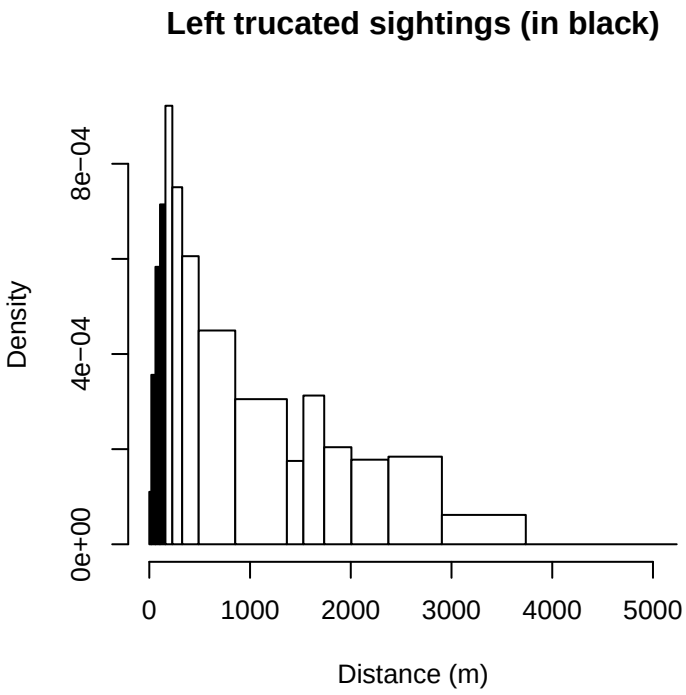

Figure 47: Density of sightings by perpendicular distance for NARWSS Twin Otters. Black bars on the left show sightings that were left truncated.

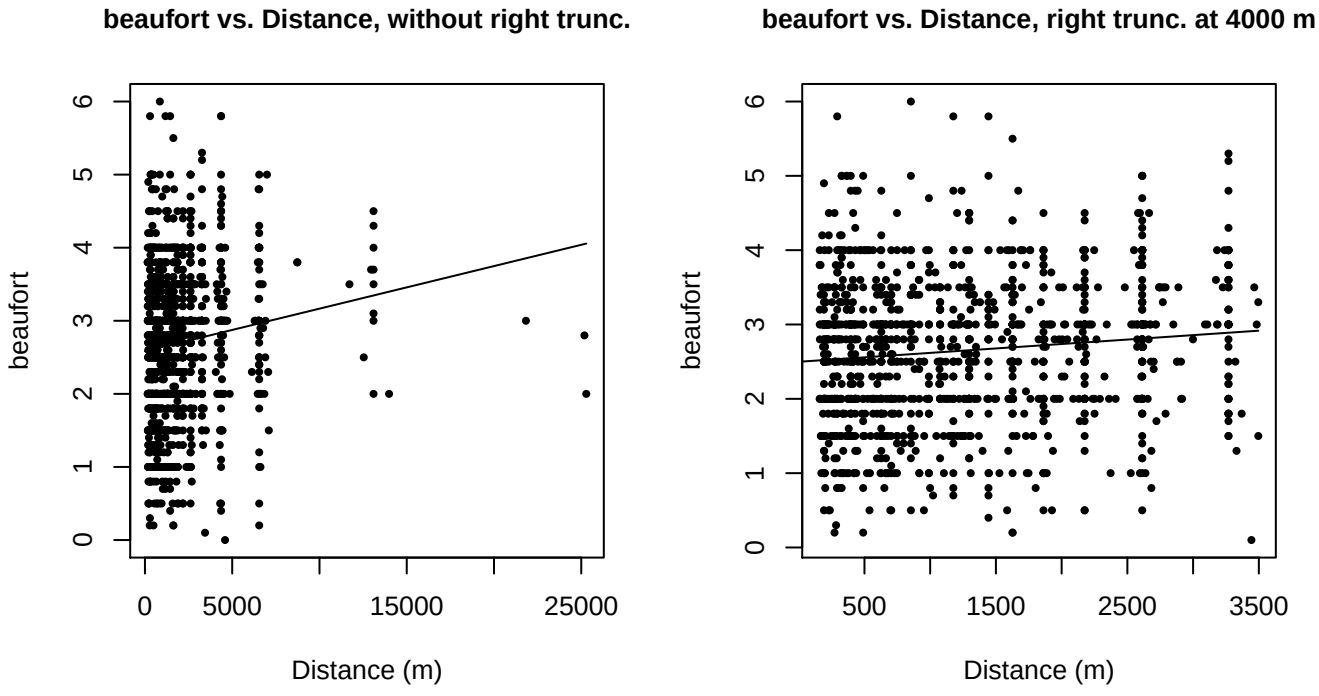

Figure 48: Scatterplots showing the relationship between Beaufort sea state and perpendicular sighting distance, for all sightings (left) and only those not right truncated (right). The line is a simple linear regression.

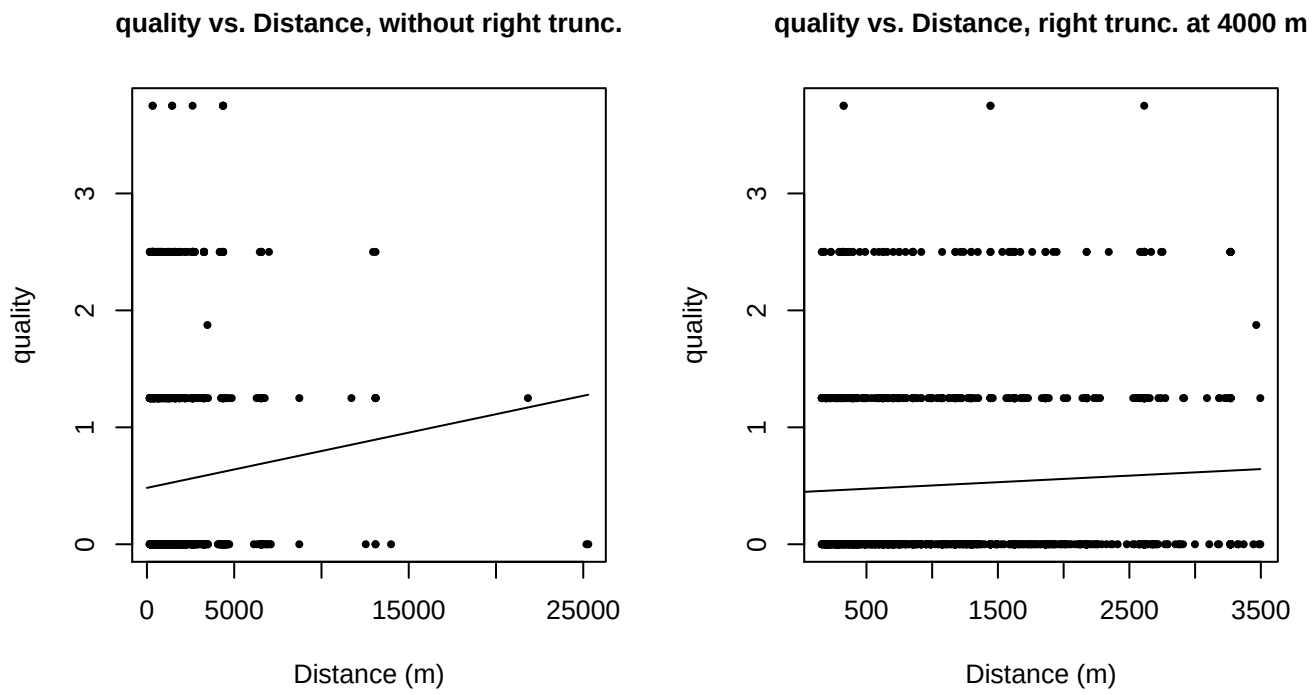

Figure 49: Scatterplots showing the relationship between the survey-specific index of the quality of observation conditions and perpendicular sighting distance, for all sightings (left) and only those not right truncated (right). Low values of the quality index correspond to better observation conditions. The line is a simple linear regression.

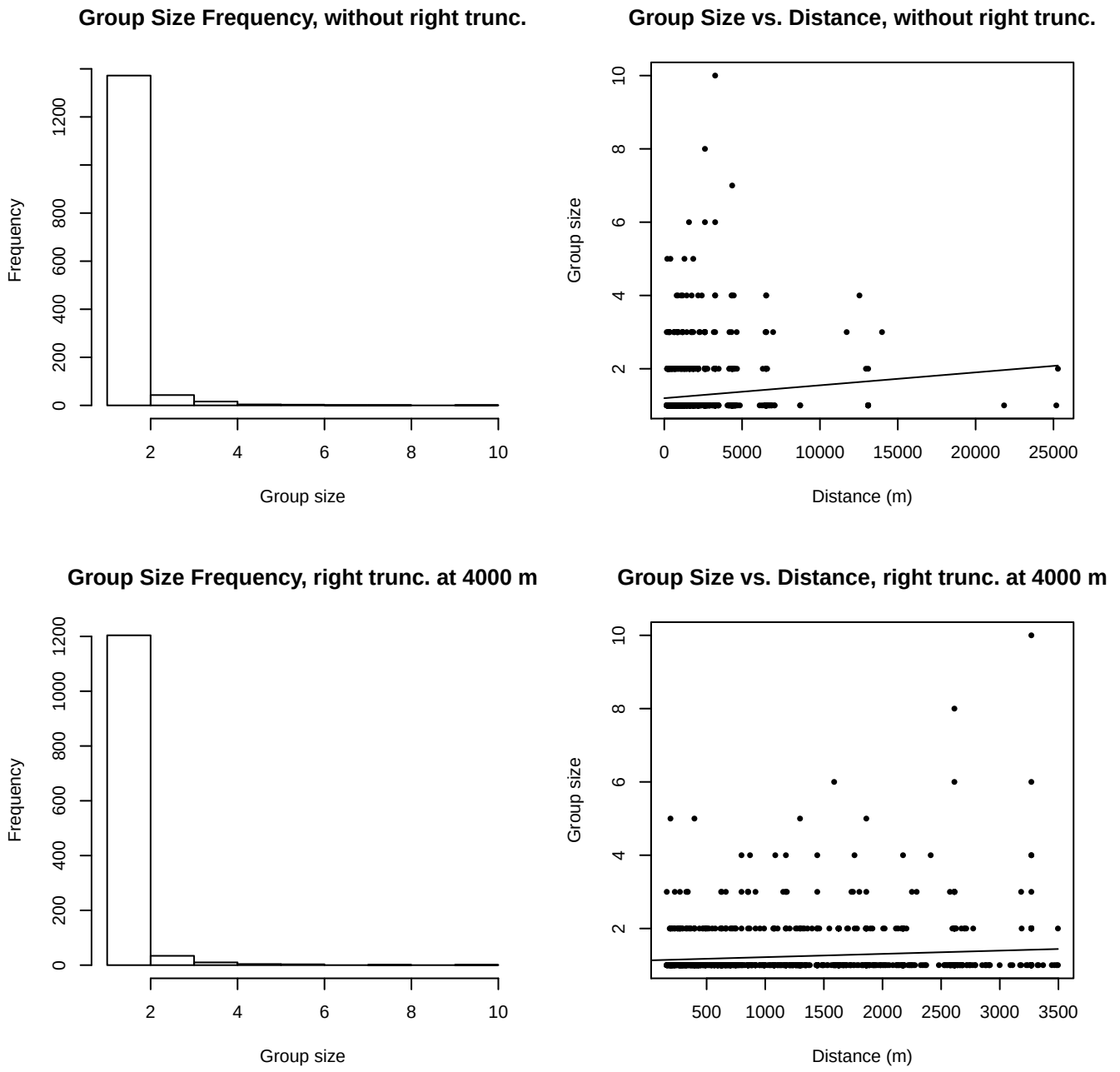

Figure 50: Histograms showing group size frequency and scatterplots showing the relationship between group size and perpendicular sighting distance, for all sightings (top row) and only those not right truncated (bottom row). In the scatterplot, the line is a simple linear regression.

g(0) Estimates

Platform	Surveys	Group Size	*g(0)*	Biases Addressed	Source
Shipboard	Binocular Surveys	Any	0.63	Perception	Palka (2006)
Shipboard	NEFSC Abel-J Binocular Surveys	Any	0.32	Perception	Palka (2006)
Shipboard	NEFSC Endeavor	Any	0.94	Perception	Palka (2006)
Shipboard	Naked Eye Surveys	Any	0.48	Perception	Palka (2006)
Aerial	All	Any	0.251	Availability	Lafortuna et al. (2003)

Table 31: Estimates of *g(0)* used in this density model.

Palka (2006) provided survey-specific g(0) estimates for fin and sei whales (pooled together) for two NOAA NEFSC shipboard surveys that used bigeye binoculars: the 1998 Abel-J survey (g(0)=0.32) and the 2004 Endeavor survey (g(0)=0.94). We used the estimates for the lower team, which was the primary team and the one for which we had sightings. All other binocular surveys did not estimate g(0); for these we used the simple mean (g(0)=0.68) of Palka's two estimates. These estimates accounted for perception bias but not availability bias (Palka 2005b), but we do not believe availability to be a major factor affecting detectability of fin whales from shipboard surveys, as they are not a particularly long-diving species.

As above, Palka (2006) provided a survey-specific, pooled fin and sei whale estimate of g(0) for the NOAA NEFSC Abel-J 1999 naked eye shipboard survey. We used the estimate for the upper team, which was the primary team and the one for which we had sightings. We also used this estimate with the European naked eye surveys, which did not publish g(0) estimates. (The European surveys were not used in the East Coast model documented here, but may have been used in the AFTT model. Please consult the AFTT model documentation for more information.)

We found no species-specific g(0) estimate for fin whales observed from aerial surveys in the literature. Utilizing equation (3) of Carretta et al. (2000) (which follows Barlow et al. 1988), we computed the availability bias component of g(0) from the mean surface and dive intervals (62 s and 225 s) for fin whales reported by Lafortuna et al. (2003). We preferred this approach to the generic large whale g(0) estimate reported by Palka (2006), as the availability bias component we estimated here was substantially lower than Palka's g(0) estimate (0.53) that accounted for both availability and perception biases. We did not obtain an estimate of perception bias, but perception bias for whales is expected to be negligible (Carretta et al. 2000).

Density Models

Surveys conducted from 1978-1989 reported that fin whales were the most frequently sighted large whale on the U.S. continental shelf north of Cape Hatteras and were present throughout this region during all four seasons (Hain et al. 1992; CETAP, 1982). Despite their prevalence, little is known about fin whale migration patterns. Similar to other baleen whales, they may undertake seasonal migrations north to feed and south to breed, but these patterns have not been described in the literature. Hain et al. (1992, Table 3), using data from CeTAP and subsequent surveys in the 1980s, reported markedly decreased fin whale abundance in fall compared to spring and summer.

The surveys used in our density models, conducted in the 1990s and later, carried out routine flights and cruises over the continental shelf in the New England area between 40 N and Canadian waters during all seasons and reported numerous fin whale sightings during every month of the year. Survey effort in the mid-Atlantic shelf region, between 35-40 N, was sparser but survey teams reported at least one sighting for each month of the year. South of 35 N, survey effort was variable, with several areas surveyed consistently throughout the year and other areas receiving coverage only a few months of the year. The surveys reported no sightings south of 33 N.

Other sources have reported fin whales at more southerly latitudes. A fin whale was photographed off Sapelo Island, Georgia in March 2012 (Florida Fish and Wildlife Conservation Commission, unpublished data, photo here). Acoustic data from SOSUS arrays suggested that in the fall fin whales may migrate south past Bermuda and into the West Indies (Clark 1995). There was at least one report of a fin whale stranding in the Bahamas (Bahamas Marine Mammal Research Organisation, unpublished data, see OBIS-SEAMAP dataset 327).

Lacking a definitive description of fin whale migration patterns, and given the year-round presence of fin whales throughout the northern half of the study area, we elected to fit a year-round model using all of the survey data.

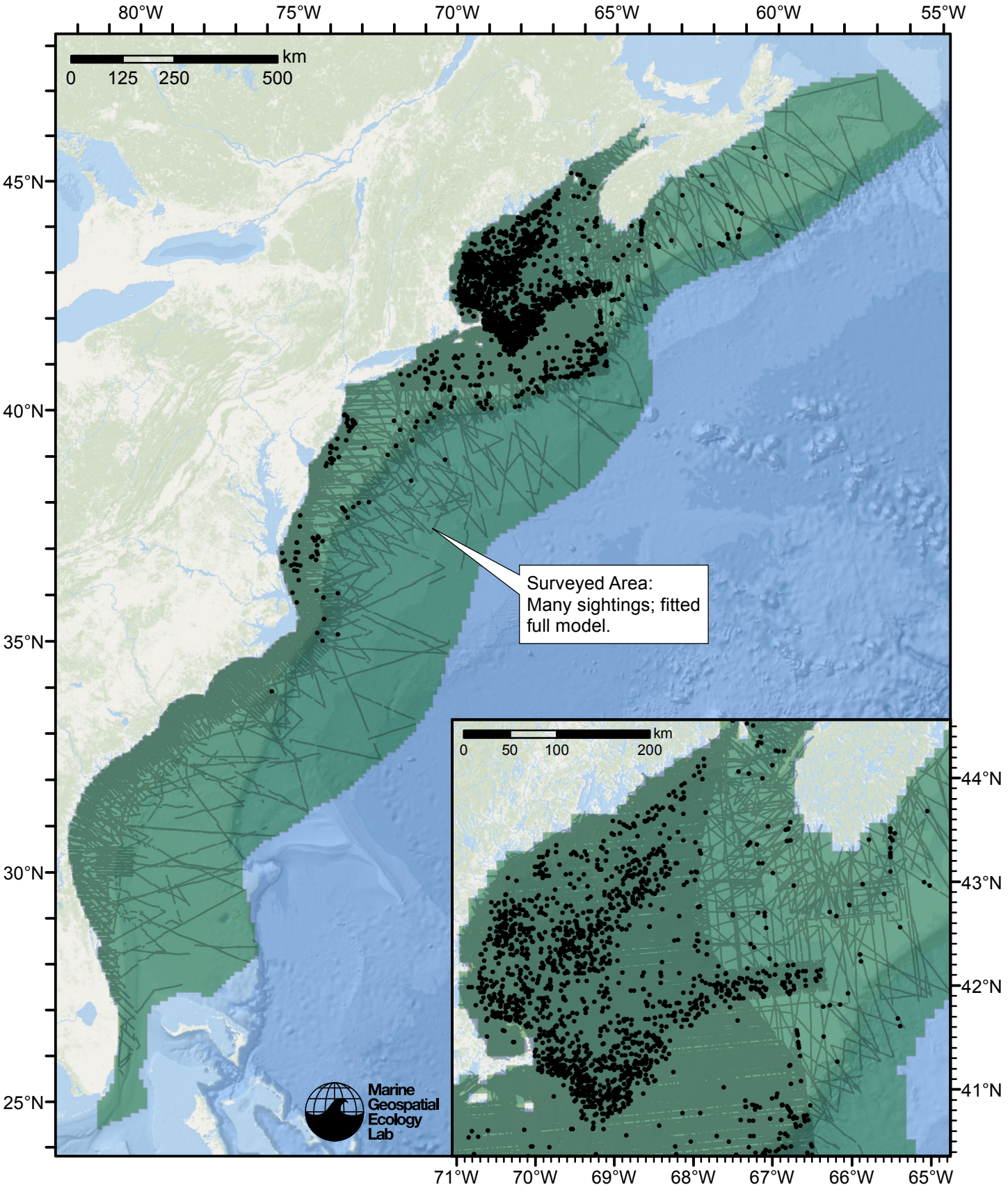

Figure 51: Fin whale density model schematic. All on-effort sightings are shown, including those that were truncated when detection functions were fitted.

Climatological Model

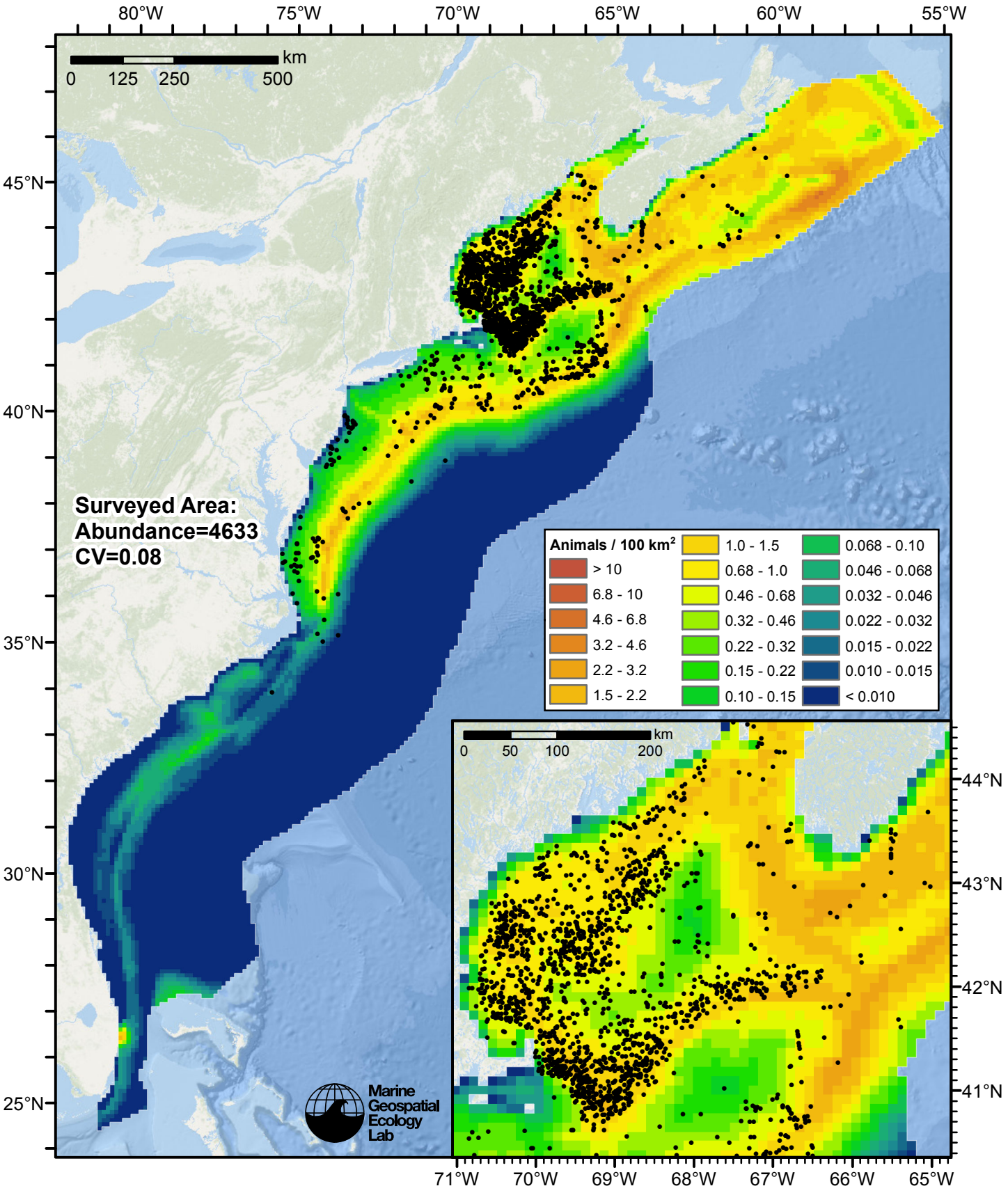

Figure 52: Fin whale density predicted by the climatological model that explained the most deviance. Pixels are 10x10 km. The legend gives the estimated individuals per pixel; breaks are logarithmic. Abundance for each region was computed by summing the density cells occuring in that region.

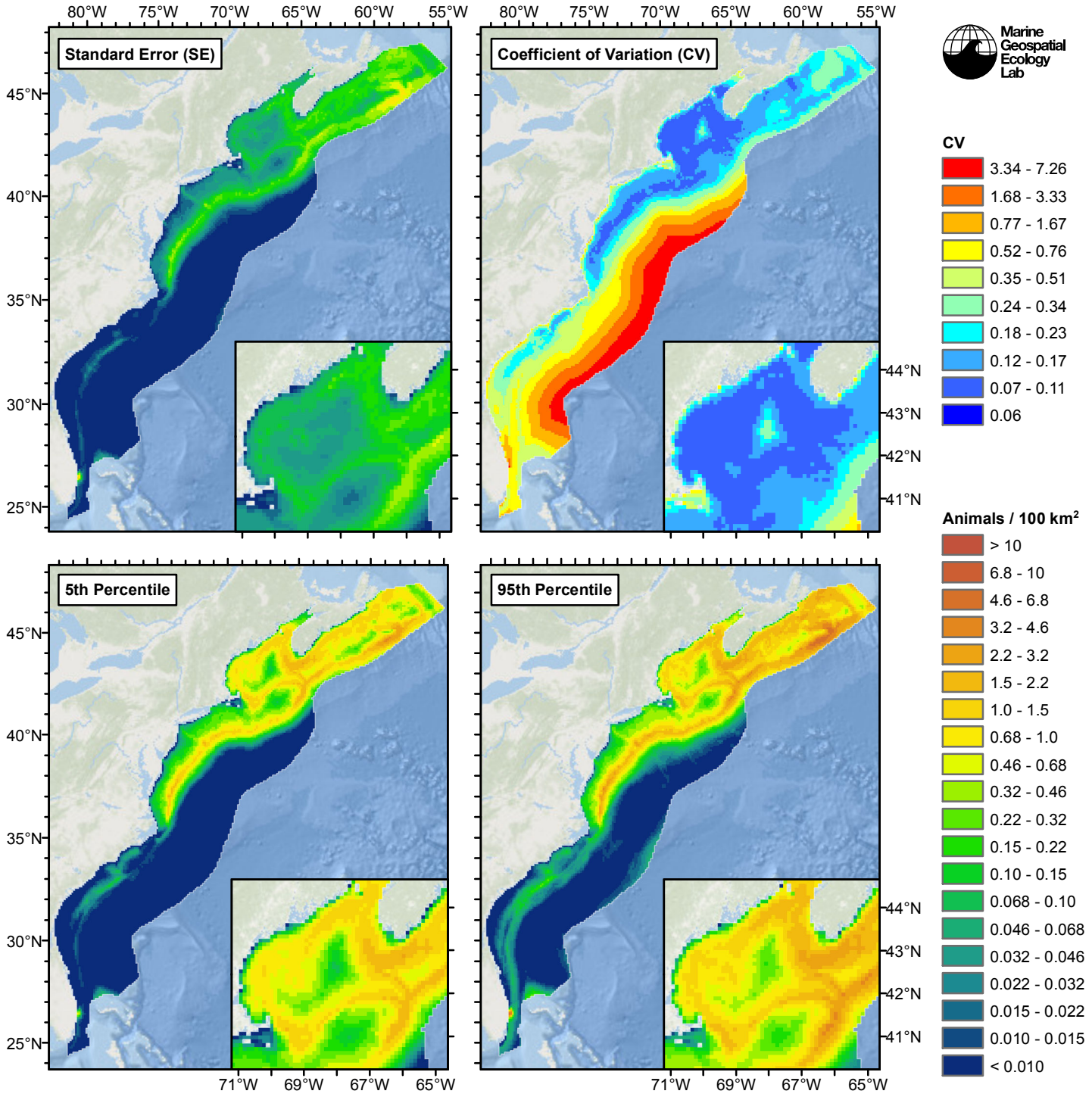

Figure 53: Estimated uncertainty for the climatological model that explained the most deviance. These estimates only incorporate the statistical uncertainty estimated for the spatial model (by the R mgcv package). They do not incorporate uncertainty in the detection functions, g(0) estimates, predictor variables, and so on.

Surveyed Area

Statistical output

```
Rscript.exe: This is mgcv 1.8-3. For overview type 'help("mgcv-package")'.


Family: Tweedie(p=1.185)
```

```
Link function: log

Formula:
abundance ~ offset(log(area_km2)) + s(log10(Depth), bs = "ts",
    k = 5) + s(sqrt(DistToShore/1000), bs = "ts", k = 5) + s(log10(Slope),
    bs = "ts", k = 5) + s(I(DistTo125m/1000), bs = "ts", k = 5) +
    s(I(DistTo300m/1000), bs = "ts", k = 5) + s(ClimSST, bs = "ts",
    k = 5) + s(I(ClimDistToFront1^(1/3)), bs = "ts", k = 5) +
    s(log10(pmax(ClimTKE, 1e-04)), bs = "ts", k = 5) + s(log10(pmax(ClimPkPB,
    0.01)), bs = "ts", k = 5)

Parametric coefficients:
            Estimate Std. Error t value Pr(>|t|)
(Intercept)  -6.8912     0.1262   -54.6   <2e-16 ***
---
Signif. codes:  0 '***' 0.001 '**' 0.01 '*' 0.05 '.' 0.1 ' ' 1

Approximate significance of smooth terms:
                                edf Ref.df      F  p-value
s(log10(Depth))               3.551      4 14.447 1.05e-13 ***
s(sqrt(DistToShore/1000))     3.315      4 10.399 7.84e-10 ***
s(log10(Slope))               1.201      4  9.498 1.69e-10 ***
s(I(DistTo125m/1000))         3.443      4 21.241  < 2e-16 ***
s(I(DistTo300m/1000))         1.273      4 21.037  < 2e-16 ***
s(ClimSST)                    3.548      4  5.375 8.48e-05 ***
s(I(ClimDistToFront1^(1/3)))  3.745      4 11.389 6.71e-10 ***
s(log10(pmax(ClimTKE, 1e-04))) 3.311      4  5.519 3.23e-05 ***
s(log10(pmax(ClimPkPB, 0.01))) 3.360      4 35.685  < 2e-16 ***
---
Signif. codes:  0 '***' 0.001 '**' 0.01 '*' 0.05 '.' 0.1 ' ' 1

R-sq.(adj) =  0.0172   Deviance explained = 23.2%
-REML =  12084  Scale est. = 23.781    n = 104236

All predictors were significant. This is the final model.
Creating term plots.
Diagnostic output from gam.check():

Method: REML   Optimizer: outer newton
full convergence after 14 iterations.
Gradient range [-1.382342e-06,1.049295e-06]
(score 12083.52 & scale 23.7807).
Hessian positive definite, eigenvalue range [0.4057875,8250.628].
Model rank =  37 / 37

Basis dimension (k) checking results. Low p-value (k-index<1) may
indicate that k is too low, especially if edf is close to k'.

                                k'   edf k-index p-value
s(log10(Depth))               4.000 3.551   0.778    0.00
s(sqrt(DistToShore/1000))     4.000 3.315   0.810    0.25
s(log10(Slope))               4.000 1.201   0.769    0.00
s(I(DistTo125m/1000))         4.000 3.443   0.806    0.12
s(I(DistTo300m/1000))         4.000 1.273   0.777    0.00
s(ClimSST)                    4.000 3.548   0.743    0.00
s(I(ClimDistToFront1^(1/3)))  4.000 3.745   0.825    0.78
s(log10(pmax(ClimTKE, 1e-04))) 4.000 3.311   0.768    0.00
s(log10(pmax(ClimPkPB, 0.01))) 4.000 3.360   0.758    0.00
```

```
Predictors retained during the model selection procedure: Depth, DistToShore, Slope, DistTo125m,
DistTo300m, ClimSST, ClimDistToFront1, ClimTKE, ClimPkPB

Predictors dropped during the model selection procedure:
```

Model term plots

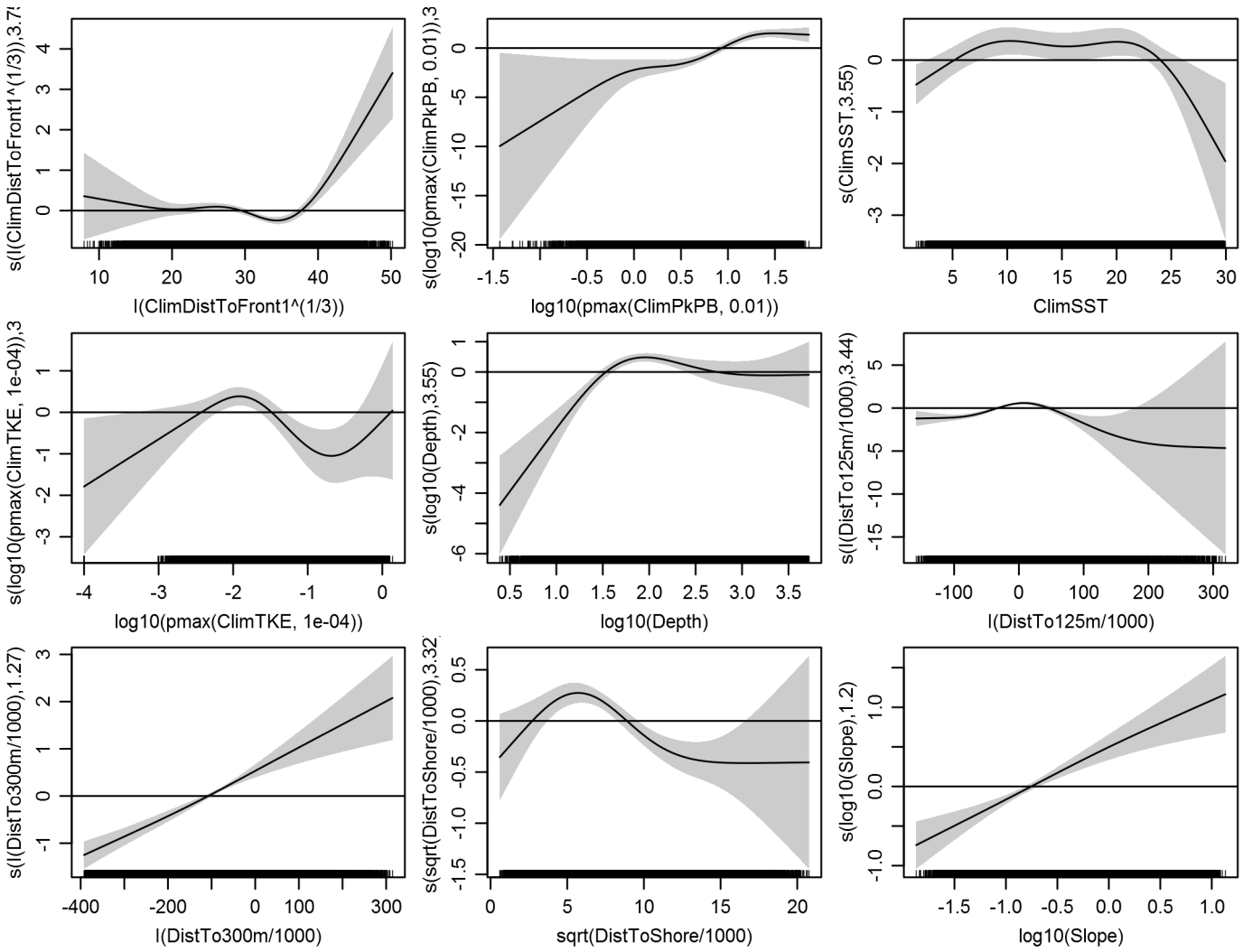

Diagnostic plots

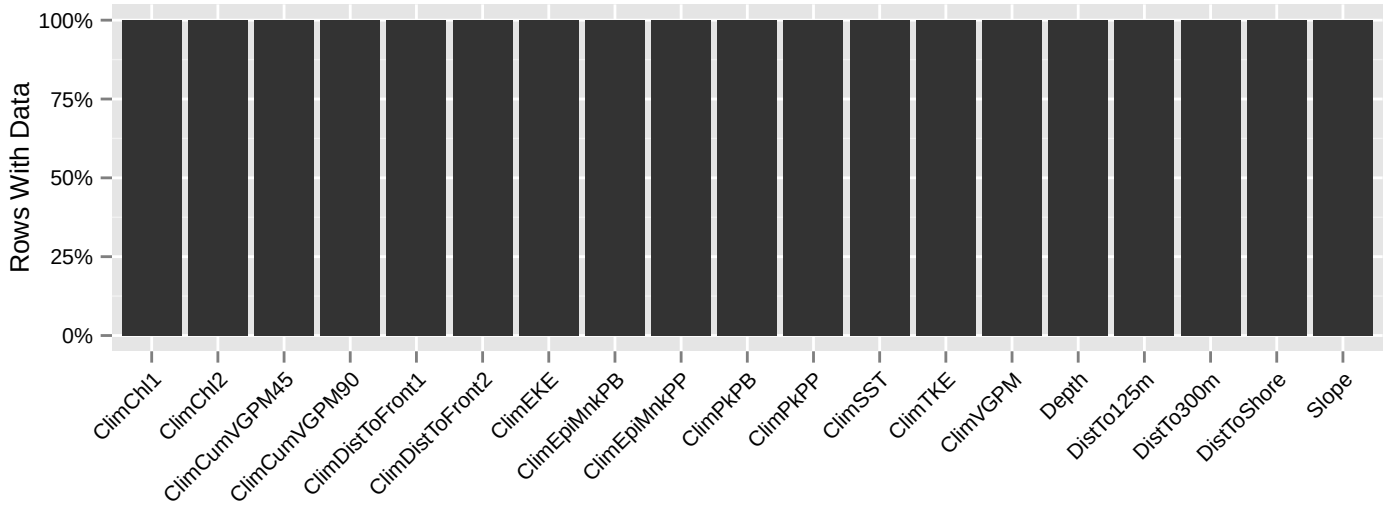

Figure 54: Segments with predictor values for the Fin whale Climatological model, Surveyed Area. This plot is used to assess how many segments would be lost by including a given predictor in a model.

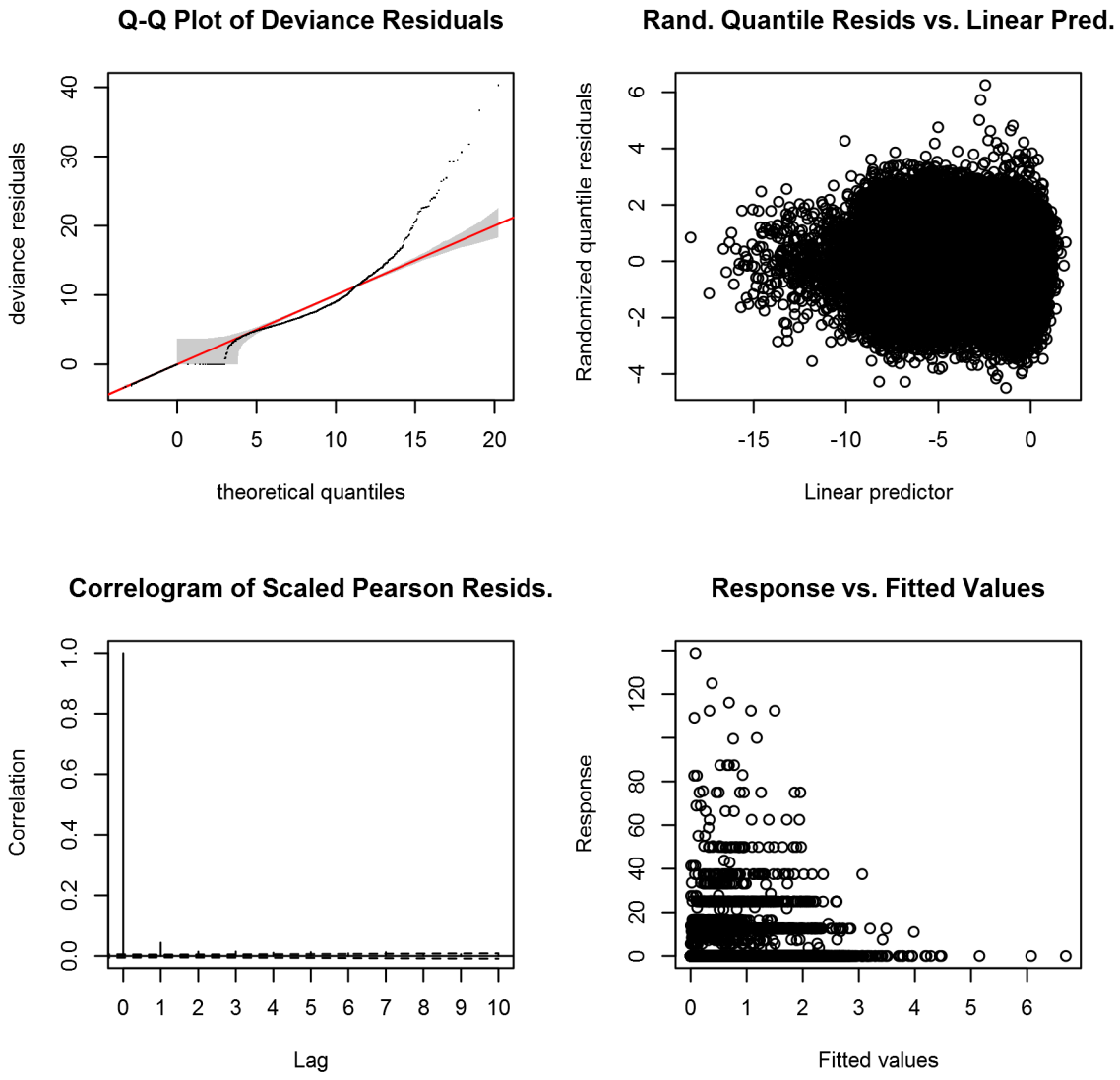

Figure 55: Statistical diagnostic plots for the Fin whale Climatological model, Surveyed Area.

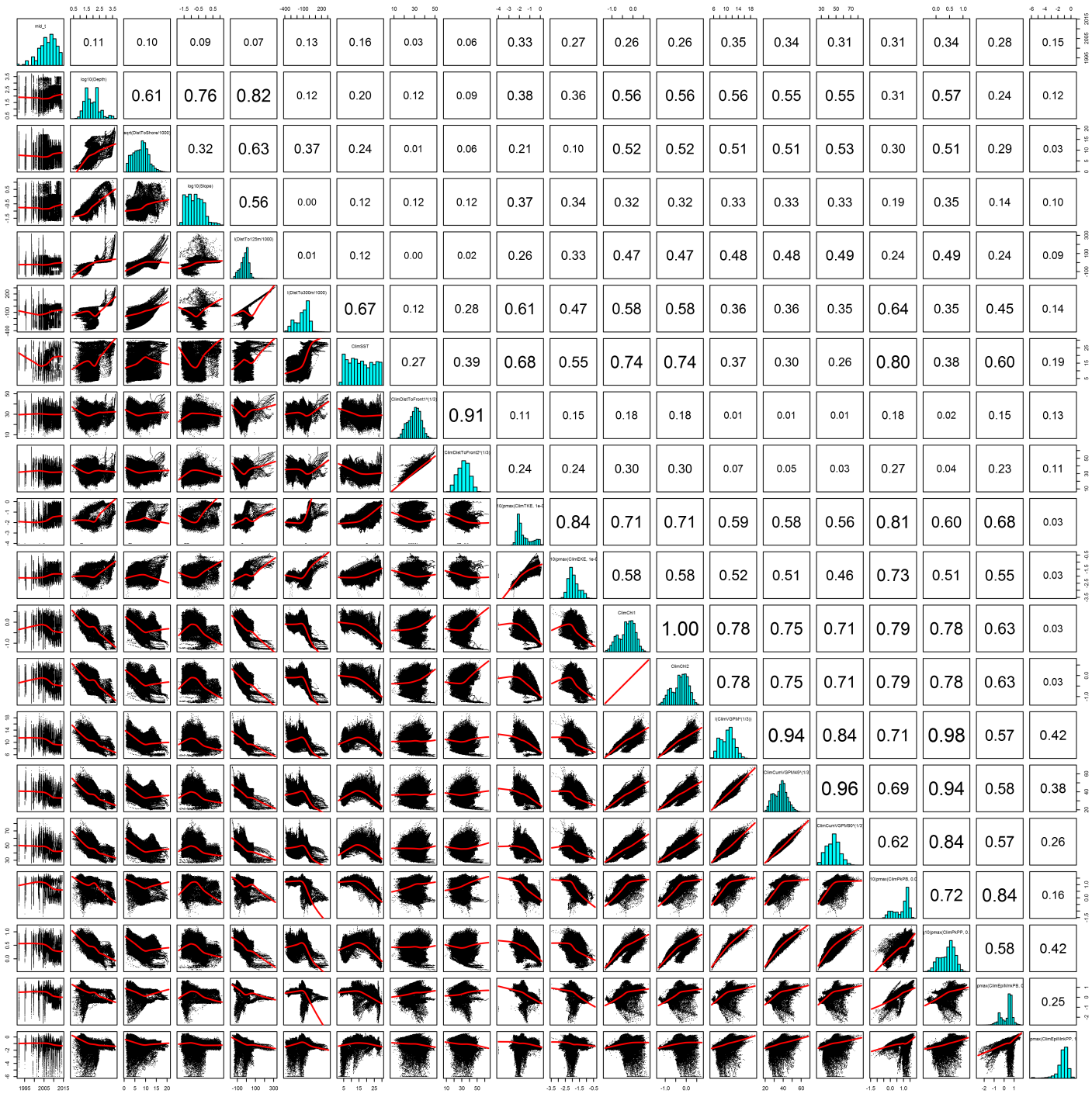

Figure 56: Scatterplot matrix for the Fin whale Climatological model, Surveyed Area. This plot is used to inspect the distribution of predictors (via histograms along the diagonal), simple correlation between predictors (via pairwise Pearson coefficients above the diagonal), and linearity of predictor correlations (via scatterplots below the diagonal). This plot is best viewed at high magnification.

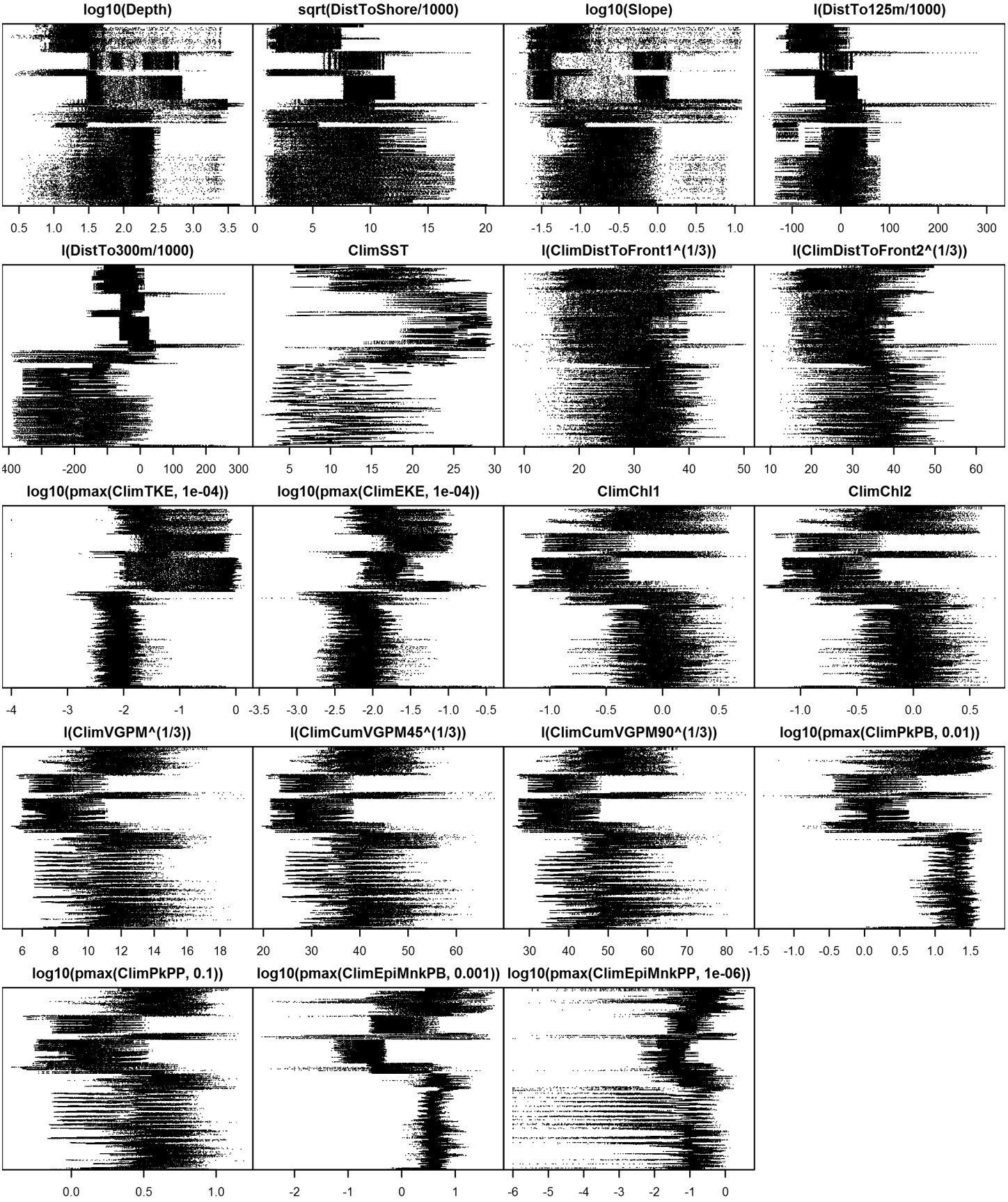

Figure 57: Dotplot for the Fin whale Climatological model, Surveyed Area. This plot is used to check for suspicious patterns and outliers in the data. Points are ordered vertically by transect ID, sequentially in time.

Contemporaneous Model

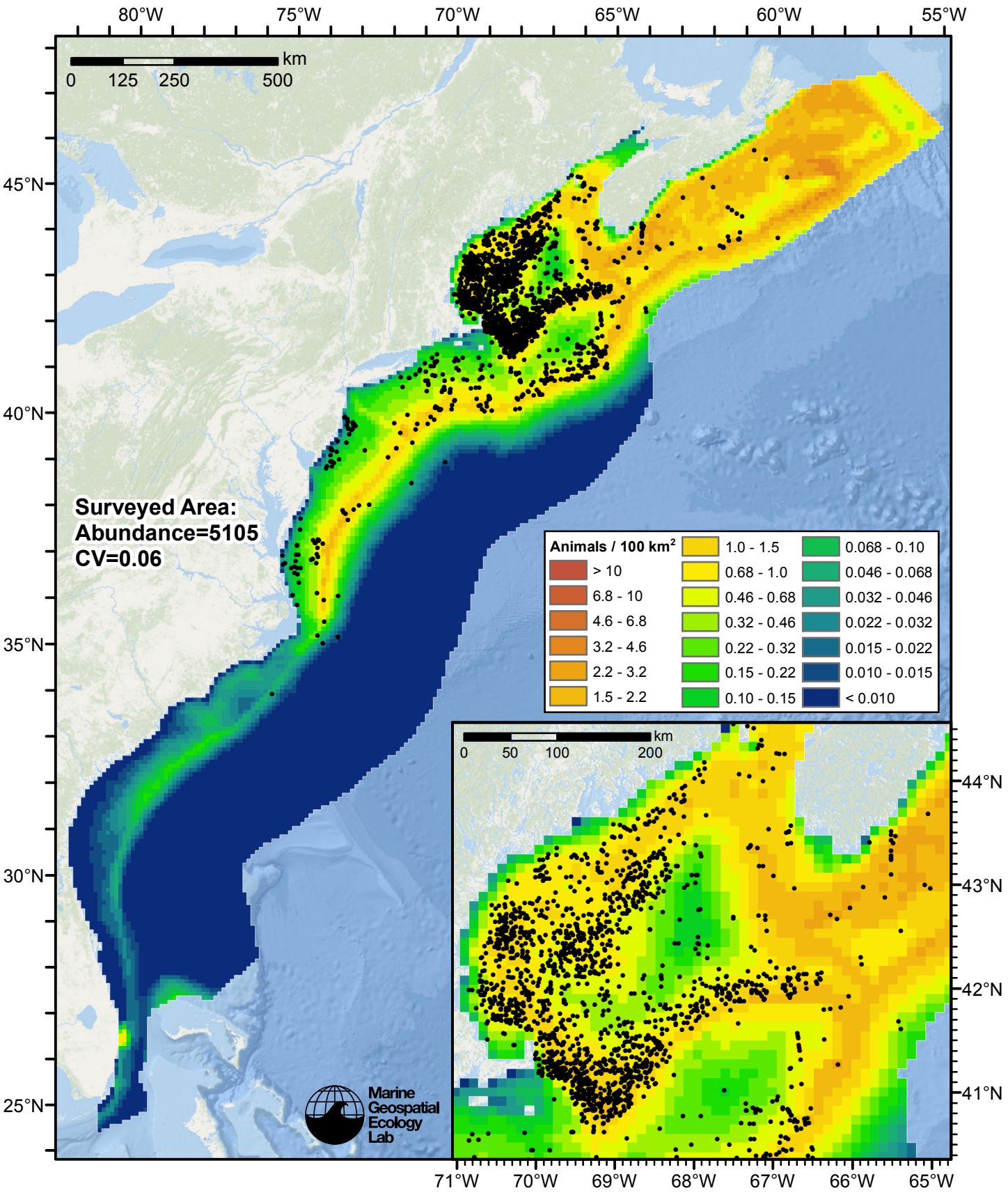

Figure 58: Fin whale density predicted by the contemporaneous model that explained the most deviance. Pixels are 10x10 km. The legend gives the estimated individuals per pixel; breaks are logarithmic. Abundance for each region was computed by summing the density cells occuring in that region.

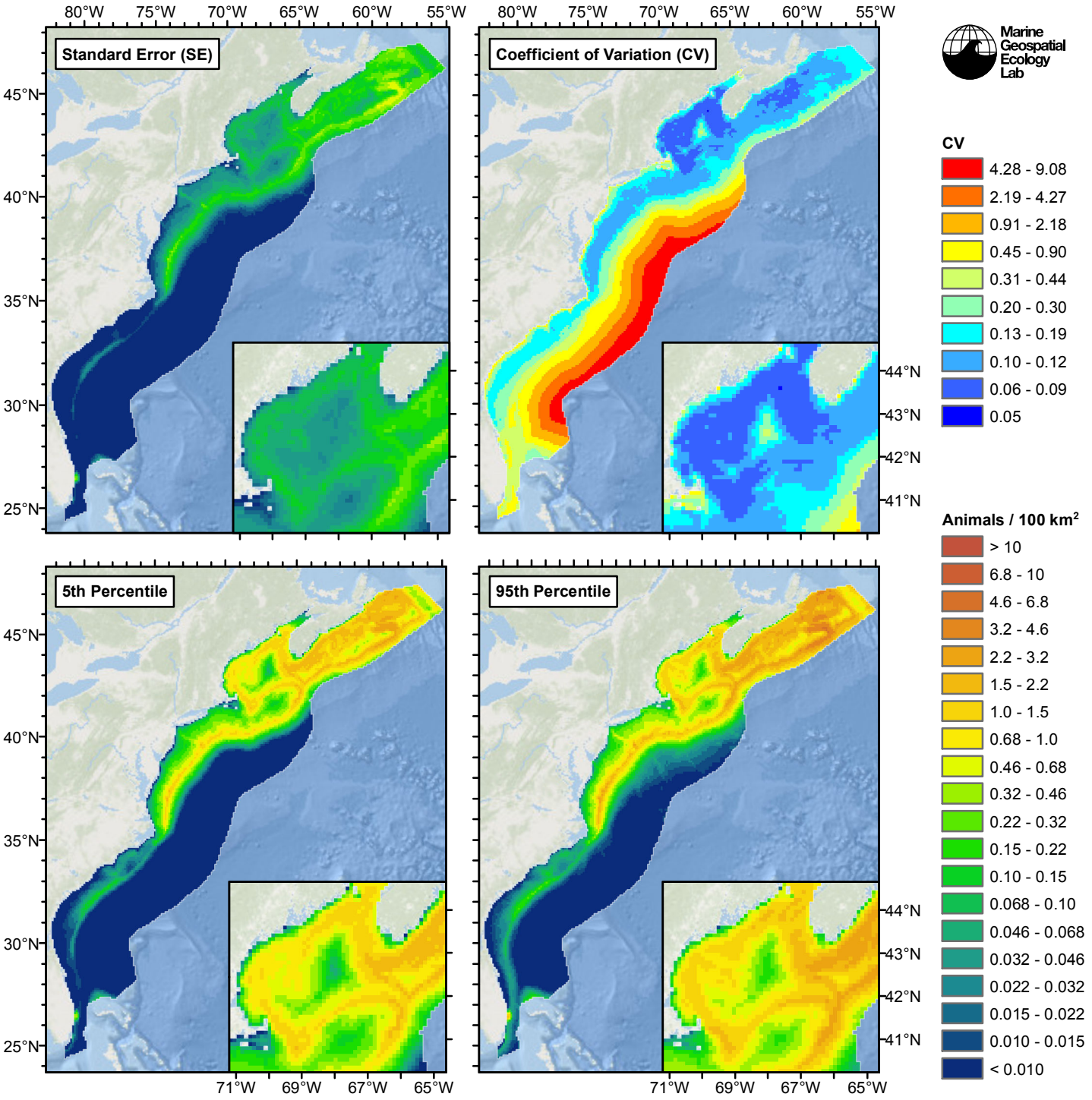

Figure 59: Estimated uncertainty for the contemporaneous model that explained the most deviance. These estimates only incorporate the statistical uncertainty estimated for the spatial model (by the R mgcv package). They do not incorporate uncertainty in the detection functions, g(0) estimates, predictor variables, and so on.

Surveyed Area

Statistical output

```
Rscript.exe: This is mgcv 1.8-3. For overview type 'help("mgcv-package")'.


Family: Tweedie(p=1.182)
```

```
Link function: log

Formula:
abundance ~ offset(log(area_km2)) + s(log10(Depth), bs = "ts",
    k = 5) + s(sqrt(DistToShore/1000), bs = "ts", k = 5) + s(log10(Slope),
    bs = "ts", k = 5) + s(I(DistTo125m/1000), bs = "ts", k = 5) +
    s(I(DistTo300m/1000), bs = "ts", k = 5) + s(SST, bs = "ts",
    k = 5) + s(I(DistToFront2^(1/3)), bs = "ts", k = 5) + s(log10(pmax(TKE,
    1e-04)), bs = "ts", k = 5) + s(log10(pmax(PkPB, 0.01)), bs = "ts",
    k = 5)

Parametric coefficients:
            Estimate Std. Error t value Pr(>|t|)
(Intercept)   -6.831      0.135  -50.59   <2e-16 ***
---
Signif. codes:  0 '***' 0.001 '**' 0.01 '*' 0.05 '.' 0.1 ' ' 1

Approximate significance of smooth terms:
                              edf Ref.df      F  p-value
s(log10(Depth))            3.3571      4 10.487 3.36e-10 ***
s(sqrt(DistToShore/1000))  3.3612      4  8.919 2.51e-08 ***
s(log10(Slope))            1.2460      4  9.133 3.81e-10 ***
s(I(DistTo125m/1000))      3.3985      4 24.795  < 2e-16 ***
s(I(DistTo300m/1000))      1.1550      4 15.949 2.35e-16 ***
s(SST)                     3.5176      4  9.657 1.17e-08 ***
s(I(DistToFront2^(1/3)))   0.9173      4  1.722 0.004890 **
s(log10(pmax(TKE, 1e-04))) 0.9614      4  2.750 0.000522 ***
s(log10(pmax(PkPB, 0.01))) 3.5020      4 48.390  < 2e-16 ***
---
Signif. codes:  0 '***' 0.001 '**' 0.01 '*' 0.05 '.' 0.1 ' ' 1

R-sq.(adj) =  0.0167   Deviance explained = 22.2%
-REML =  11875  Scale est. = 23.844    n = 99937

All predictors were significant. This is the final model.
Creating term plots.
Diagnostic output from gam.check():

Method: REML   Optimizer: outer newton
full convergence after 13 iterations.
Gradient range [-0.0006144122,0.0001825469]
(score 11874.54 & scale 23.84371).
Hessian positive definite, eigenvalue range [0.2942918,8200.162].
Model rank =  37 / 37

Basis dimension (k) checking results. Low p-value (k-index<1) may
indicate that k is too low, especially if edf is close to k'.

                              k'   edf k-index p-value
s(log10(Depth))            4.000 3.357   0.821    0.02
s(sqrt(DistToShore/1000))  4.000 3.361   0.850    0.18
s(log10(Slope))            4.000 1.246   0.842    0.09
s(I(DistTo125m/1000))      4.000 3.398   0.851    0.22
s(I(DistTo300m/1000))      4.000 1.155   0.821    0.03
s(SST)                     4.000 3.518   0.775    0.00
s(I(DistToFront2^(1/3)))   4.000 0.917   0.822    0.02
s(log10(pmax(TKE, 1e-04))) 4.000 0.961   0.815    0.01
s(log10(pmax(PkPB, 0.01))) 4.000 3.502   0.798    0.00
```

```
Predictors retained during the model selection procedure: Depth, DistToShore, Slope, DistTo125m,
DistTo300m, SST, DistToFront2, TKE, PkPB

Predictors dropped during the model selection procedure:
```

Model term plots

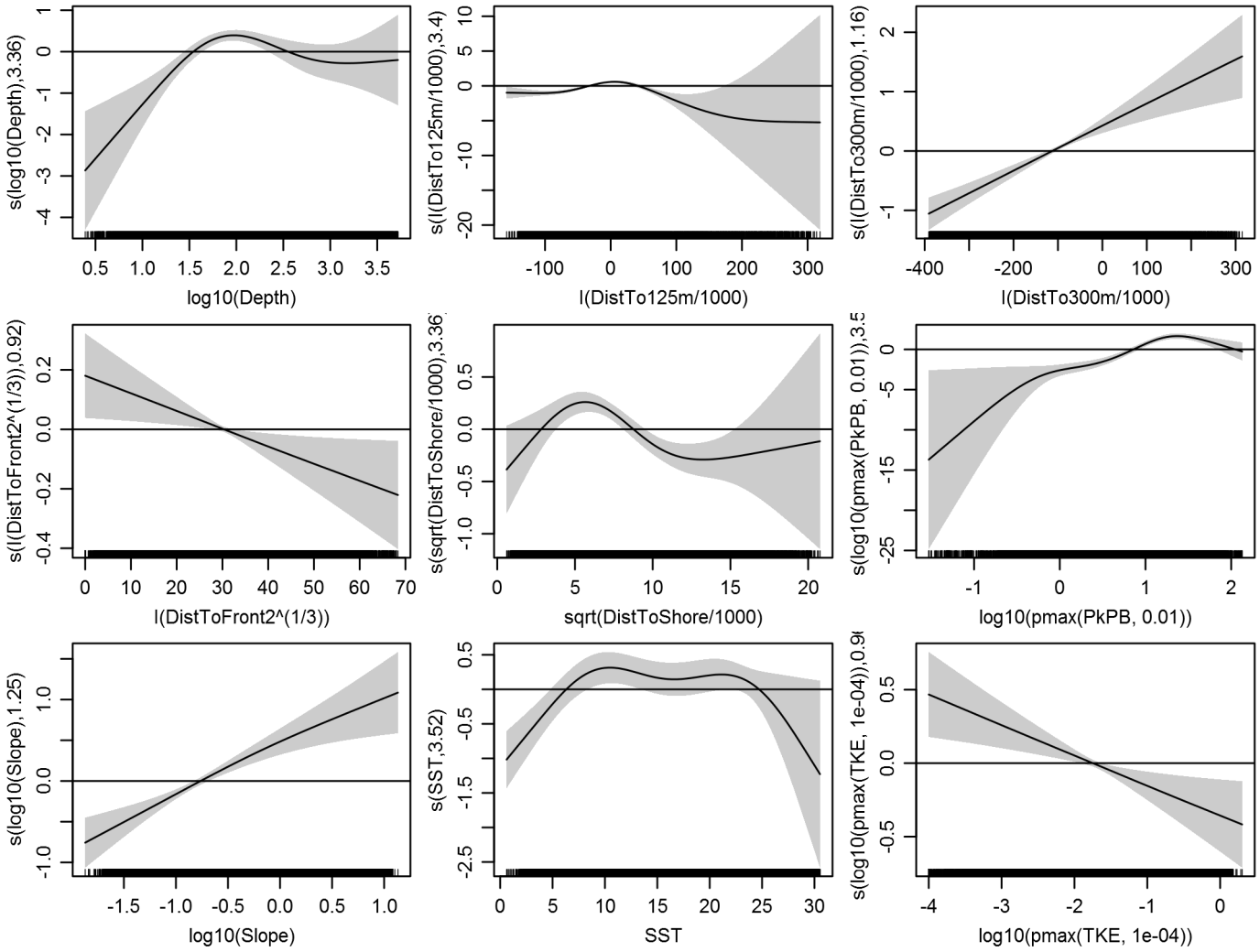

Diagnostic plots

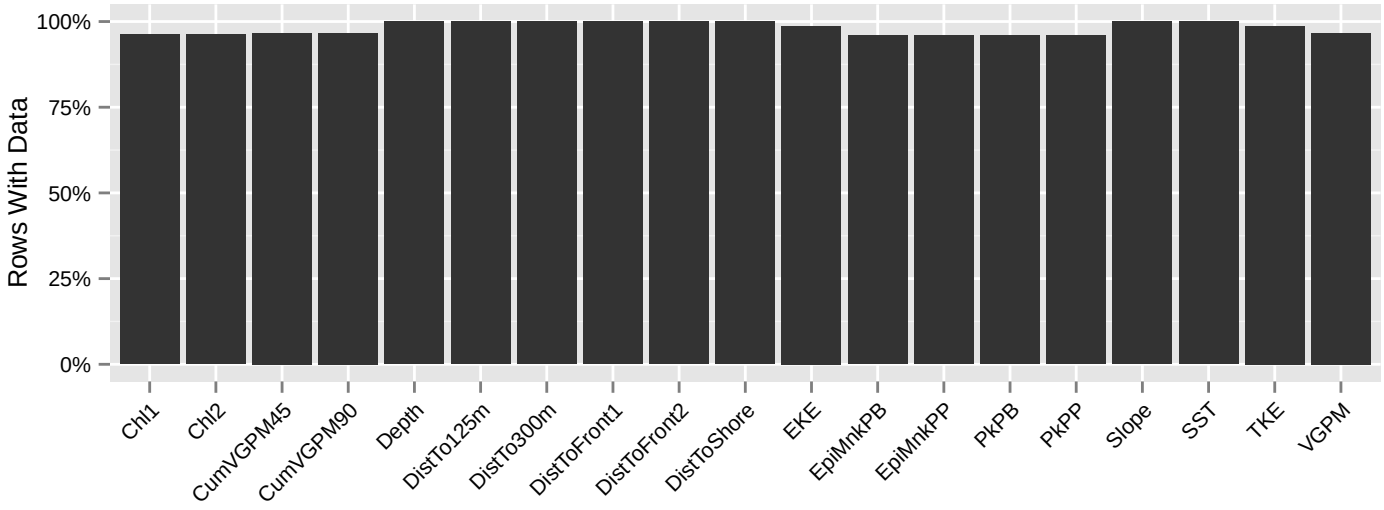

Figure 60: Segments with predictor values for the Fin whale Contemporaneous model, Surveyed Area. This plot is used to assess how many segments would be lost by including a given predictor in a model.

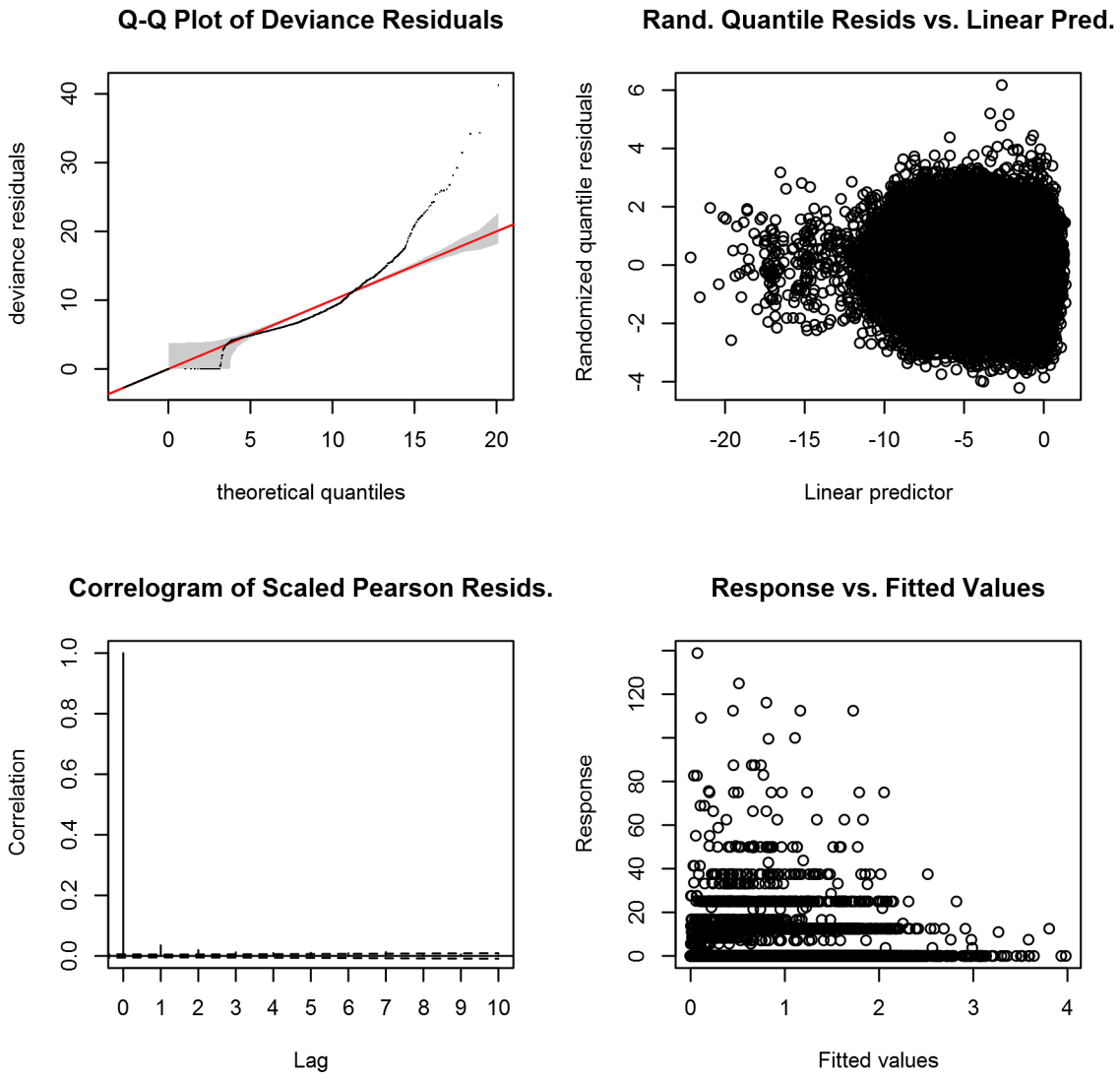

Figure 61: Statistical diagnostic plots for the Fin whale Contemporaneous model, Surveyed Area.

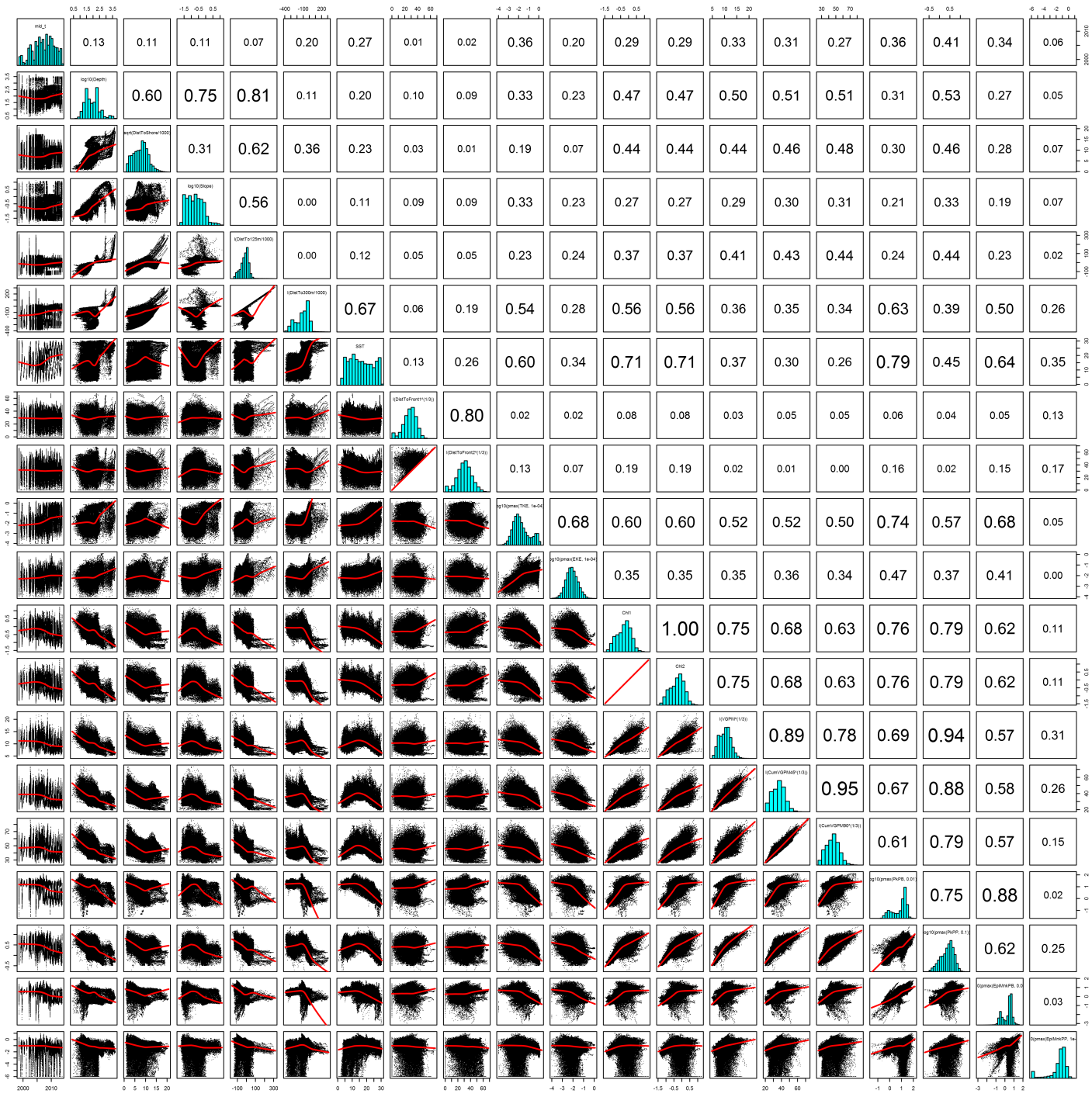

Figure 62: Scatterplot matrix for the Fin whale Contemporaneous model, Surveyed Area. This plot is used to inspect the distribution of predictors (via histograms along the diagonal), simple correlation between predictors (via pairwise Pearson coefficients above the diagonal), and linearity of predictor correlations (via scatterplots below the diagonal). This plot is best viewed at high magnification.

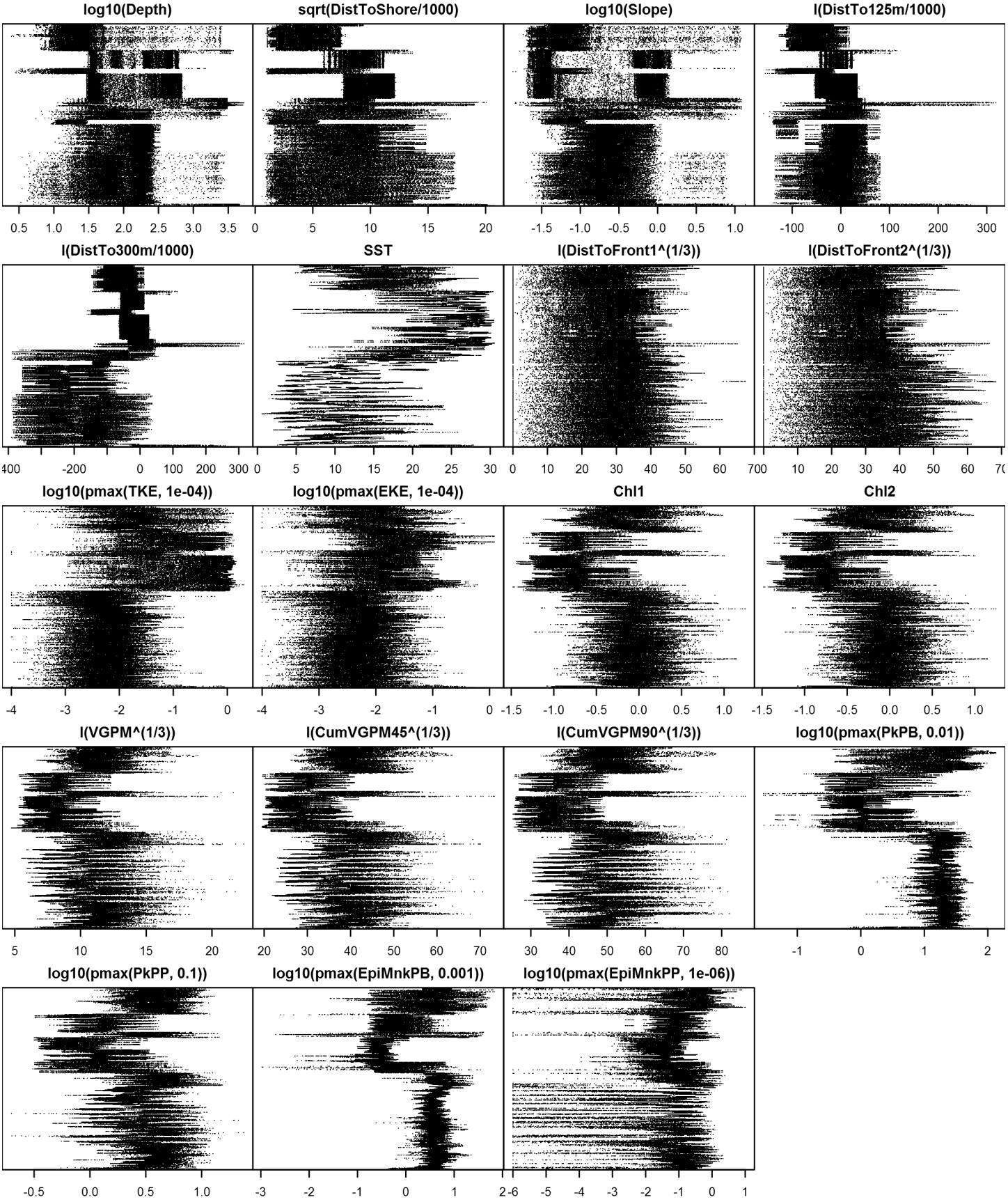

Figure 63: Dotplot for the Fin whale Contemporaneous model, Surveyed Area. This plot is used to check for suspicious patterns and outliers in the data. Points are ordered vertically by transect ID, sequentially in time.

Climatological Same Segments Model

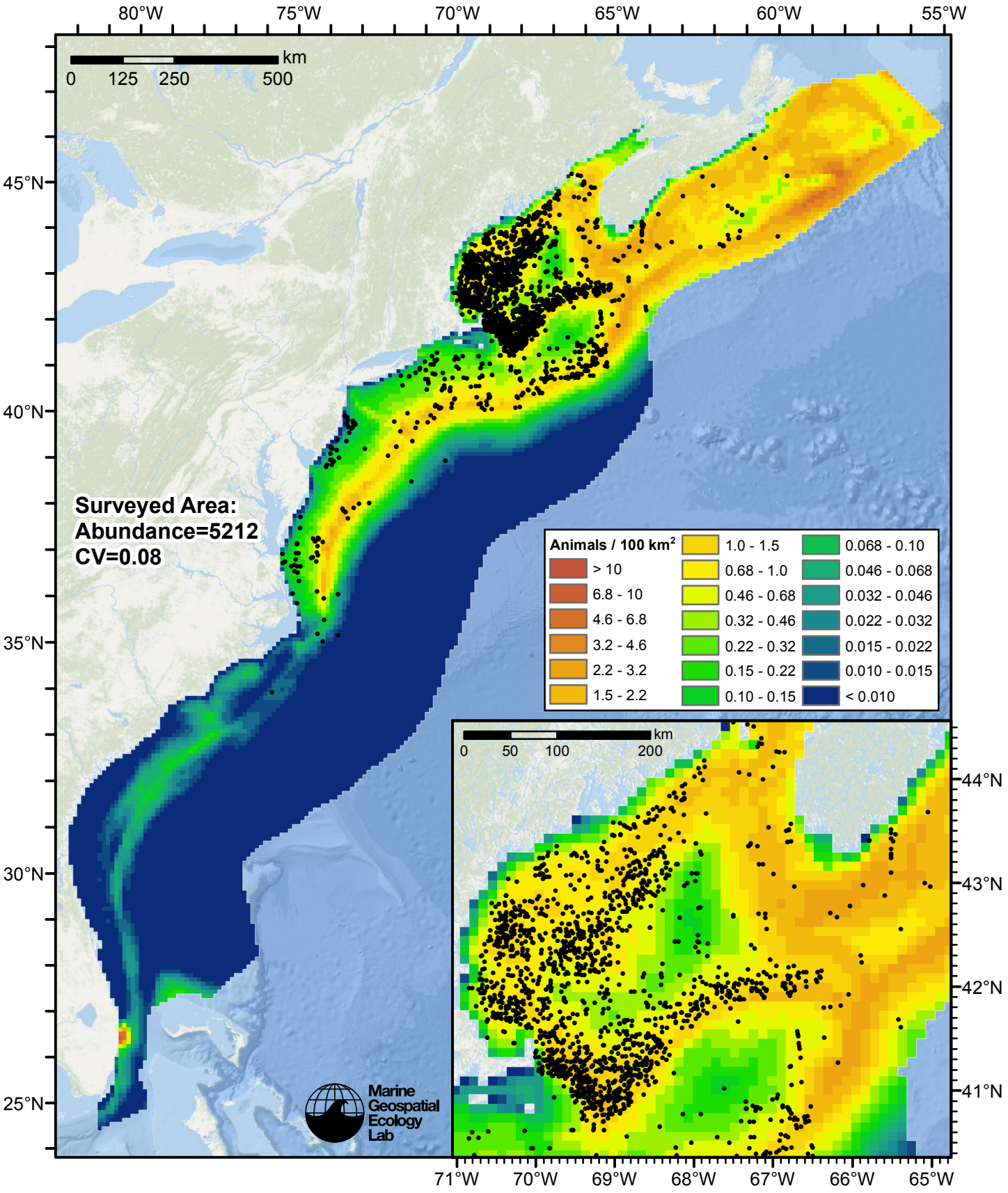

Figure 64: Fin whale density predicted by the climatological same segments model that explained the most deviance. Pixels are 10x10 km. The legend gives the estimated individuals per pixel; breaks are logarithmic. Abundance for each region was computed by summing the density cells occuring in that region.

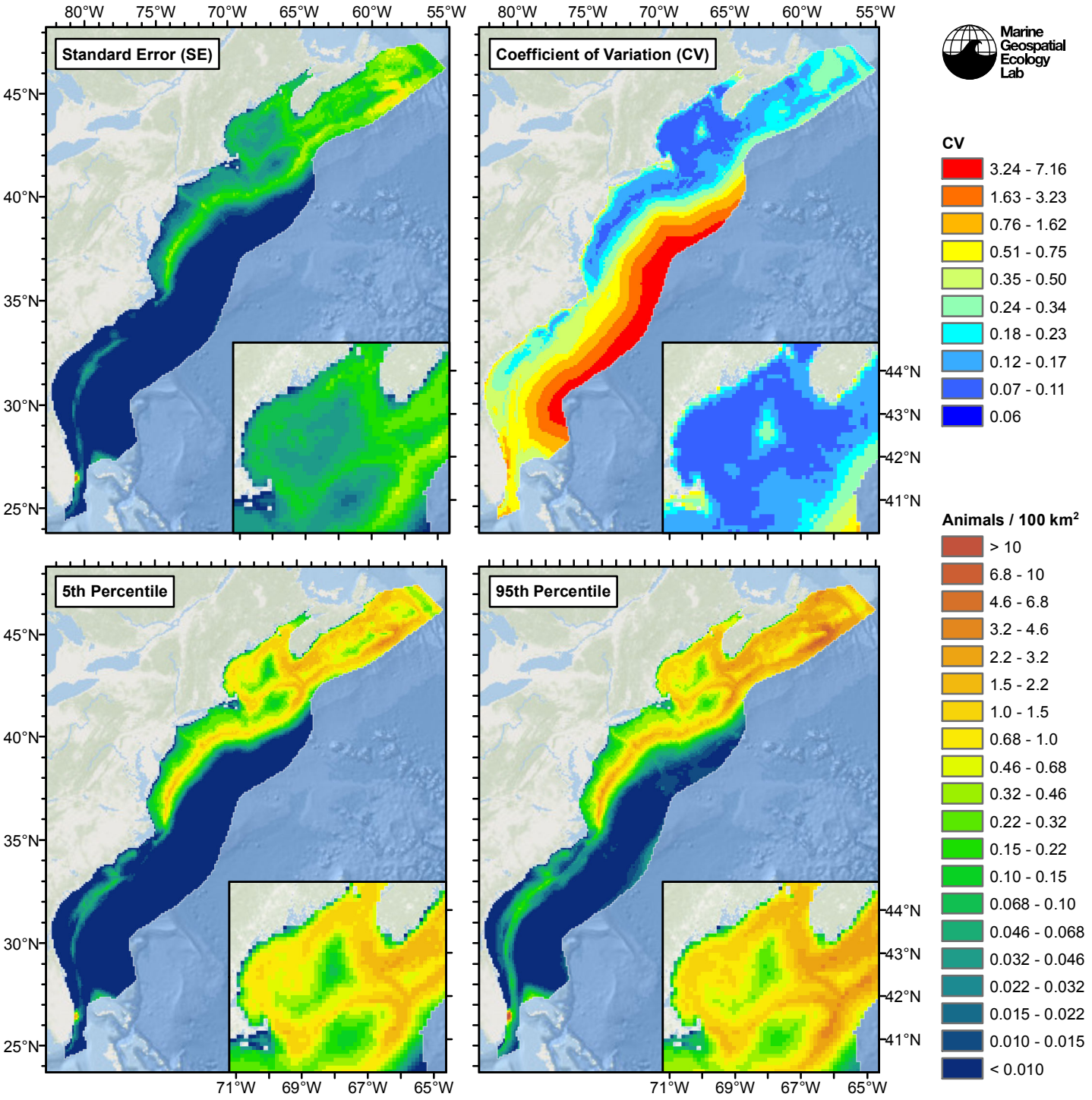

Figure 65: Estimated uncertainty for the climatological same segments model that explained the most deviance. These estimates only incorporate the statistical uncertainty estimated for the spatial model (by the R mgcv package). They do not incorporate uncertainty in the detection functions, g(0) estimates, predictor variables, and so on.

Surveyed Area

Statistical output

```
Rscript.exe: This is mgcv 1.8-3. For overview type 'help("mgcv-package")'.


Family: Tweedie(p=1.182)
```

```
Link function: log

Formula:
abundance ~ offset(log(area_km2)) + s(log10(Depth), bs = "ts",
    k = 5) + s(sqrt(DistToShore/1000), bs = "ts", k = 5) + s(log10(Slope),
    bs = "ts", k = 5) + s(I(DistTo125m/1000), bs = "ts", k = 5) +
    s(I(DistTo300m/1000), bs = "ts", k = 5) + s(ClimSST, bs = "ts",
    k = 5) + s(I(ClimDistToFront1^(1/3)), bs = "ts", k = 5) +
    s(log10(pmax(ClimTKE, 1e-04)), bs = "ts", k = 5) + s(log10(pmax(ClimPkPB,
    0.01)), bs = "ts", k = 5)

Parametric coefficients:
            Estimate Std. Error t value Pr(>|t|)
(Intercept)  -6.8439     0.1259  -54.36   <2e-16 ***
---
Signif. codes:  0 '***' 0.001 '**' 0.01 '*' 0.05 '.' 0.1 ' ' 1

Approximate significance of smooth terms:
                                edf Ref.df      F  p-value
s(log10(Depth))               3.5362      4 13.957 2.65e-13 ***
s(sqrt(DistToShore/1000))     3.3892      4 11.092 2.28e-10 ***
s(log10(Slope))               1.1861      4  8.895 6.81e-10 ***
s(I(DistTo125m/1000))         3.4743      4 22.758  < 2e-16 ***
s(I(DistTo300m/1000))         1.4176      4 22.708  < 2e-16 ***
s(ClimSST)                    0.9072      4  1.558 0.007316 **
s(I(ClimDistToFront1^(1/3)))  3.7558      4 12.054 1.77e-10 ***
s(log10(pmax(ClimTKE, 1e-04))) 3.3064      4  4.299 0.000422 ***
s(log10(pmax(ClimPkPB, 0.01))) 3.3724      4 56.071  < 2e-16 ***
---
Signif. codes:  0 '***' 0.001 '**' 0.01 '*' 0.05 '.' 0.1 ' ' 1

R-sq.(adj) =  0.0167   Deviance explained = 22.7%
-REML =  11860  Scale est. = 23.795    n = 99937

All predictors were significant. This is the final model.
Creating term plots.
Diagnostic output from gam.check():

Method: REML   Optimizer: outer newton
full convergence after 12 iterations.
Gradient range [-0.002400136,0.001286385]
(score 11859.77 & scale 23.79488).
Hessian positive definite, eigenvalue range [0.2284005,8168.818].
Model rank =  37 / 37

Basis dimension (k) checking results. Low p-value (k-index<1) may
indicate that k is too low, especially if edf is close to k'.

                                k'   edf k-index p-value
s(log10(Depth))               4.000 3.536   0.824    0.12
s(sqrt(DistToShore/1000))     4.000 3.389   0.845    0.70
s(log10(Slope))               4.000 1.186   0.810    0.01
s(I(DistTo125m/1000))         4.000 3.474   0.853    0.94
s(I(DistTo300m/1000))         4.000 1.418   0.793    0.00
s(ClimSST)                    4.000 0.907   0.809    0.02
s(I(ClimDistToFront1^(1/3)))  4.000 3.756   0.831    0.22
s(log10(pmax(ClimTKE, 1e-04))) 4.000 3.306   0.800    0.00
s(log10(pmax(ClimPkPB, 0.01))) 4.000 3.372   0.807    0.04
```

```
Predictors retained during the model selection procedure: Depth, DistToShore, Slope, DistTo125m,
DistTo300m, ClimSST, ClimDistToFront1, ClimTKE, ClimPkPB

Predictors dropped during the model selection procedure:
```

Model term plots

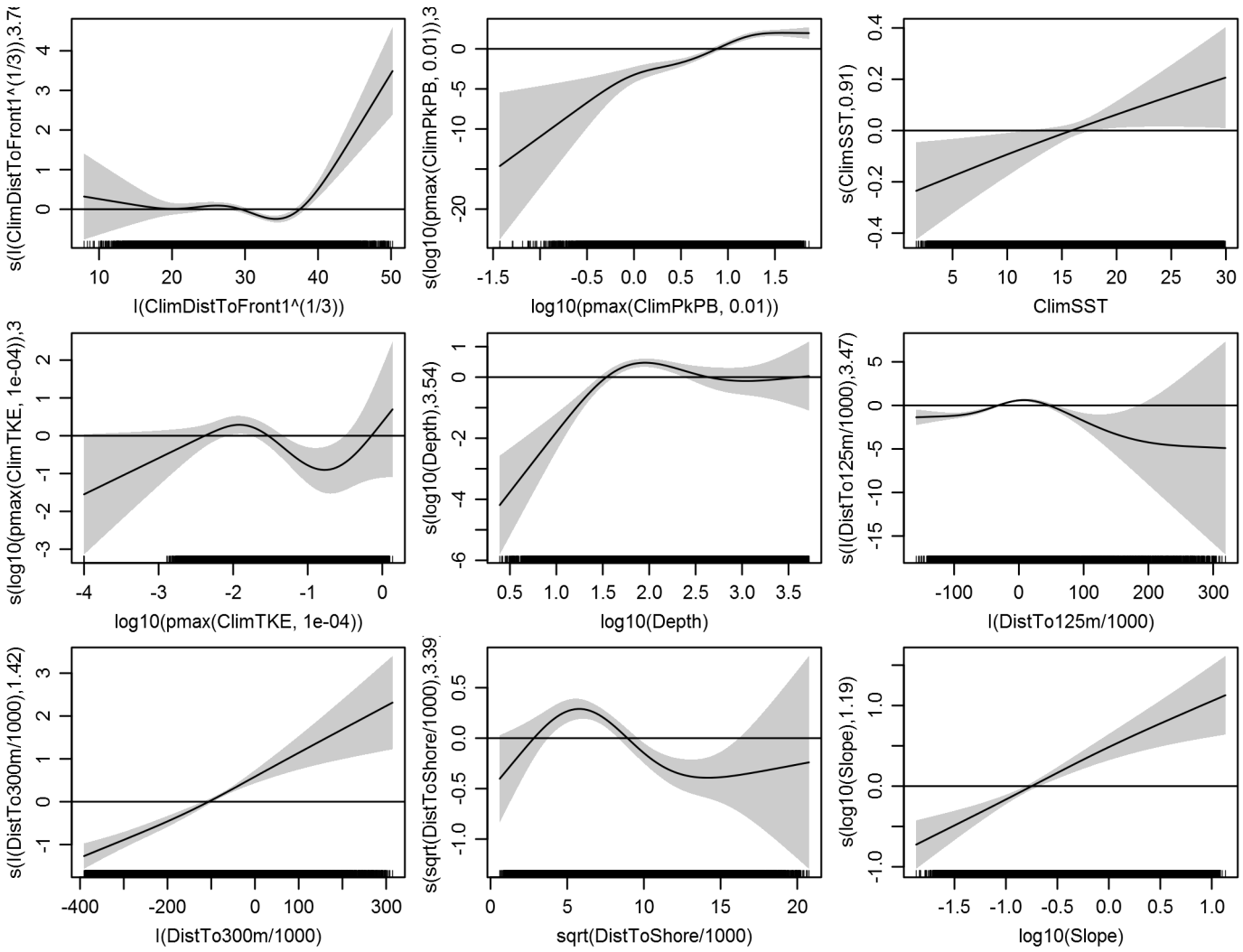

Diagnostic plots

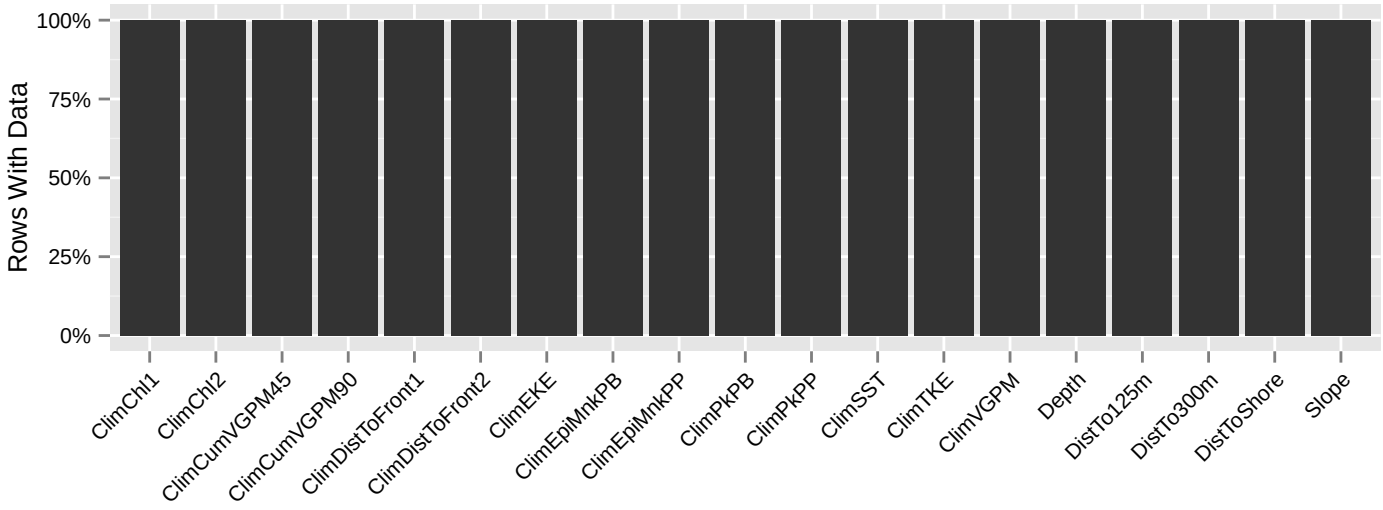

Figure 66: Segments with predictor values for the Fin whale Climatological model, Surveyed Area. This plot is used to assess how many segments would be lost by including a given predictor in a model.

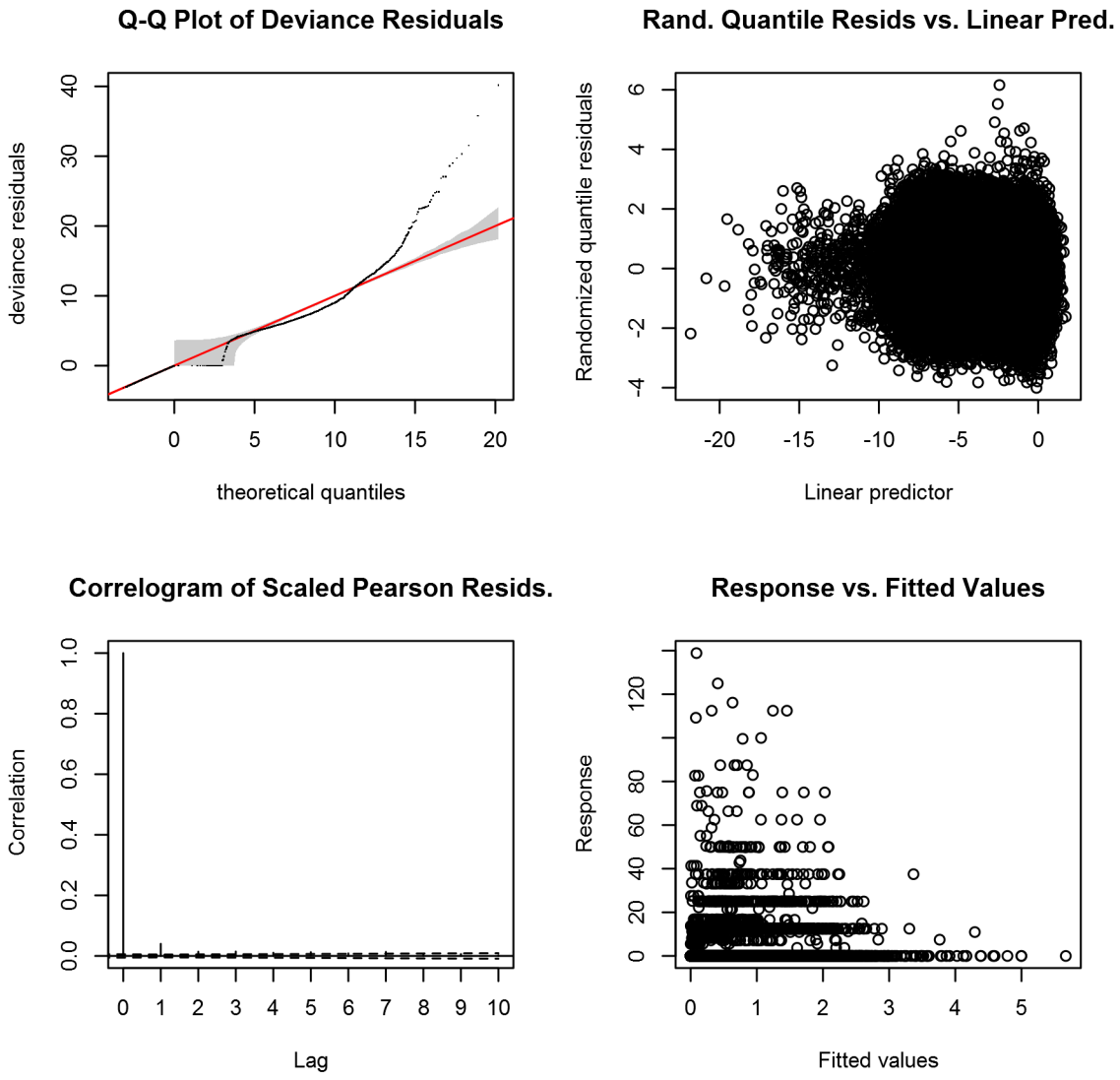

Figure 67: Statistical diagnostic plots for the Fin whale Climatological model, Surveyed Area.

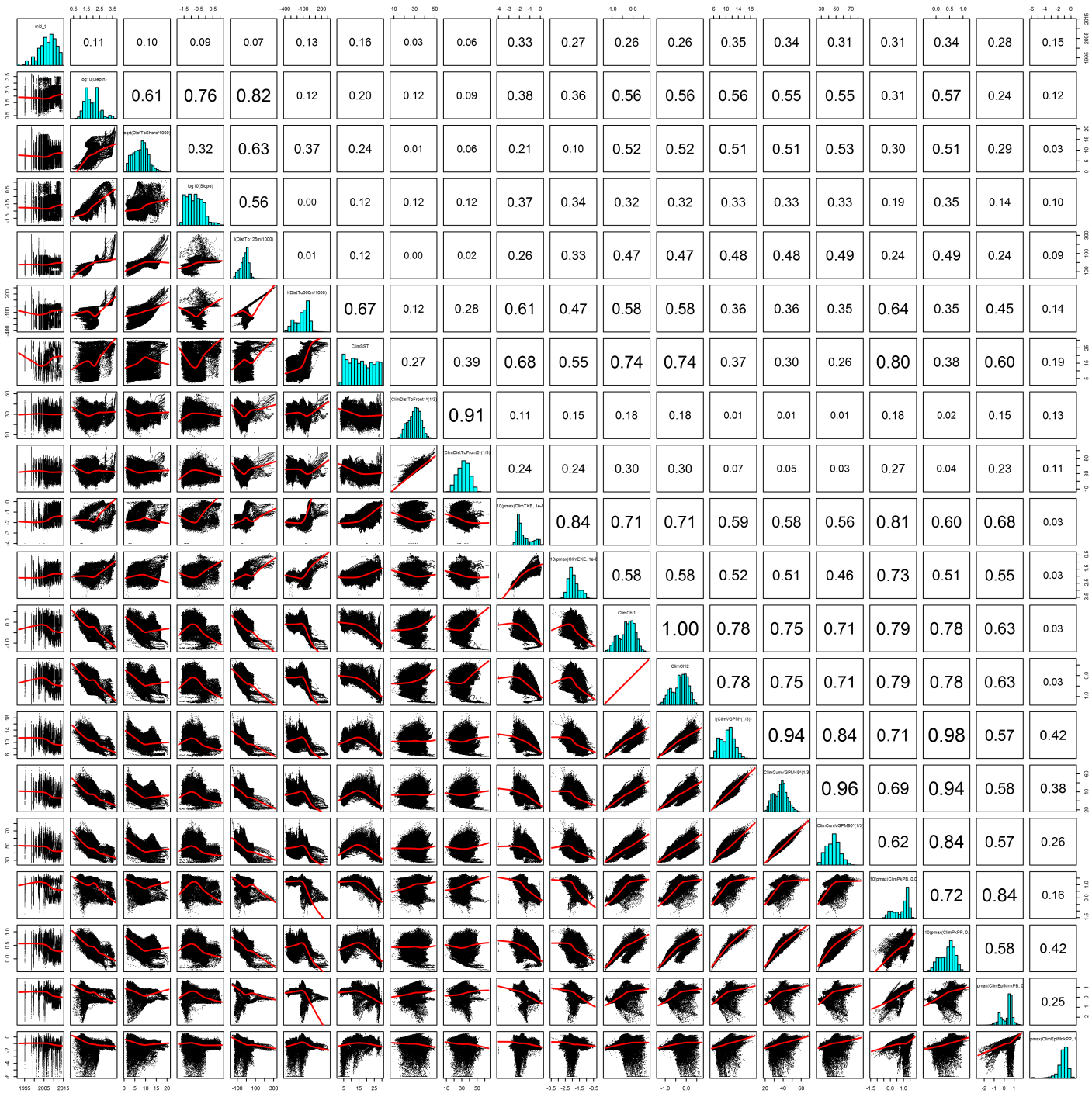

Figure 68: Scatterplot matrix for the Fin whale Climatological model, Surveyed Area. This plot is used to inspect the distribution of predictors (via histograms along the diagonal), simple correlation between predictors (via pairwise Pearson coefficients above the diagonal), and linearity of predictor correlations (via scatterplots below the diagonal). This plot is best viewed at high magnification.

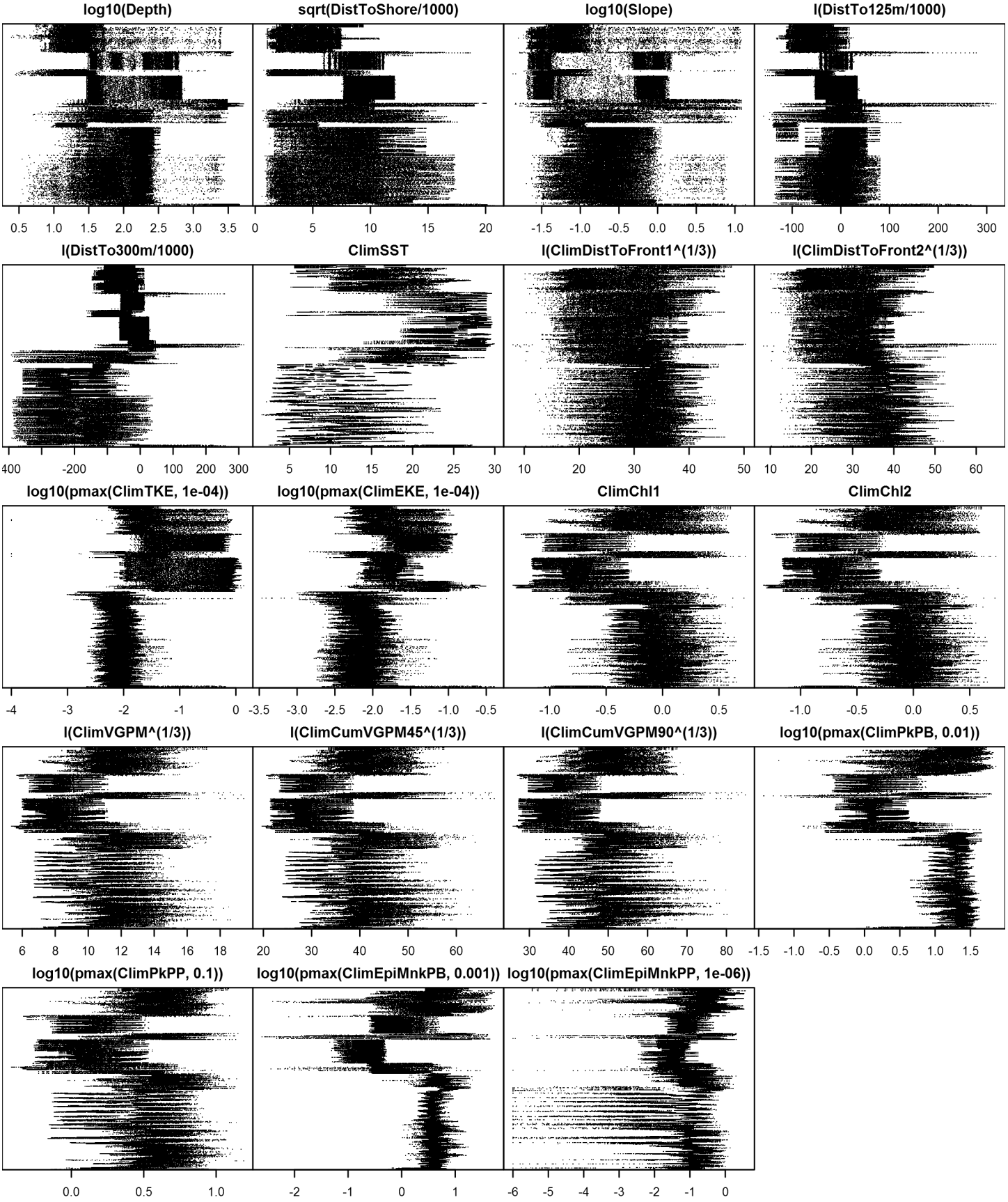

Figure 69: Dotplot for the Fin whale Climatological model, Surveyed Area. This plot is used to check for suspicious patterns and outliers in the data. Points are ordered vertically by transect ID, sequentially in time.

Model Comparison

Spatial Model Performance

The table below summarizes the performance of the candidate spatial models that were tested. The first model contained only physiographic predictors. Subsequent models added additional suites of predictors of based on when they became available via remote sensing.

For each model, three versions were fitted; the % Dev Expl columns give the % deviance explained by each one. The "climatological" models were fitted to 8-day climatologies of the environmental predictors. Because the environmental predictors were always available, no segments were lost, allowing these models to consider the maximal amount of survey data. The "contemporaneous" models were fitted to day-of-sighting images of the environmental predictors; these were smoothed to reduce data loss due to clouds, but some segments still failed to retrieve environmental values and were lost. Finally, the "climatological same segments" models fitted climatological predictors to the segments retained by the contemporaneous model, so that the explantory power of the two types of predictors could be directly compared. For each of the three models, predictors were selected independently via shrinkage smoothers; thus the three models did not necessarily utilize the same predictors.

Predictors derived from ocean currents first became available in January 1993 after the launch of the TOPEX/Poseidon satellite; productivity predictors first became available in September 1997 after the launch of the SeaWiFS sensor. Contemporaneous and climatological same segments models considering these predictors usually suffered data loss. Date Range shows the years spanned by the retained segments. The Segments column gives the number of segments retained; % Lost gives the percentage lost.

Predictors	Climatol % Dev Expl	Contemp % Dev Expl	Climatol Same Segs % Dev Expl	Segments	% Lost	Date Range
Phys	17.6			104236		1992-2014
Phys+SST	20.5	20.0	20.5	104236	0.0	1992-2014
Phys+SST+Curr	21.9	20.8	21.7	102911	1.3	1995-2013
Phys+SST+Curr+Prod	23.2	22.2	22.7	99937	4.1	1998-2013

Table 32: Deviance explained by the candidate density models.

Abundance Estimates

The table below shows the estimated mean abundance (number of animals) within the study area, for the models that explained the most deviance for each model type. Mean abundance was calculated by first predicting density maps for a series of time steps, then computing the abundance for each map, and then averaging the abundances. For the climatological models, we used 8-day climatologies, resulting in 46 abundance maps. For the contemporaneous models, we used daily images, resulting in 365 predicted abundance maps per year that the prediction spanned. The Dates column gives the dates to which the estimates apply. For our models, these are the years for which both survey data and remote sensing data were available.

The Assumed g(0)=1 column specifies whether the abundance estimate assumed that detection was certain along the survey trackline. Studies that assumed this did not correct for availability or perception bias, and therefore underestimated abundance. The In our models column specifies whether the survey data from the study was also used in our models. If not, the study provides a completely independent estimate of abundance.

Dates	Model or study	Estimated abundance	CV	Assumed g(0)=1	In our models
1992-2014	Climatological model*	4633	0.08	No	
1998-2013	Contemporaneous model	5105	0.06	No	
1992-2014	Climatological same segments model	5212	0.08	No	

Jun-Aug 2011	Central Virginia to lower Bay of Fundy (Waring et al. 2014)	1595	0.33	No	No
Jun-Aug 2011	Central Florida to central Virginia (Waring et al. 2014)	23	0.76	No	No
Jun-Aug 2011	Central Florida to lower Bay of Fundy, combined	1618	0.33	No	No
Jul-Aug 2007	Scotian Shelf to Northern Labrador (Lawson and Gosselin 2011)	3522	0.27	No	No
August 2006	Southern Gulf of Maine to Bay of Fundy and Gulf of St. Lawrence (Waring et al. 2014)	2269	0.37	No	Yes
Jun-Aug 2004	Maryland to Bay of Fundy (Waring et al. 2007)	1925	0.55	No	Yes
Aug 2002	Southern Gulf of Maine to Maine (Palka 2006)	2933	0.49	No	Yes

Table 33: Estimated mean abundance within the study area. We selected the model marked with * as our best estimate of the abundance and distribution of this taxon. For comparison, independent abundance estimates from NOAA technical reports and/or the scientific literature are shown. Please see the Discussion section below for our evaluation of our models compared to the other estimates. Note that our abundance estimates are averaged over the whole year, while the other studies may have estimated abundance for specific months or seasons. Our coefficients of variation (CVs) underestimate the true uncertainty in our estimates, as they only incorporated the uncertainty of the GAM stage of our models. Other sources of uncertainty include the detection functions and g(0) estimates. It was not possible to incorporate these into our CVs without undertaking a computationally-prohibitive bootstrap; we hope to attempt that in a future version of our models.

Density Maps

Climatological Model

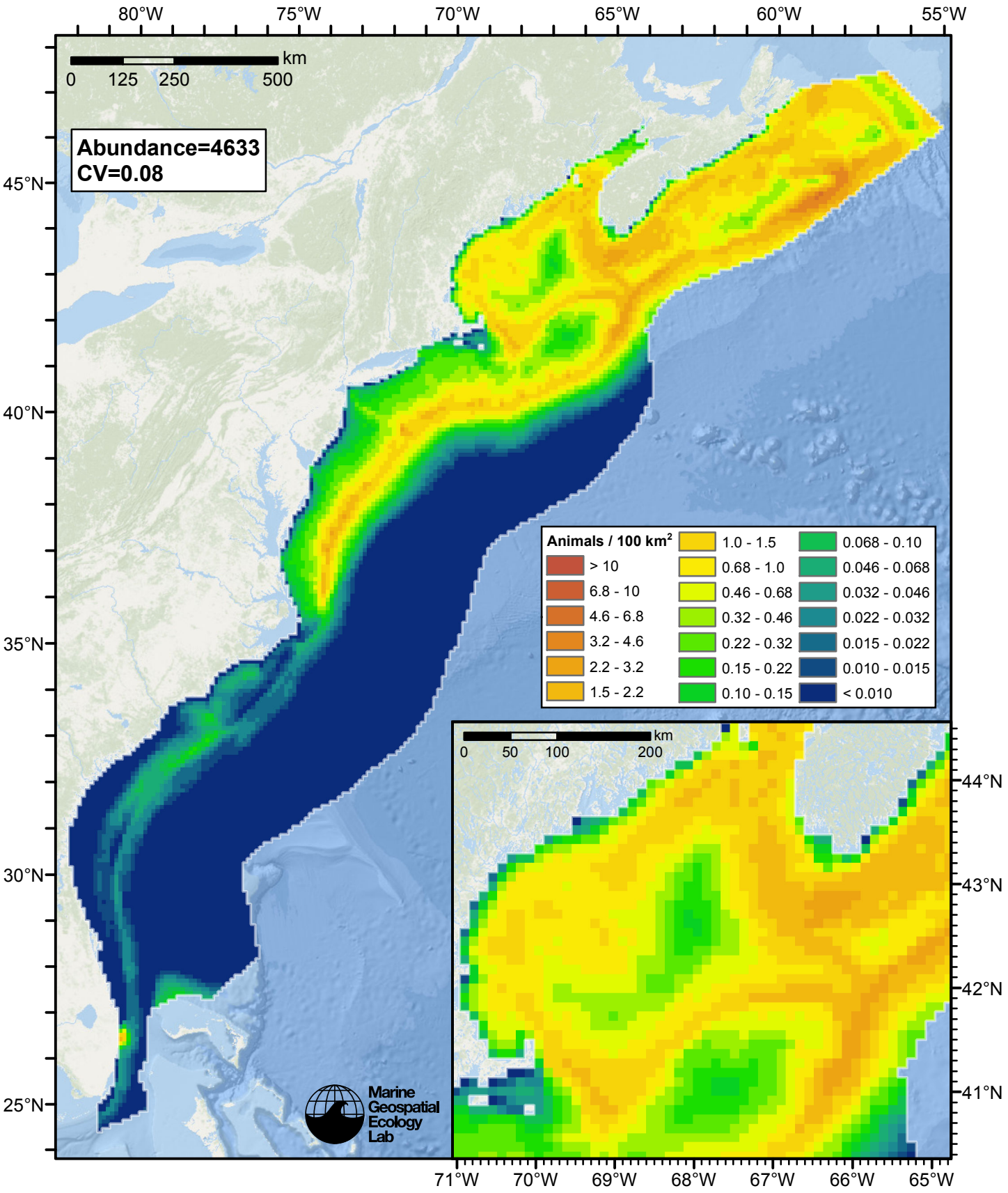

Figure 70: Fin whale density and abundance predicted by the climatological model that explained the most deviance. Regions inside the study area (white line) where the background map is visible are areas we did not model (see text).

Contemporaneous Model

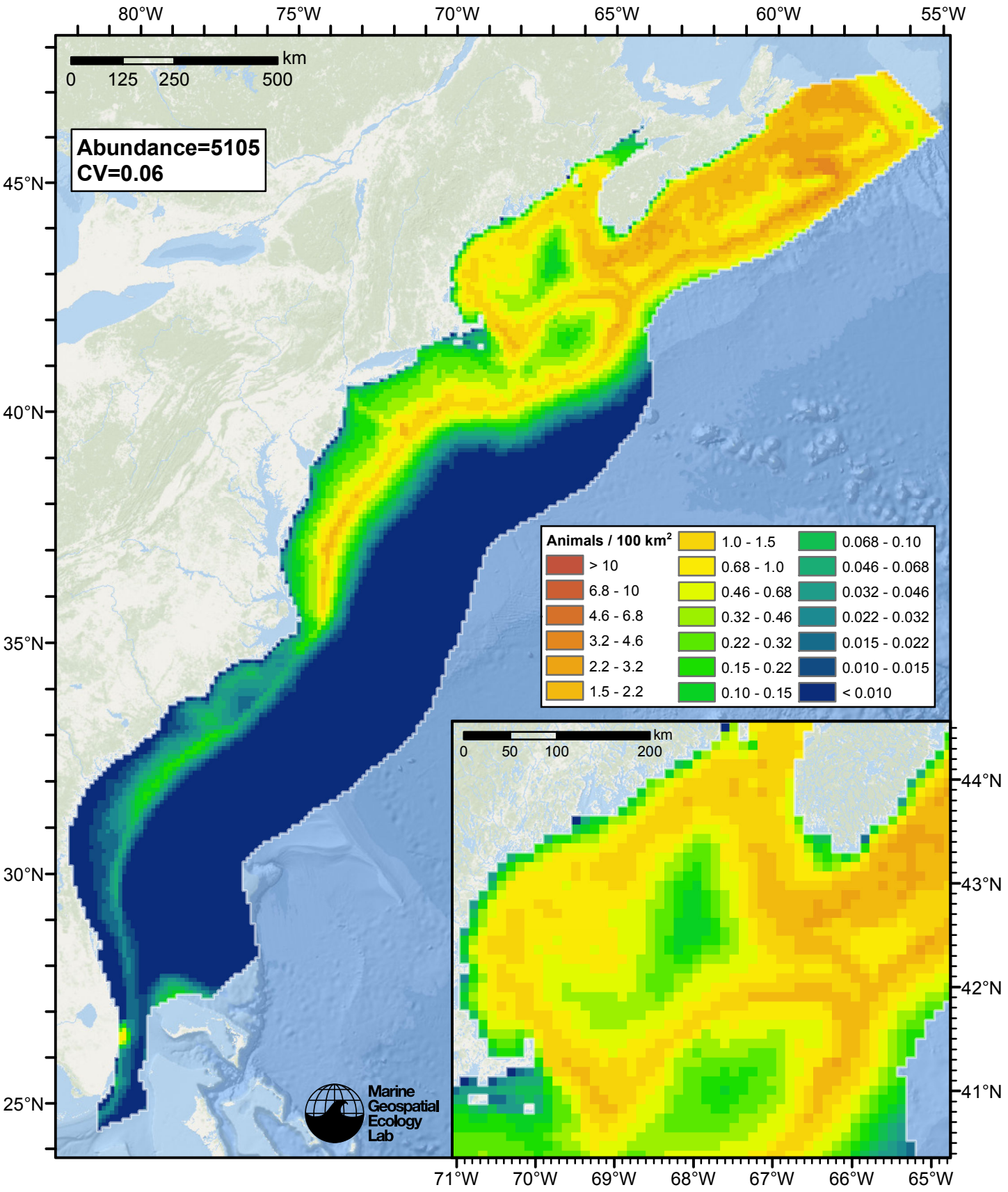

Figure 71: Fin whale density and abundance predicted by the contemporaneous model that explained the most deviance. Regions inside the study area (white line) where the background map is visible are areas we did not model (see text).

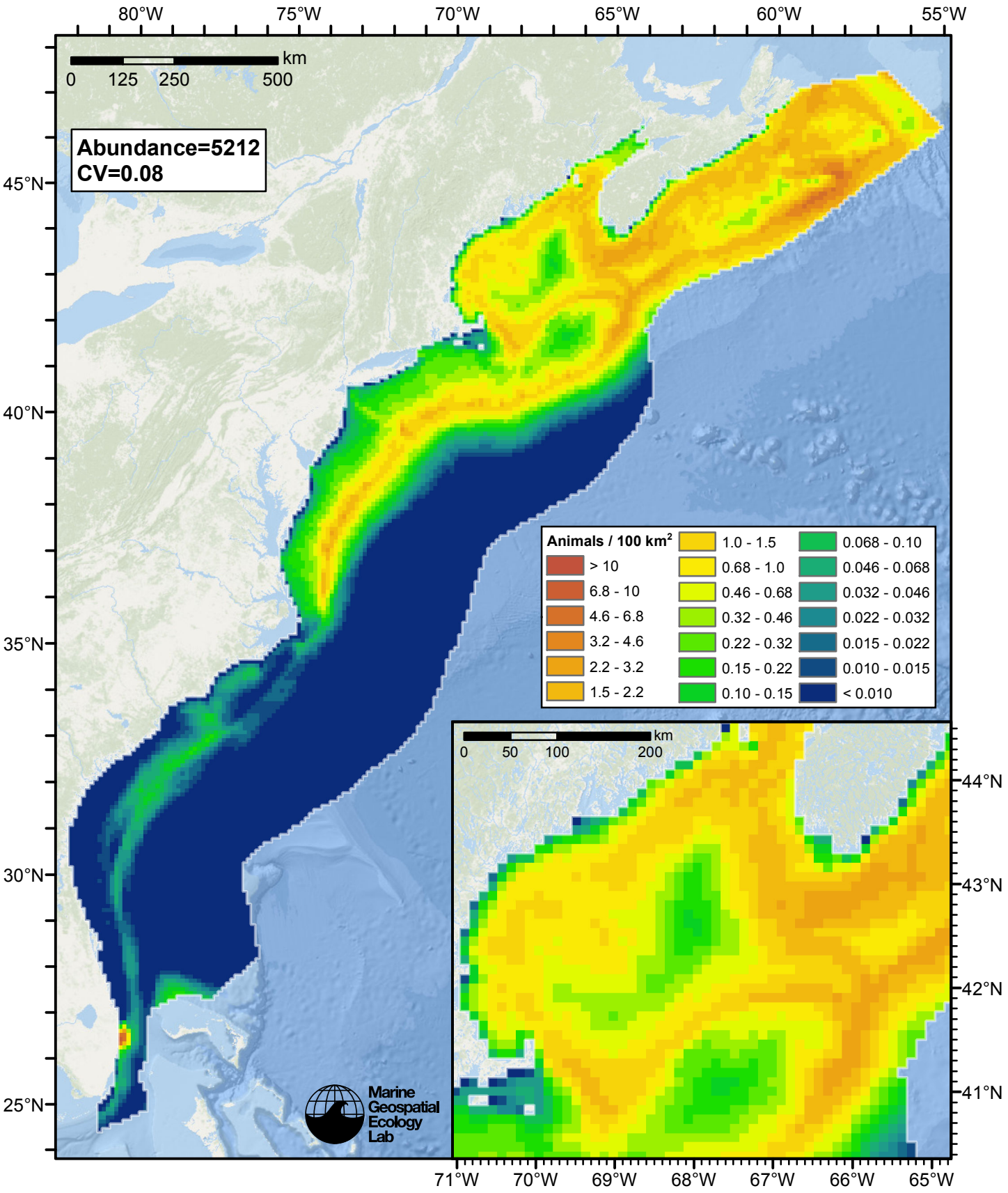

Figure 72: Fin whale density and abundance predicted by the climatological same segments model that explained the most deviance. Regions inside the study area (white line) where the background map is visible are areas we did not model (see text).

Temporal Variability

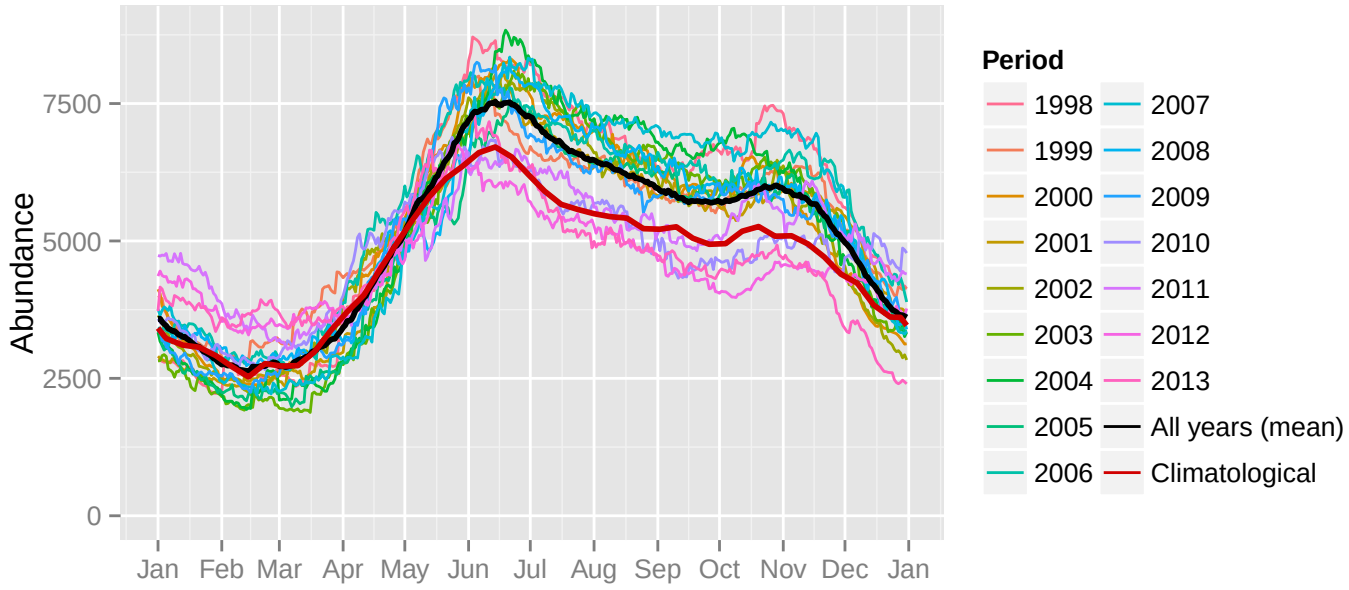

Figure 73: Comparison of Fin whale abundance predicted at a daily time step for different time periods. Individual years were predicted using contemporaneous models. "All years (mean)" averages the individual years, giving the mean annual abundance of the contemporaneous model. "Climatological" was predicted using the climatological model. The results for the climatological same segments model are not shown.

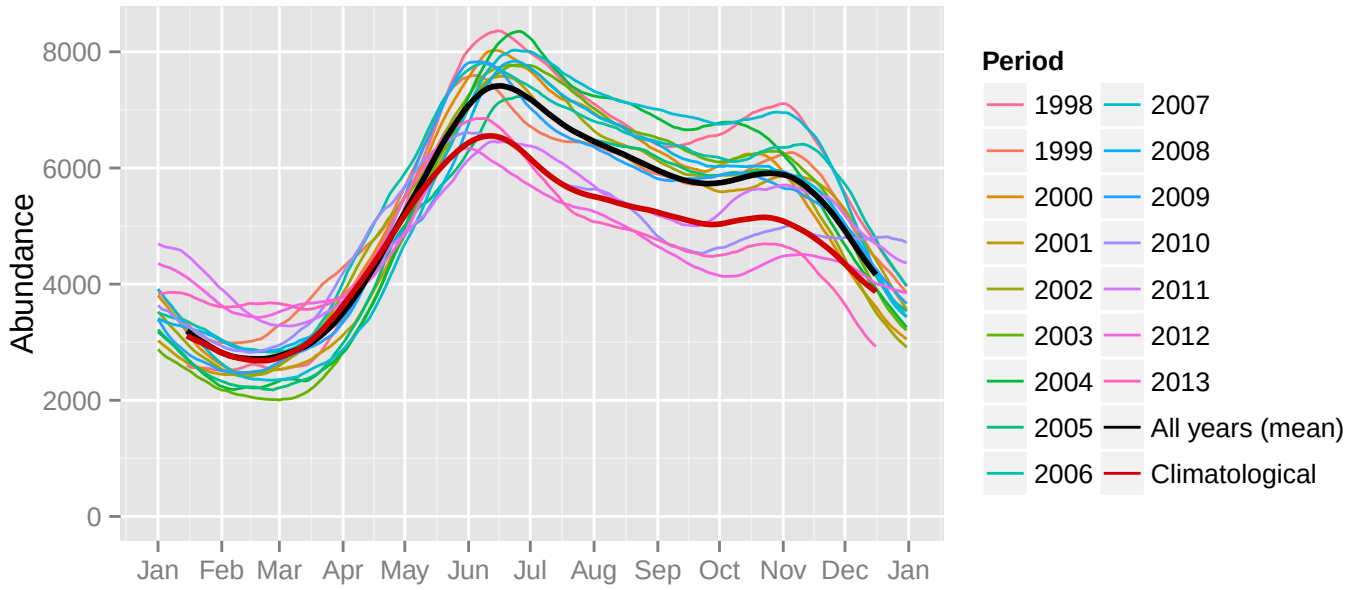

Figure 74: The same data as the preceding figure, but with a 30-day moving average applied.

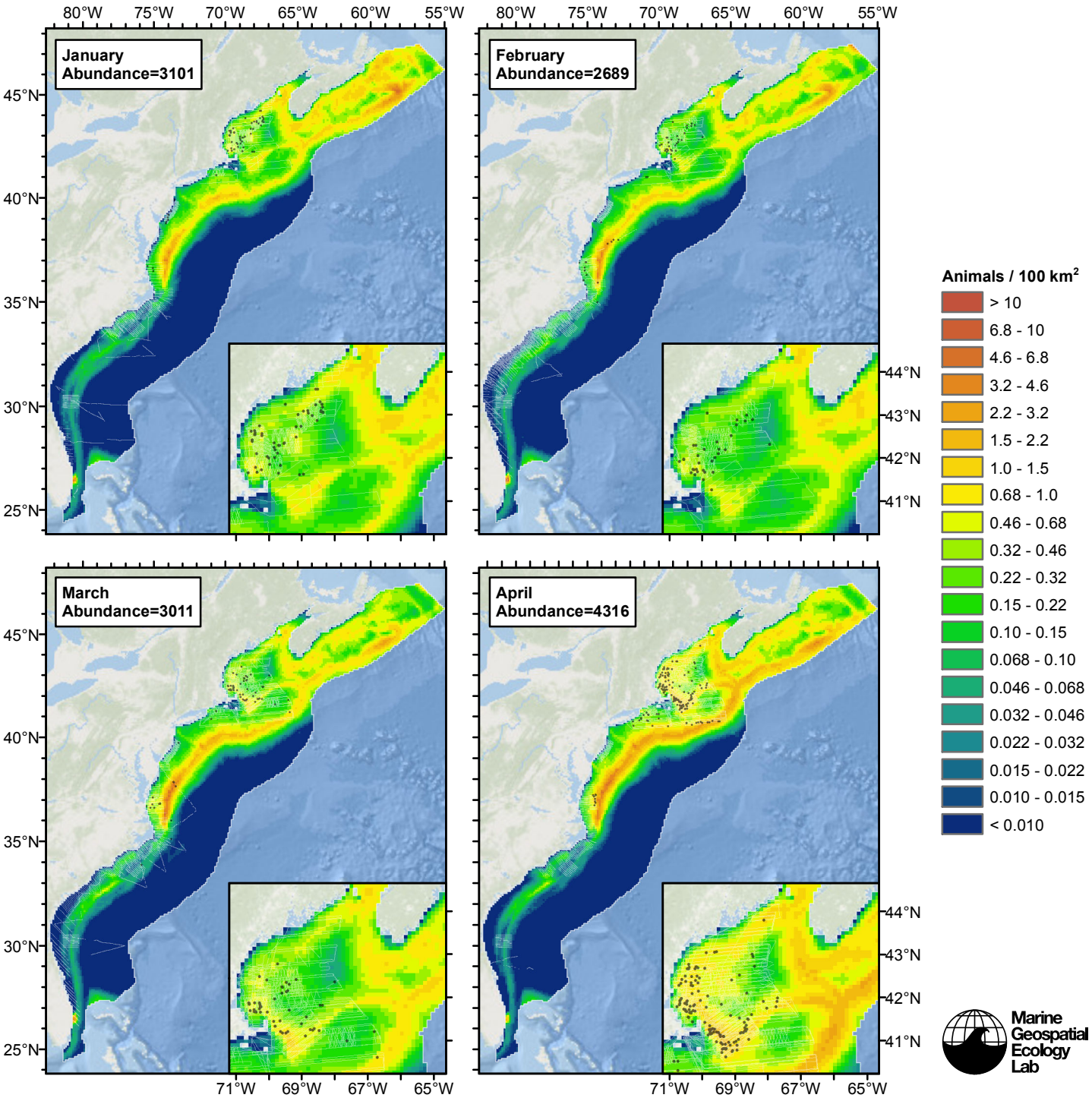
January
Abundance=3101
February
Abundance=2689
March
Abundance=3011
April
Abundance=4316
80°W
75°W
70°W
65°W
60°W
55°W
45°N
40°N
35°N
30°N
25°N
44°N
43°N
42°N
41°N
71°W
69°W
67°W
65°W
Animals / 100 km²
> 10
6.8 - 10
4.6 - 6.8
3.2 - 4.6
2.2 - 3.2
1.5 - 2.2
1.0 - 1.5
0.68 - 1.0
0.46 - 0.68
0.32 - 0.46
0.22 - 0.32
0.15 - 0.22
0.10 - 0.15
0.068 - 0.10
0.046 - 0.068
0.032 - 0.046
0.022 - 0.032
0.015 - 0.022
0.010 - 0.015
< 0.010
Marine
Geospatial
Ecology
Lab

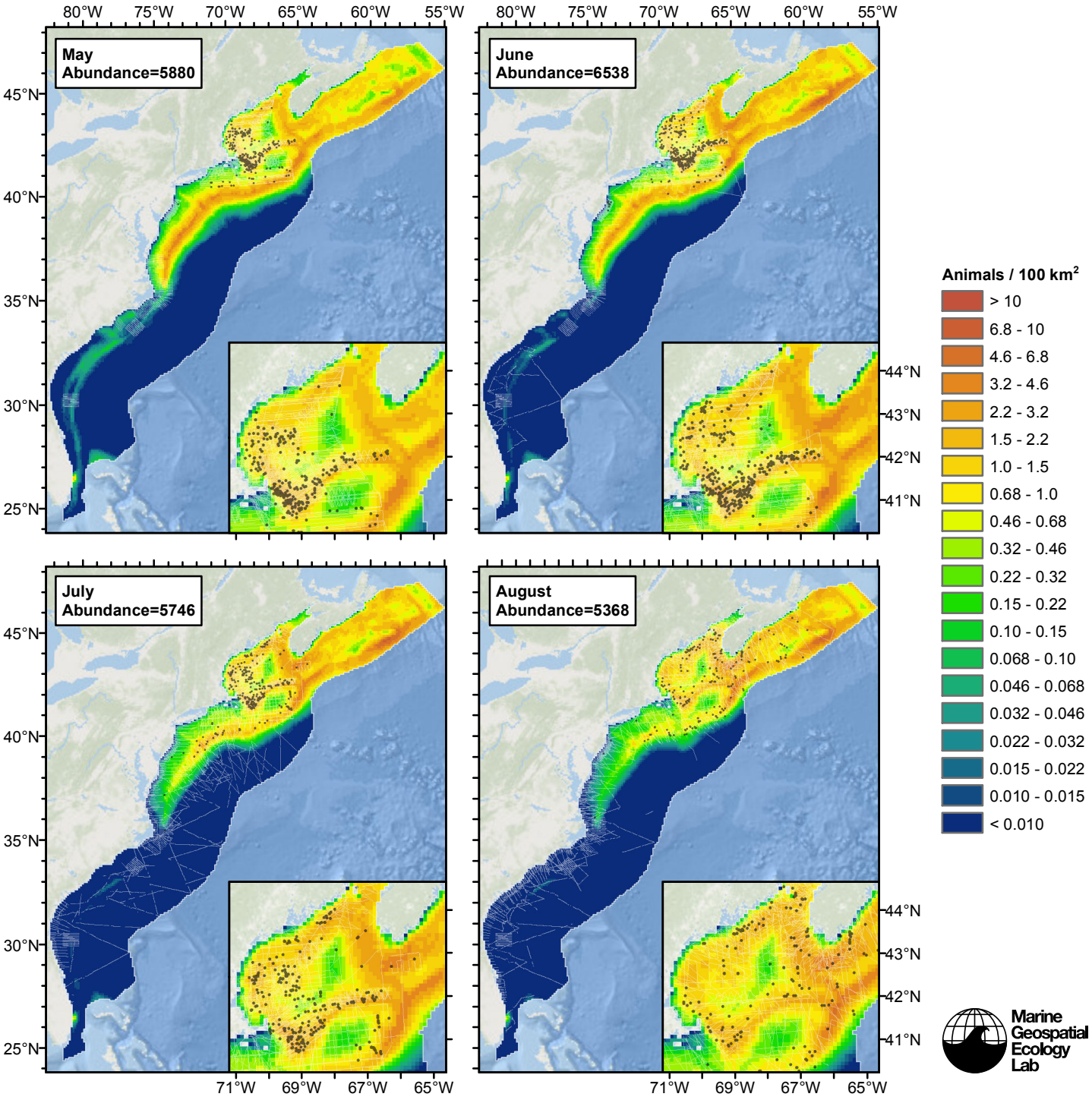
May
Abundance=5880
June
Abundance=6538
July
Abundance=5746
August
Abundance=5368
80°W
75°W
70°W
65°W
60°W
55°W
45°N
40°N
35°N
30°N
25°N
44°N
43°N
42°N
41°N
71°W
69°W
67°W
65°W
Animals / 100 km²
> 10
6.8 - 10
4.6 - 6.8
3.2 - 4.6
2.2 - 3.2
1.5 - 2.2
1.0 - 1.5
0.68 - 1.0
0.46 - 0.68
0.32 - 0.46
0.22 - 0.32
0.15 - 0.22
0.10 - 0.15
0.068 - 0.10
0.046 - 0.068
0.032 - 0.046
0.022 - 0.032
0.015 - 0.022
0.010 - 0.015
< 0.010
Marine
Geospatial
Ecology
Lab

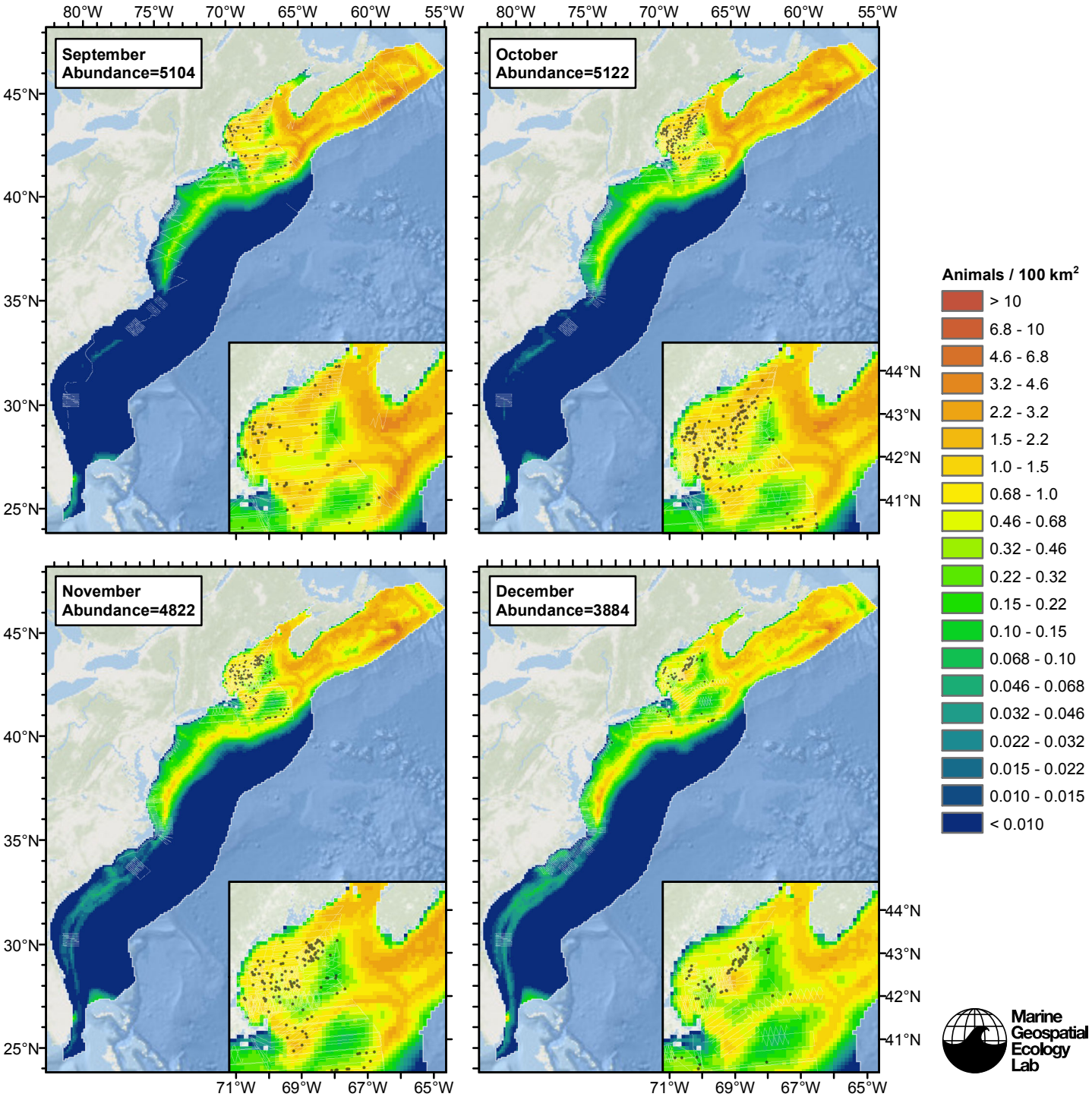
September
Abundance=5104
October
Abundance=5122
November
Abundance=4822
December
Abundance=3884
80°W
75°W
70°W
65°W
60°W
55°W
45°N
40°N
35°N
30°N
25°N
44°N
43°N
42°N
41°N
71°W
69°W
67°W
65°W
Animals / 100 km²
> 10
6.8 - 10
4.6 - 6.8
3.2 - 4.6
2.2 - 3.2
1.5 - 2.2
1.0 - 1.5
0.68 - 1.0
0.46 - 0.68
0.32 - 0.46
0.22 - 0.32
0.15 - 0.22
0.10 - 0.15
0.068 - 0.10
0.046 - 0.068
0.032 - 0.046
0.022 - 0.032
0.015 - 0.022
0.010 - 0.015
< 0.010
Marine
Geospatial
Ecology
Lab

Contemporaneous Model

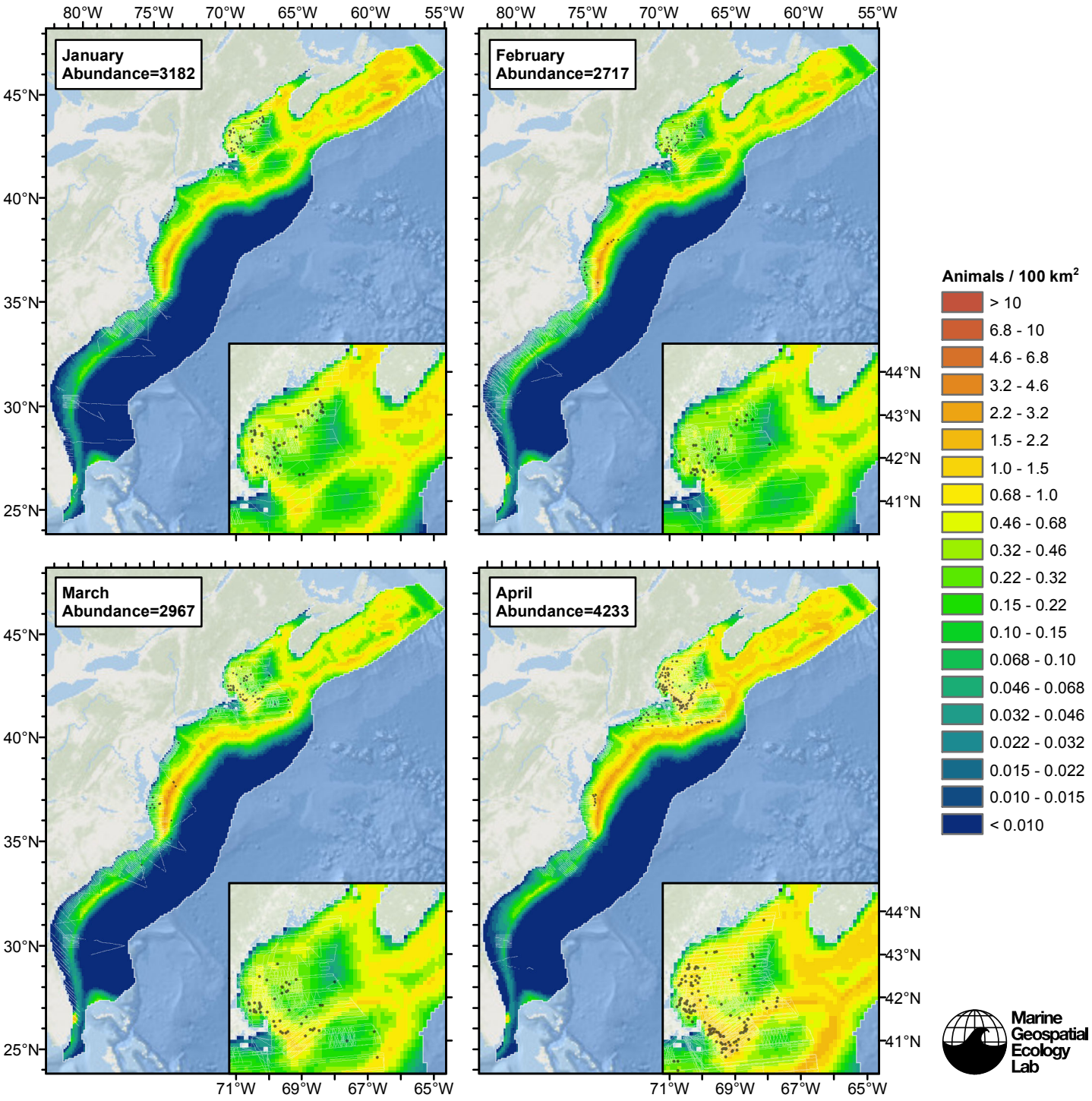

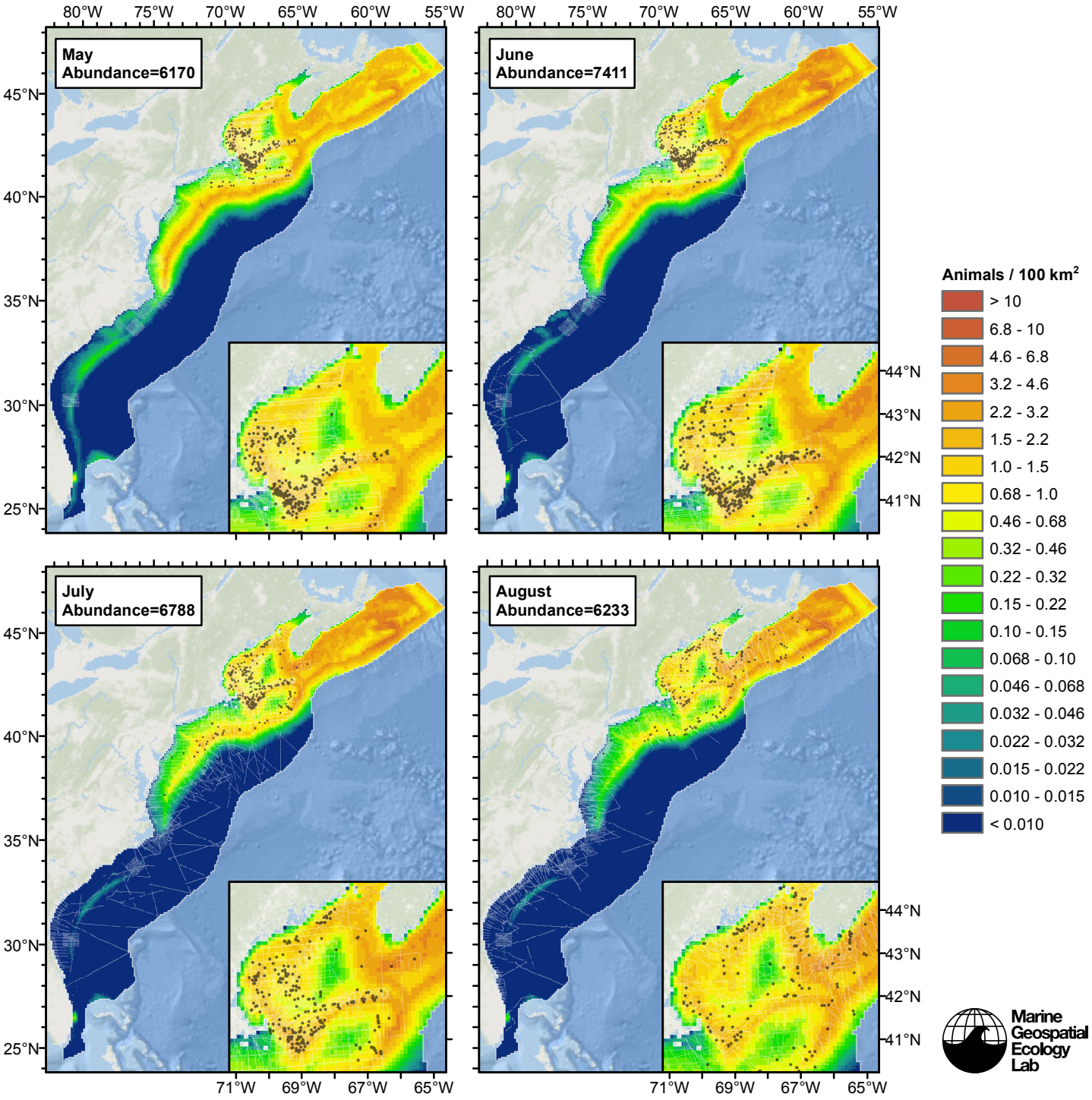
May
Abundance=6170
June
Abundance=7411
July
Abundance=6788
August
Abundance=6233
80°W
75°W
70°W
65°W
60°W
55°W
45°N
40°N
35°N
30°N
25°N
44°N
43°N
42°N
41°N
71°W
69°W
67°W
65°W
Animals / 100 km²
> 10
6.8 - 10
4.6 - 6.8
3.2 - 4.6
2.2 - 3.2
1.5 - 2.2
1.0 - 1.5
0.68 - 1.0
0.46 - 0.68
0.32 - 0.46
0.22 - 0.32
0.15 - 0.22
0.10 - 0.15
0.068 - 0.10
0.046 - 0.068
0.032 - 0.046
0.022 - 0.032
0.015 - 0.022
0.010 - 0.015
< 0.010
Marine
Geospatial
Ecology
Lab

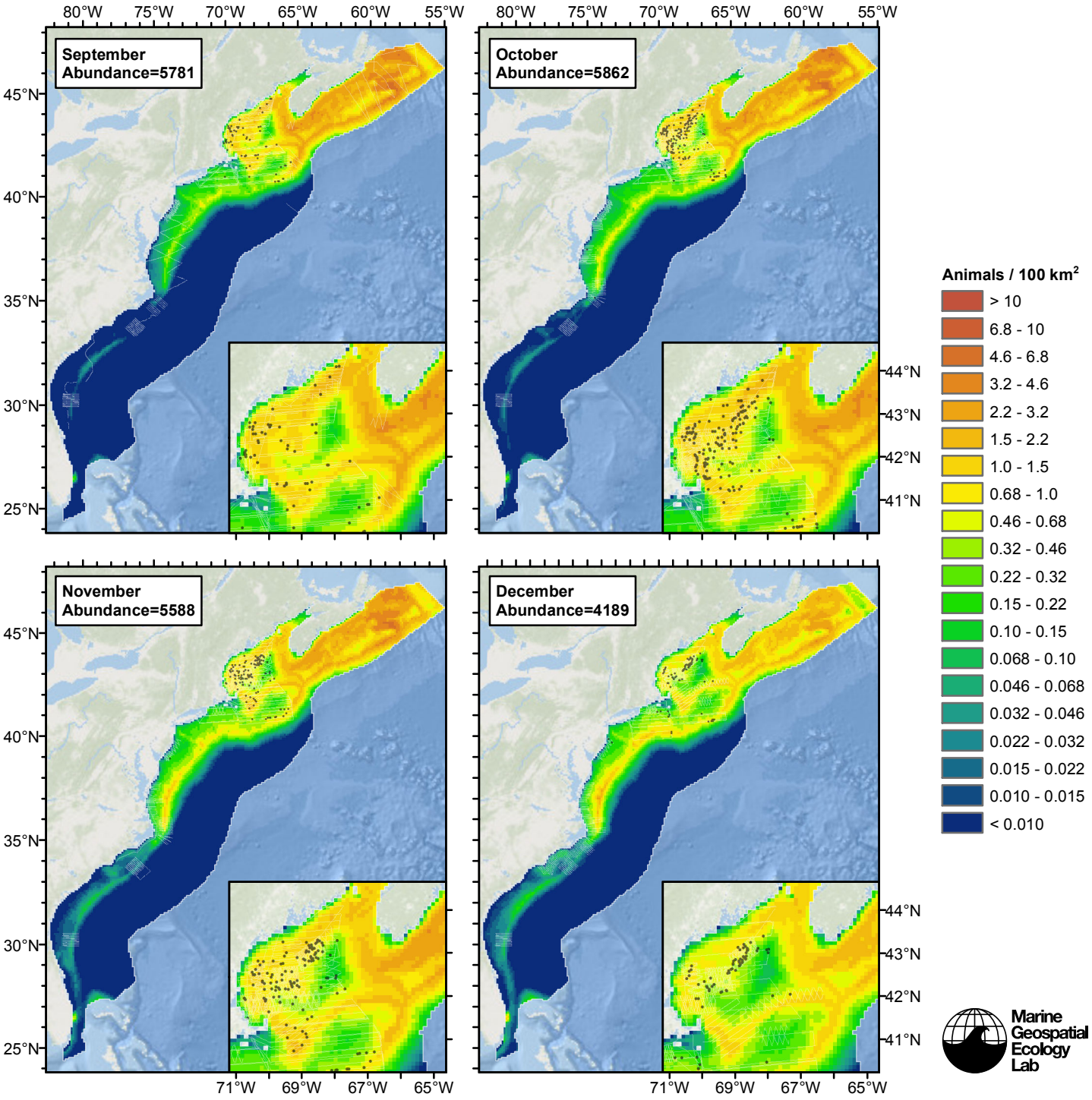
September
Abundance=5781
October
Abundance=5862
November
Abundance=5588
December
Abundance=4189
80°W
75°W
70°W
65°W
60°W
55°W
45°N
40°N
35°N
30°N
25°N
44°N
43°N
42°N
41°N
71°W
69°W
67°W
65°W
Animals / 100 km²
> 10
6.8 - 10
4.6 - 6.8
3.2 - 4.6
2.2 - 3.2
1.5 - 2.2
1.0 - 1.5
0.68 - 1.0
0.46 - 0.68
0.32 - 0.46
0.22 - 0.32
0.15 - 0.22
0.10 - 0.15
0.068 - 0.10
0.046 - 0.068
0.032 - 0.046
0.022 - 0.032
0.015 - 0.022
0.010 - 0.015
< 0.010
Marine
Geospatial
Ecology
Lab

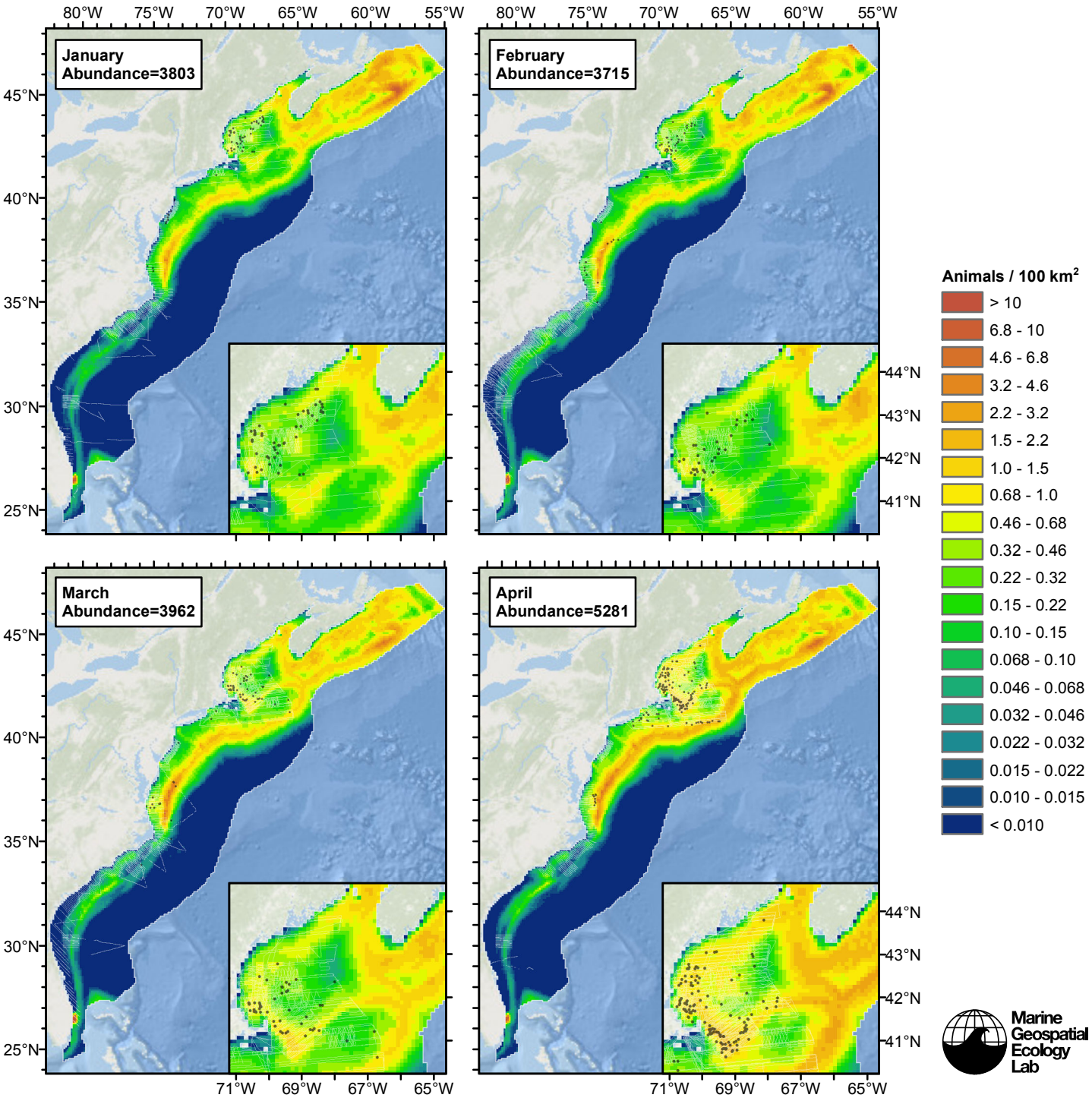
January
Abundance=3803
February
Abundance=3715
March
Abundance=3962
April
Abundance=5281
80°W
75°W
70°W
65°W
60°W
55°W
45°N
40°N
35°N
30°N
25°N
44°N
43°N
42°N
41°N
71°W
69°W
67°W
65°W
Animals / 100 km²
> 10
6.8 - 10
4.6 - 6.8
3.2 - 4.6
2.2 - 3.2
1.5 - 2.2
1.0 - 1.5
0.68 - 1.0
0.46 - 0.68
0.32 - 0.46
0.22 - 0.32
0.15 - 0.22
0.10 - 0.15
0.068 - 0.10
0.046 - 0.068
0.032 - 0.046
0.022 - 0.032
0.015 - 0.022
0.010 - 0.015
< 0.010
Marine
Geospatial
Ecology
Lab

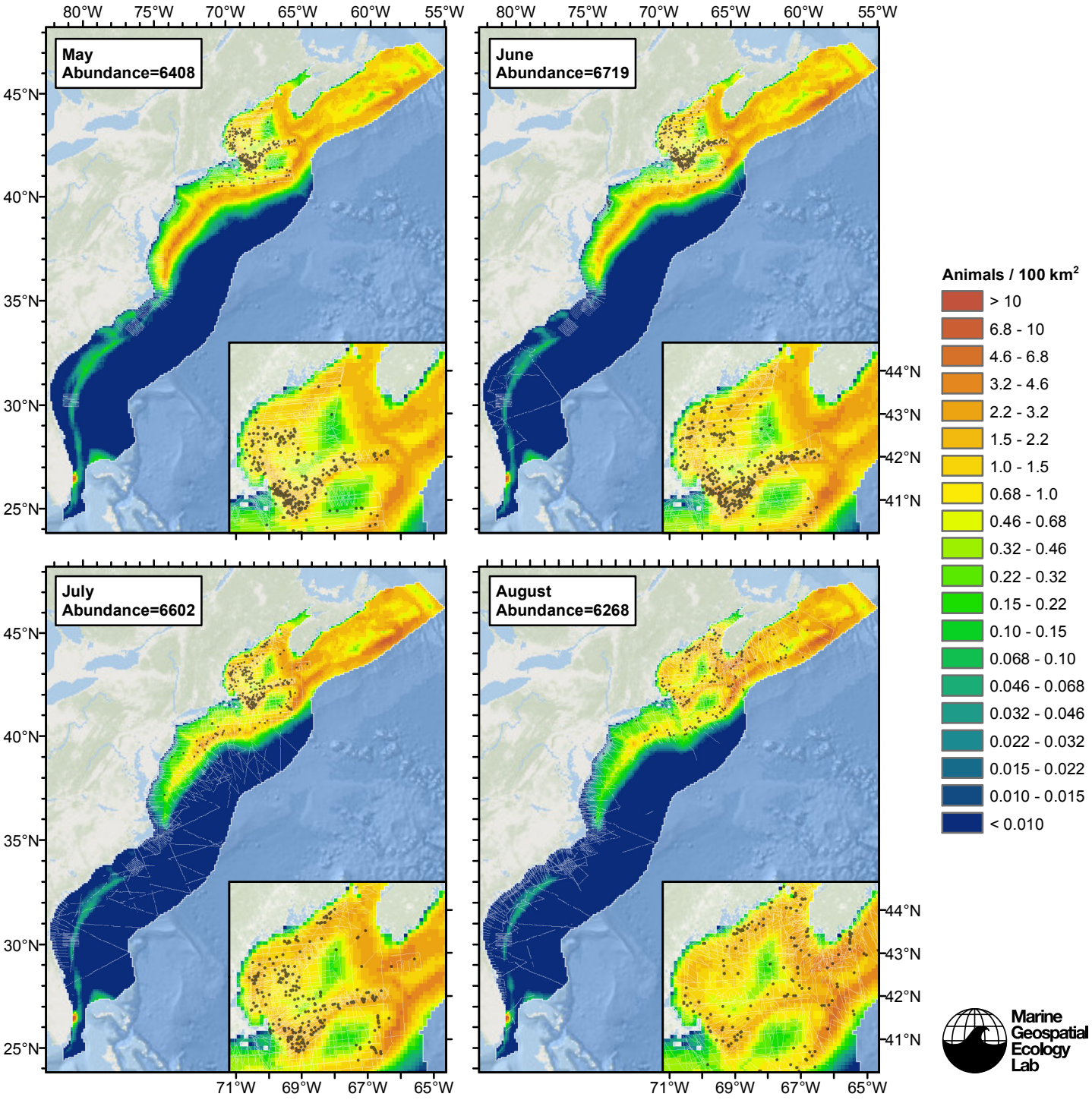
May
Abundance=6408
June
Abundance=6719
July
Abundance=6602
August
Abundance=6268
80°W
75°W
70°W
65°W
60°W
55°W
45°N
40°N
35°N
30°N
25°N
44°N
43°N
42°N
41°N
71°W
69°W
67°W
65°W
Animals / 100 km²
> 10
6.8 - 10
4.6 - 6.8
3.2 - 4.6
2.2 - 3.2
1.5 - 2.2
1.0 - 1.5
0.68 - 1.0
0.46 - 0.68
0.32 - 0.46
0.22 - 0.32
0.15 - 0.22
0.10 - 0.15
0.068 - 0.10
0.046 - 0.068
0.032 - 0.046
0.022 - 0.032
0.015 - 0.022
0.010 - 0.015
< 0.010
Marine
Geospatial
Ecology
Lab

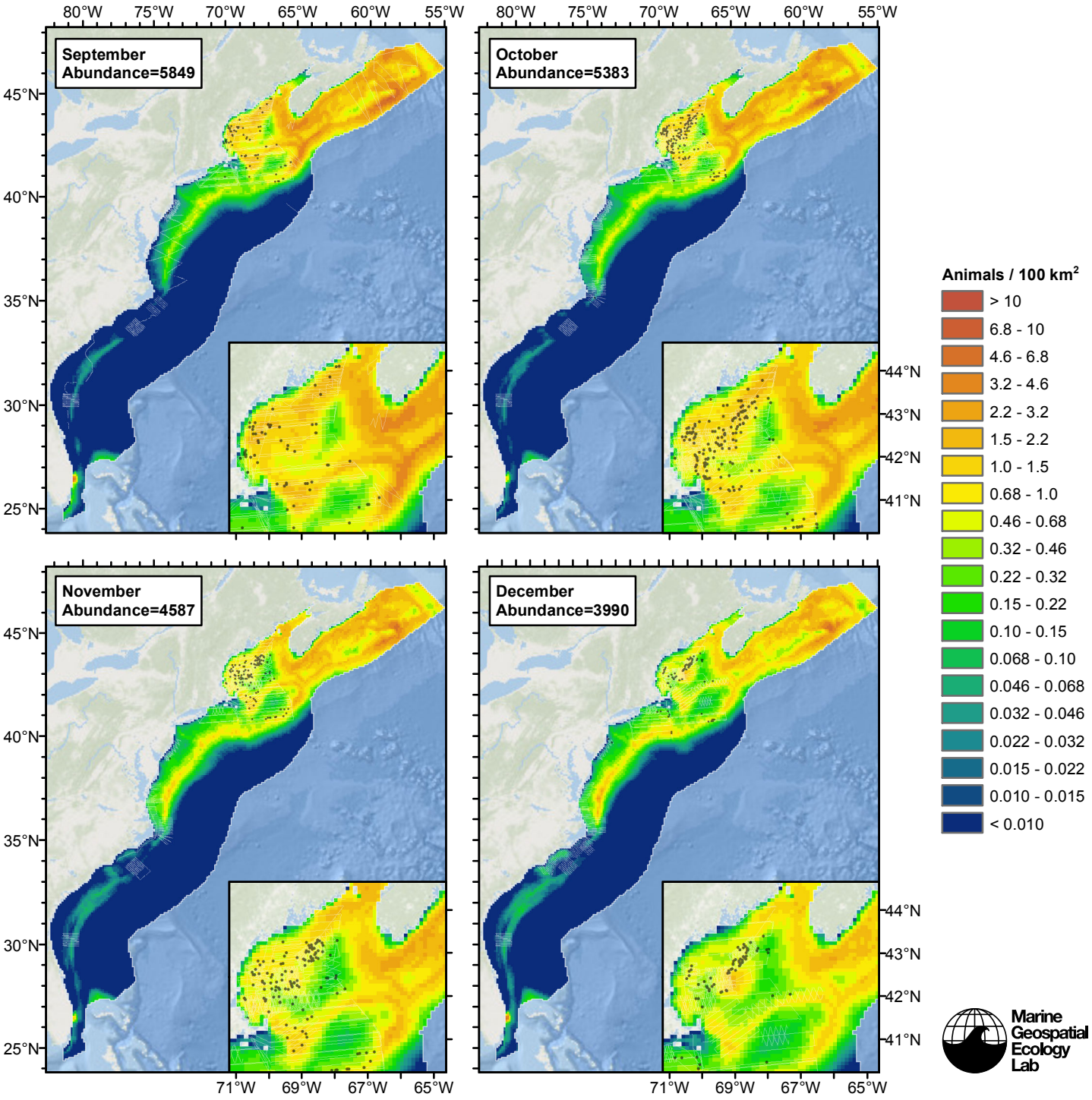

Discussion

The models that used climatological predictor variables explained more deviance than the models that used contemporaneous predictors. The spatial distribution of predicted abundance was similar across all models (see Density Maps section). The climatological model that considered all segments predicted roughly 10% lower total abundance than contemporaneous model or the climatological model that considered only the contemporaneous model's segments. The difference occurred mainly between June-December; the models estimated similar abundance during January-May (Figure 73). Given the overall similarity between the models, we selected the climatological model that considered all segments as our best estimate of fin whale distribution and abundance, on the basis of its higher explained deviance and consideration of more survey data.

At the broad scale, the model displayed plausible temporal dynamics for a migratory baleen whale that feeds in the northern

part of the study area, with low abundance in winter months, an increase in spring, high abundance in summer concentrated in the northern part of the study area, and a decrease in fall. Although fin whale migration patterns for this area have not been fully described in the literature, we are confident enough in the temporal dynamics of our model to recommend that our monthly predictions be used for federal regulatory purposes and marine spatial planning applications.

We do offer two cautions regarding the temporal dynamics. First the model predicts high abundance for nearly every month of the year for part of the Scotian Shelf near an area known as the Gully. This pattern may not be real. Hooker et al. (1999) reported that fin whales were the second most abundant baleen whale in the Gully (humpbacks were first), but seemed to suggest that they were not present throughout the year (although Hooker's study did not perform any surveying outside of summer). Second, when we reviewed our model's predictions with Andy Read, he indicated that the winter abundance was higher than he expected for a baleen whale that presumably migrates to the tropical calving grounds in the winter.

As an experiment, we fitted a two-season model to see whether it would yield a substantially lower abundance in winter. For seasons, we used December-March for winter and April-November for summer. The results were discouraging: the two-season model exacerbated the problem. Abundance was predicted to be higher in winter than in summer, with extreme concentrations predicted along the mid-Atlantic shelf break. Low effort occurred along the shelf break in winter, yet fin whales were sighted in most of the bouts of it that occurred there. We presume these sightings led to the extreme shelf-break prediction. We concluded that our single-season model was a better choice. In any case, to fully resolve this uncertainty we recommend additional surveying be performed in non-summer months, particularly along the shelf break.

The total abundance predicted by our model is higher than the other estimates reported in recent NOAA stock assessment reports (Table 33). A direct comparison is difficult due to the differing spatial and temporal extents of those studies and ours, and the different g(0) estimates that were used. We believe the differences in g(0) may play a large role in explaining the differences in estimated abundance. For example, our aerial g(0) estimate (0.251), based on fin whale diving data to account for availability bias, was about half of that (0.53) used for NOAA's August 2006 estimate (Palka 2006), while our abundance estimate is about twice that of NOAA's. Most fin whale sightings occurred during aerial surveys of the continental shelf, thus halving the aerial g(0) should double the abundance estimate, given that density is inversely proportional to g(0) in the density estimation equation. As an experiment, we refitted an earlier version of our models with Palka's (2006) aerial g(0). The results confirmed our expectation: our abundance estimate was halved by a factor of 1.98.

We believe our models could be improved by incorporating the Canadian TNASS survey from July 2007 (Lawson and Gosselin, 2009). We made several attempts to contact J. Lawson regarding this survey, in the hope of incorporating it into our models, but received no response. We remain hopeful that a collaboration can be established in the future, and the Canadian TNASS data may be incorporated into a new version of our models.

References

Barlow J, Oliver CW, Jackson TD, Taylor BL (1988) Harbor Porpoise, Phocoena phocoena, Abundance Estimation for California, Oregon, and Washington: II. Aerial Surveys. Fishery Bulletin 86: 433-444.

Carretta JV, Lowry MS, Stinchcomb CE, Lynn MS, Cosgrove RE (2000) Distribution and abundance of marine mammals at San Clemente Island and surrounding offshore waters: results from aerial and ground surveys in 1998 and 1999. Administrative Report LJ-00-02, available from Southwest Fisheries Science Center, P.O. Box 271, La Jolla, CA USA 92038. 44 p.

Chelton DB, Schlax MG, Samelson RM (2011) Global observations of nonlinear mesoscale eddies. Prog. Oceanogr. 91: 167-216.

Clark CW (1995) Application of US Navy underwater hydrophone arrays for scientific research on whales. Rep. Int. Whale Commn. 45: 210-212.

Hain JH, Ratnaswamy MJ, Kenney RD, Winn HE (1992) The fin whale, Balaenoptera physalus, in waters of the northeastern United States continental shelf. Rep. Int. Whale Commn. 42: 653-669.

Hooker SK, Whitehead H, Gowans S (1999) Marine Protected Area Design and the Spatial and Temporal Distribution of Cetaceans in a Submarine Canyon. Conservation Biology 13: 592-602.

Lafortuna CL, Jahoda M, Azzellino A, Saibene F, Colombini A (2003) Locomotor behaviours and respiratory pattern of the Mediterranean fin whale (Balenoptera physalus). Eur. J. Appl. Physiol. 90, 387-395.

Lawson JW, Gosselin J-F (2011) Fully-corrected cetacean abundance estimates from the Canadian TNASS survey. Working Paper 10. National Marine Mammal Peer Review Meeting. Ottawa, Can. 28 p.

Palka DL (2005b) Shipboard surveys in the northwest Atlantic: estimation of g(0). In: Proceedings of a Workshop on Estimation of g(0) in Line-Transect Surveys of Cetaceans (Thomsen F, Ugarte F, Evans PGH, eds.). European Cetacean Society's 18th Annual Conference; Kolmarden, Sweden; Mar. 28, 2004. pp. 32-37.

Palka DL (2006) Summer Abundance Estimates of Cetaceans in US North Atlantic Navy Operating Areas. US Dept Commer, Northeast Fish Sci Cent Ref Doc. 06-03: 41 p.

Waring GT, Josephson E, Fairfield-Walsh CP, Maze-Foley K, eds. (2007) U.S. Atlantic and Gulf of Mexico Marine Mammal Stock Assessments – 2007. NOAA Tech Memo NMFS NE 205; 415 p.

Waring GT, Josephson E, Maze-Foley K, Rosel PE, eds. (2014) U.S. Atlantic and Gulf of Mexico Marine Mammal Stock Assessments – 2013. NOAA Tech Memo NMFS NE 228; 464 p.